AGING OF POLYURETHANE FOAMS

by

Aleksandar G. Ostrogorsky

Dipl. Eng. M.E. University of Beograd
(1977)

M.S. N.E. Rensselaer Polytechnic Institute
(1981)

SUBMITTED TO THE DEPARTMENT OF
MECHANICAL ENGINEERING
IN PARTIAL FULFILLMENT OF THE REQUIREMENT
FOR THE DEGREE OF

DOCTOR OF SCIENCE

at the

MASSACHUSETTS INSTITUTE OF TECHNOLOGY
December 1985

Signiture of the Author___
Department of Mechanical Engineering
December 5, 1985

Certified by _____
Leon R. Glicksman
Thesis Supervisor

Accepted by _____
Ain A. Sonin
Chairman, Departmental Graduate Committee

AGING OF POLYURETHANE FOAMS

by

Aleksandar G. ostrogorsky

Submitted to the Department of Mechanical Engineering
on December 5, 1985 in partial fulfillment of the
requirements for the Degree of Doctor of Science

ABSTRACT

Several experimental and analytical techniques were developed to quantify the aging (i.e., degradation rate of the thermal properties) of unfaced and faced closed-cell polyurethane foams.

An analytical model, called the Successive Membrane Model, was developed. The model relates the geometry of the foam cells and the cell wall permeability to the effective foam diffusion coefficient. The model predictions of the foam effective diffusion coefficient are within 29% of the foam data or better.

An innovative experimental steady state technique was developed to measure the foam permeability and diffusion coefficients. Reference data were obtained with N_2, O_2, CO_2 and flourocarbon 11 at different temperatures. To test the new technique, the N_2 data were first obtained by the long-term steady state technique, and then reproduced with equal accuracy but 10 times faster by the rapid steady state technique. The data for flourocarbon 11 were obtained 30 times faster compared to the long-term steady state tests. To estimate if steady state has been achieved in tested foam samples, special charts were developed.

An experimental technique was developed to measure the permeability of the cell walls. Samples of cell walls were taken from large bubble-cells which appear on the surface of free-rise foam. The membranes forming the bubble-cells have the same composition and thermal history as the cells forming the foam. Permeability data were obtained with N_2, O_2 and CO_2. The limited number of data obtained on these membranes without flaws agreed within 4.6%.

A method to obtain the electrical analogy of the two-dimensional mass transport process in closed-cell foams was developed. The electrical analogy was used to measure the resistance of the foam-cell structure to permeation, the 2-D enhancement parameter, and the effect of the direction of staggerness on the effective diffusion coefficient. The electrical analogy method, combined with the cell was permeability data, can be used instead of the analytical model or foam tests, to rapidly obtain the value of the foam effective diffusion coefficient.

A computer code was developed to compute the aging of foam panels. The effective diffusion coefficients of air components

and fluorocarbon 11 obtained by measurement or modeling are the main code inputs. Based on given initial and boundary conditions, the code computes the change of the gas composition and conductivity of the gas mixture inside foam panels. The code prediction of the effective conductivity of foam panels is within 6% or better of the conductivity versus age data obtained in long-term tests under three different thermal environments.

The permeability of several materials used for facing was tested. Two fast laboratory tests "The Leak Cell" and "The Dye Technique" were developed to measure the porosity of the foam and foam-foil interface. For most samples tested, the air bypassed the facing by flowing laterally along the interface.

Thesis Supervisor: Dr. Leon R. Glicksman
Title: Senior Research Scientist

ACKNOWLEDGMENTS

I wish to thank Dr. Leon R. Glicksman, the thesis supervisor, for his encouragement and guidance and for being always available for consultations and advice. I would also like to thank Professor B.B. Mikic for his frequent suggestions and valuable discussions which I enjoyed throughout my studies at M.I.T. Both Dr. Glicksman and Professor Mikic have very much influenced my professional interests and development as a researcher.

I would also like to thank:

Professors W. M. Rohsenow and D. K. Roylance, members of the thesis committee, for their discussions, time and interest in this research project.

Professors E. P. Gyftopoulos and G. P. Beretta for their helpful suggestions concerning the thermodynamical aspect of this project.

Dr. Stephen Smith and Dr. Andre Desjarlais of Dynatech Research Corp., Mr. Doug Reitz of Owens Corning Fiberglas Corp., Mr. Thomas Allen and Mr. David Fair of Mobay Chemical Company, for their support in the form of materials and expertise.

Keith Gawlik and my other colleagues in the Heat Transfer Laboratory for providing a great help in the writing stage of this project.

Sponsorship by the U.S. Department of Energy, Energy Conversion and Utilisation Technologies (ECUT) Program and the Building Thermal Envelope Systems and Materials Program is gratefully acknowledged. Special thanks are extended to Mr. Joseph Carpenter and Mr. David McElroy of Oak Ridge National Laboratories for their suggestions and their support of this project.

TABLE OF CONTENTS

LIST OF TABLES

LIST OF FIGURES

NOMENCLATURE

A	Area
C	Storage capacity
d	Diameter
D	Diffusion coefficient
e	Energy
E	energy of activation
Fo = Dt/L^2	Fourier number
h	Entalphy
J	Flux
K	Conductivity
K_o	Reference value of K
<l>	Average distance between cell walls
L	Length or thickness
m	Mass
P	Gas pressure or gas partial pressure
Pe	Permeability coefficient
Pe_o	Reference value of Pe
q	Flux
R	Resistance or gas constant
s	Specific entropy
S	Solubility
S_o	Reference value of S
Sv	Surface to volume ratio
T	Temperature
t	Time
u	Internal energy
v	Specific volume
V	Volume

GREEK

α	Void fraction
ε	Enhancement parameter
μ	Chemical potential
ρ	Density

SUBSCRIPTS

c.w. Cell wall

eff Effective

el Electrical

i Initial

m Mass

p Plane

SM Successive membranes

ss Steady state

STP Standard temperature and pressure

t Transient

2 Side of the high potential

1 Side of the low potential

SUPERSCRIPT

* Dimensionless form

I INTRODUCTION

Buildings and appliances are frequently insulated with closed-cell foams made of polymers such as polyurethane. Closed-cell foams have the lowest conductivity of any insulation material that is currently available, other than vacuum insulation systems.

Heat is transferred through closed cell foam insulation by conduction through the solid polymer making up the cell structure, conduction through the gas within the cells and by thermal radiation. Because of the small cell size there is no convective heat transfer. At least 50 percent of the total heat is transferred by conduction through the gas so that it is advantageous to have a low conductivity gas inside of the foam, for example Fluorocarbon 11. The total conductivity of new closed-cell polyurethane foam is only two-thirds of the conductivity of stagnant air. It is one half the conductivity of glass fiber insulation, allowing buildings with conventional construction practices to approach super insulation values.

The increase of foam conductivity with age, i.e, the aging effect, is a major drawback of the closed cell foams. Aging occurs as air components diffuse into the foam while freon vapor diffuses out. Air components diffuse much faster than Fluorocarbon 11, so that the aging process can be divided into two stages: the diffusion of the air components, which lasts typically 1 year for a 2.5 cm (1 in) thick unfaced sample, and diffusion of Fluorocarbon 11, which is expected to last approximately twenty times longer.

The diffusion of the air components into the foam increases the foam conductivity by about 60%. The diffusion of the Fluorocarbon 11 out from the foam increases the conductivity of the foam by another 50% of the initial value.

In an attempt to reduce the diffusion process, closed cell foams are often faced with various materials such as aluminum or plastic foils, bonded to the surface to act as diffusion barriers. For faced foams, the aging rate becomes a function of both the foam internal resistance to diffusion and effectiveness of the diffusion barriers.

The main goal of the present research project is to provide accurate and reliable techniques to quantify the foam aging rate. The techniques developed include anccurate analytical model which relates the geometry of the closed cells and the cell wall permeability to an effective foam diffusion coefficient. An electrical analogy of the foam effective diffusion coeffisient is also developed. Experimental techniques developed to obtain data on the foam effective diffusion coefficient and permeability of the cell walls will be described. These data will be used to verify the model and will be used directly in a computer code to predict the change of gas composition inside the foam cells. From the change of the gas composition, the change of the conductivity of the foam panels is computed.

Two fast laboratory test to study the effectiveness of the diffusion barriers are also developed.

1.1 Previous Work: Accelerated Aging Tests

To quantify the aging rate of closed-cell foam, a test, called the accelerated aging test, is presently performed by industry [1]. A fresh foam sample is kept for 90 to 180 days at 60°C (140°F). This temperature increases the rate of the diffusion process although the exact increase for different air components is not well known. The overall foam thermal conductivity is measured before and after the accelerated aging. Foams having a smaller increase in the thermal conductivity in this test are assumed to age more slowly over their entire life. The accelerated aging test quantifies the foam resistance to aging, and therefore enables industry to distinguish foams with good and bad aging properties. Still it has several major disadvantages:

- It does not give any insight into the physics of the aging process.
- It is unclear if the foams have reached their ultimate aged values at the end of the accelerated aging test.
- It is imposible to extrapolate the results of an accelerated aging test, to the ultimate aged values, if the foam has not completely aged.
- It is difficult to relate the aging that occurred during the accelerated test to the aging that would occur in different operating conditions. Some foams are used at low and others at high temperatures. However, all foams are used as heat insulators and therefore are exposed to unequal temperatures at the

boundaries.

- It is too lengthy to enable fast feed-back between production conditions and quality of the foam.

Because of the above deficiencies of the accelerated aging tests, industry at present is not able to determine and guarantee the properties of the closed cell foams over its life time.

1.2 Previous Work: Measurements and Models of the Foam Effective Diffusion Coefficients

If the effective diffusion coefficients of freon and air components are determined, they can be used in the transient diffusion equation to predict the change of the gas composition with time in foams. The gas composition can be related to the effective conductivity of the foam. The effective foam diffusion coefficient can be determined by lengthy foam permeability measurements (which give little physical insight into foam aging behavior) or it can be modeled based on the knowledge of the foam geometry, and permeability of the solid polymer cell walls. The important geometry parameters are: the cell wall thickness, cell size, arrangement and percent of open cells.

Models of the effective diffusion coefficient have been developed in the past [2] and [3]. However, they assumed oversimplified geometries with unrealistically thick cell walls. For example Norton [3] used cubical model of the foam cell structure and estimated that 50% of the polymer is in the cell walls. In addition, they could not be validated because the published data of foam diffusion coefficients

varied substantially.

Reitz at M.I.T. developed an embedding technique to obtain a clear two dimensional view of the foam structure. He determined that cell walls contain only 10 to 20 percent ofthe total polymer material. Based on the geometry measurement Reitz suggested a model with an accurate distribution of solid polymer [4]. Using the existing data for the permeability of solid polymer and his own data for the permeability of cell walls, Reitz computed, for N_2, O_2 and CO_2 the effective foam diffusion coefficient of three foams having different densities. The model predicted that the foam effective diffusion coefficient decreases as the foam density increases, while the data had the opposite trend.

The existing data on the cell wall permeability coefficient are also uncertain. Some data on solid polyurethane have been published by Hallian et al.,[5], but it is not known if the foam cell walls have the same permeability coefficient since they have a different formation and thermal history.

Reitz has measured the permeability of the cell walls obtained from large bubbles that are often created on the free rised foam surface [6]. He obtained data on the permeability of cell walls to O_2 and CO_2. The permeability coefficient of CO_2 was measured to be only 2.6 times higher than the permeability coefficient of O_2. These data are in reasonable agreement with the data of Hallian et al., Table 1. It is interesting to note that CO_2 permeability coefficients vary more than O_2 permeability coefficients, although CO_2 permeates faster, and therefore should be measured more accurately.

Lee measured the foam permeability coefficient of O_2 and CO_2 at

TABLE 1

PUBLISHED DATA ON THE PERMEABILITY OF THE SOLID POLYMER

TYPE	DENSITY kg/m^3	Pe $[cm^3_{STP}\text{-}mm/cm^2\text{-}s\text{-}cmHg]$ Pe_{CO2}	Pe_{O2}	Pe_{N2}	AUTOR
-	-	$4.00x10^{-10}$	$1.07x10^{-10}$	$.27x10^{-10}$	Hallian et. al.[5]
TDI	20.7	$2.35x10^{-10}$	$.89x10^{-10}$	-	Reitz [6]

room temperature [7]. Reitz measured the foam permeability coefficient of O_2 and CO_2 at different temperatures [6]. He applied various pressure differences to the foam samples and measured a substantial decrease in foam permeability coefficient with the increase of the applied pressure differential. The data of Reitz also show an increase of the foam permeability and diffusion coefficient with foam density although one would expect the foam permeability to decrease as foam density increases. Still, the O_2 data obtained from steady-state permeability measurements by Lee and Reitz vary much less than the other published data [8], [9], and [10]. The published data are given in Table 2.

1.3 Previous Work: Diffusion Barriers

The accelerated aging test performed on faced foams by Dynatech Research and Development Corporation [11] have shown that most of the diffusion barriers are inefficient. The aging rate of most faced foam samples was only 10% to 20% slower than the aging rate of the unfaced foams, while an one to two orders of magnitude slower rate was expected. The explanation for the failure of the facings was not apparent.

TABLE 2

PUBLISHED DATA ON THE FOAM EFFECTIVE DIFFUSION COEFFICIENT

DENSITY kg/m^3	D_{eff} $[cm^2/s]$ D_{O2}	D_{N2}	D_{R11}	Reference
33.5	200. x10-8	100. x10-8	3.0 x10-8	Ball[8]*****
35.2	11.2x10-8	6.3x10-8	0.225x10-8	Norton[9]**
35.9(TDI)	4.0 to 7.0x10-8	5.5 to 16. x10-8	0.006 to 0.25 x10-8	Brandreth[10]*
33.5(MDI)	6.0x10-8	2.0 to 3.0 x10-8	.025 to .046x10-8	Brandreth[10]*
35.2	-	-	.042x10-8	Norton[3]****
24.5(MDI)	196.2x10-8	-	-	Lee[7]***
25.6(TDI)	147.6x10-8	-	-	Lee[7]***
20.7(TDI)	76.8x10-8	-	-	Reitz[6]***
28.3(MDI)	119.0x10-8	-	-	Reitz[6]***
30.4(MDI)	193.0x10-8	-	-	Reitz[6]***

* Stored plugs of foam for various times and measured transient change of gas composition by gas chromatogaphy

** Measured effusion from the plugs by mass spectrometry

*** Permeability coefficient was measured

**** Film data and a model

***** Thermal conductivity was measured

2. MASS TRANSPORT IN CLOSED-CELL FOAMS

2.1 Phenomenological, Kinetic and Thermodynamic Approach to Mass and Energy Transport Porcesses

Transport of mass and heat is usualy described by so-called phenomenological laws. These laws are experimentally verified and are valid for systems that are not too far from equilibrium. The phenomenological laws are in the form of proportionalities between the flux of the transported property and the gradient of a driving potential. If an irreversible process occurs in a system that is too far from the equilibrium state, linearity might not exist between the gradient of the driving potential and the flux. Also continuum assumptions for the system are called into question. For example, when a concentration difference is initially imposed on a semi infinite body, infinite gradient occurs but does not cause an infinite flux of matter.

The proportionality constants are usually obtained by imposing a gradient of the potential, which is belived to be the driving potential, and measuring the resulting flux of the property. However, it is not certain that other potentials do not cause the flow of the same property. For example, Gibbs [12] [13], has established that chemical potential is the quantity that determines the value of the mass flux (of a simple substance). Still, the phenomenological law of mass transport, the Fick's law, states the proportionality between the

mass flux and the concentration gradient,

$$J_m = -D\, dc/dx \qquad (2.1)$$

Equation (2.1) implies that, besides concentration, other driving potentials for mass transport do not exist or that their influence is neglegable.

Phenomenological laws also do not take into account the interference that arises when two or more transport processes occur simultaneously.

The kinetic theories rely on a much more rigorous analysis of the physics of the phenomenon. The transport phenomena are first analysed on atomic or molecular scale based on Newtonian, reversible mechanics. Motion of particles is modelled and as a result trajectories of the particles are obtained. The trajectories are used as an input for transport equations, like the Boltzman's equation, that treat the motion of the large number of particles statistically, and give the macroscopic transport coefficients as an output. Although very rigorous and informative, this theory lacks generality. Every transport process has to be modelled separately.

L. Onsager, in his famous papers published in 1931, has given a most general thermodynamic treatment of the irreversible processes. Onsager calls the gradients of the potentials forces and denotes them by X_i, $(i=1,2,\ldots n)$, [14], [15]. The fluxes of the transported properties are denoted by J_i. A force can give rise to the flow of all properties.

The irreversible processes are coupled, i.e., each flux is linked

to all driving forces present,

$$J_i = L_{i,k} X_k \qquad (i = 1,2,...n) \qquad (2.2)$$

where $L_{i,k}$ are the Onsager phenomenological coefficients. The coefficient are symetrical,

$$L_{i,k} = L_{k,i} \qquad (i,k = 1,2,...n) \qquad (2.3)$$

In the next section the general thermodynamic approach will be applied to the ireversible transport processes in closed cell foams. We will examine by methods of irreversible thermodynamics, the existance of other driving potentials for mass transport, and determine if their presence can be neglected in the case of the gas transport through closed-cell foam.

2.2 The Thermodynamic Approach to the Irreversible Process of Gass Permeation Through Cell Walls of Closed-Cell Foam

The approach of the thermodynamics for irreversible processes as described in [16] and [17] can be applied to the cells of a closed-cell foam. A schematic diagram of two neighboring foam cells is shown on Fig 2.1. Let the gas inside the left-hand side cell be a simple single component system, I, while the gas in the right-hand side is a simple single component system, II. The cell-wall membrane beween the cells is the system A, which is in steady state. Systems I

and II are in stable equilibrium states, defined by temperatures T^I and T^{II}, volumes V^I and V^{II}, and total potentials μ^I and μ^{II}. The reservoir of the systems consists of the two neigboring cells, Fig. 2.1. The cells have constant volume, impermeable walls and are adiabaticaly isolated from the rest of the foam.

If systems I and II are not in mutual stable equilibrium, they will interact via system A, which is in steady state. Since the system A is in steady state, all properties of the system A are time independent. Although properties are transfered through system A, storage of properties does not occure.

If systems I and II are in mutual stable equilibrium, any change of state of combined system I and II must yield a decrease in entropy or in the limit no change in entropy,

$$dS^I + dS^{II} \leq 0 \tag{2.4}$$

where dS^I and dS^{II} are the changes in entropy of systems I and II respectively.

We can assume that the cells have constant volume. Then for a constant volume process, the Gibbs equations yield [17],

$$dS^I = dU^I/T^I - (\mu^I/T^I)dn^I \tag{2.5}$$

$$dS^{II} = dU^{II}/T^{II} - (\mu^{II}/T^{II})dn^{II} \tag{2.6}$$

There is no storage of mass or energy in the system A which is in steady state. Consequently,

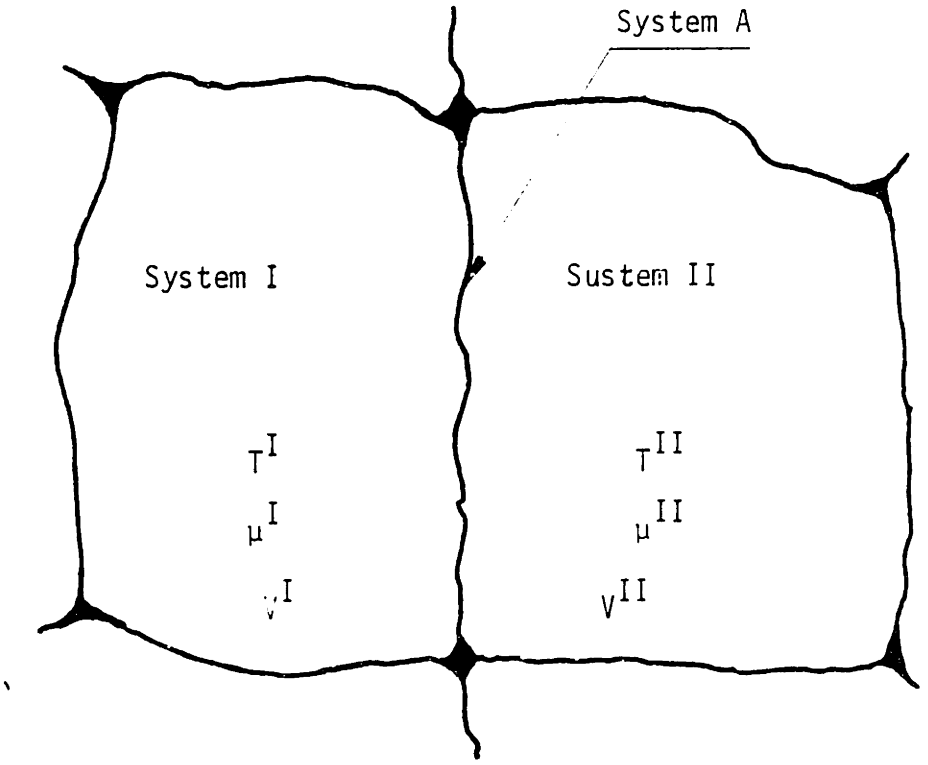

Fig. 2.1 SCHEMATIC DIAGRAM OF TWO NEIGHBORING CELLS CONTAINING SYSTEMS I, II AND A

$$dU^{I} = -dU^{II} \tag{2.7}$$

$$dn^{I} = -dn^{II} \tag{2.8}$$

It is important to note that dU^{I} and dn^{I} can be positive or negative. Then, from equations (2.4) to (2.8), it follows that systems I and II are in mutual stabile equilibrium if and only if,

$$1/T^{I} = 1/T^{II} \tag{2.9}$$

and,

$$\mu^{I}/T^{I} = \mu^{II}/T^{II} \tag{2.10}$$

or,

$$T^{I} = T^{II} \tag{2.11}$$

and,

$$\mu^{I} = \mu^{II} \tag{2.12}$$

Consequently, steady state mass or energy fluxes must be at least a function of the quantities $[1/T^{I} - 1/T^{II}]$ and $[(\mu^{I}/T^{I}) - (\mu^{II}/T^{II})]$.

To be able to regard the irreversible transport process as linear, we need to assume small magnitudes of the differences of the driving potentials, i.e.,

$$1/T^{I} = 1/T \tag{2.13}$$

$$\mu^{I}/T^{I} = \mu/T \tag{2.14}$$

$$1/T^{II} = 1/T + d(1/T) \tag{2.15}$$

$$\mu^{II}/T^{II} = \mu/T + d(\mu/T) \tag{2.16}$$

where d denotes small but finite difference of the potentials across the membrane. It can be shown [17], that the entropy generation rate J_S is related to fluxes of properties and differences of thermodynamic potentials as,

$$dJ_s = Je\ d(1/T) + J_m\ d(-\mu/T) \tag{2.17}$$

where J_e is the energy flux, and J_m is the mass flux. The fluxes are given by the Onsager phenomenological relations,

$$J_e = L_{ee}\ d(1/T) + L_{em}\ d(-\mu/T) \tag{2.18}$$

$$J_m = L_{me}\ d(1/T) + L_{mm}\ d(-\mu/T) \tag{2.19}$$

where L_{ee}, L_{em}, L_{me} and L_{mm} are the conductivities. According to the Onsager reciprocal relations,

$$L_{em} = L_{me} \tag{2.20}$$

Equation (2.19) gives the total mass flux through the system A, i.e. cell-wall membrane. The flux results from inequality of the driving potentials, (1/T) and (μ/T), in systems I and II.

By taking derivatives of the driving potentials in the equations (2.18) and (2.19) we obtain,

$$J_m = -L_{me} (dT/T^2) + L_{mm} [(-Td\mu + \mu dT)/T^2] \quad (2.21)$$

$$J_e = -L_{ee} (dT/T^2) + L_{em} [(-Td\mu + \mu dT)/T^2] \quad (2.22)$$

where dT is the temperature difference accros the membrane and $d\mu$ is the difference of the chemical potential across the membrane. For a one component system,

$$\mu = h - Ts = u + pv - Ts \quad (2.23)$$

If molecules of other gasses are present in the cells, symbol p in the equation (2.23) denotes the partial pressure of the permeated gas. By differentiating the equation (2.19), we obtain,

$$d\mu = v\, dp - s\, dT \quad (2.24)$$

Then the equations (2.21) and (2.22) become,

$$J_m = -L_{me} (dT/T^2) + L_{mm} [-(v/T)dp + (h/T^2)dT] \quad (2.25)$$

$$J_e = -L_{em} (dT/T^2) + L_{ee} [-(v/T)dp + (h/T^2)dT] \quad (2.26)$$

or,

$$J_m = - L_{mm} (v/T)dp + [(L_{mm}h - L_{me})/T^2]dT \qquad (2.27)$$

$$J_e = - L_{em} (v/T)dp + [(L_{em}h - L_{ee})/T^2]dT \qquad (2.28)$$

In the present research an experimental technique is developed to measure the mass flux due to partial pressure difference. To be able to estimate the magnitude of the mass flux caused by the temperature difference without a measurement, we need to compare the coefficients associated with the pressure and temperature differences.

The mass flux due to pressure difference according to equation (2.27) is,

$$J_m\Big|_{dT=0} = - L_{mm} (v/T)dp \qquad (2.29)$$

We can also write $J_m\Big|_{dT=0}$ in the form

$$J_m\Big|_{dT=0} = - (Pe/t)dp = -Pe'dp \qquad (2.30)$$

where Pe is the cell-wall membrane permeability coefficient, t is the thickness of the membrane and Pe'=Pe/t. An experimental technique for measurement of the membrane permeability coefficient is described in Chapter 4. By combining (2.29) and (2.30), we obtain an expression for

the coefficient L_{mm},

$$L_{mm} = Pe'/(v/T) = Pe'T/v \tag{2.31}$$

The energy flux due to a pressure difference according to the equation (2.28) is,

$$J_e\Big|_{dT=0} = - L_{em}\,(v/T)dp \tag{2.32}$$

The energy flux due to pressure gradient is equal to the amount of energy that permeating particles carry with them,

$$J_e\Big|_{dT=0} = [J_m\Big|_{dT=0}]e = [-Pe'dp]e \tag{2.33}$$

where e is the energy carried by the unit of mass of permeated particles. By combining (2.32) and (2.33), we obtain the L_{em} coefficient,

$$L_{em} = Pe'e/(v/T) \tag{2.34}$$

Since the phenomenological coefficients are symetric, i.e., $L_{em} = L_{me}$, we can write,

$$Lme = Pe'e/(v/T) = Pe'eT/v \tag{2.35}$$

Now, coefficients in the equation (2.27) can be computed in terms of the Pe',

$$J_m = - Pe'dp - [(Pe'hT/v - Pe'eT/v)/T^2]dT \qquad (2.36)$$

It is convenient to nondimensionalize the pressure and temperature difference by dividing them with their absolute value. Then, the difference of the potentials is given in terms of the fraction of the absolute value.

$$J_m = - Pe'p(dp/p) - Pe'(h/v - e/v)/(dT/T) \qquad (2.37)$$

To compare the fluxes in the equation (2.37) due to temperature and pressure differance, assuming the same magnitude of (dp/p) and (dT/T) we need to compare the term (h/v - e/v) with the pressure, p,

$$(h/v - e/v) = (u + pv - e)/v = p + (u - e)/v \qquad (2.38)$$

Therefore, if the energy per unit permeated mass is equal to u, the pressure and temperature gradients cause equal mass fluxes. If the energy per unit of the permeated mass is equal to h, then no mass is transfered due to temperature gradient.

For bulk flow of perfect gas e = h. This situation occures when perfect gas permeates through pores in a membrane, which has a characteristic diameter larger than the mean free path of the molecules. In that case a temperature gradient does not cause a mass flux.

In the case of Knudsen diffusion where the mean free path of the molecules is much greater the diameter of the pores, e = u. The molecules are isolated from each other, and each of them carry only its internal energy u with it. In that case a temperature gradient given in terms of a fraction of the absolute temperature causes the same mass flux as a pressure gradient given in terms of a fraction of the absolute pressure.

Gas molecules permeate through cell walls of the closed cell foam by diffusion through the solid polymer. It is dificult to compute the exact value of the energy that is carried by molecules diffusing through the polymer. Still we can conclude that the energy is in the range between h and u. Concequently, the proportionality coefficient next to the dimensionless temperature difference, (dT/T), can not be bigger than the coefficient next to the dimensionless pressure difference, (dp/p),

$$Pe'[(h/v - e/v)] \lesssim Pe'p \tag{2.39}$$

Next (dT/T), and (dp/p) need to be compared. The dimensionless pressure difference, (Δp/p), across one half of the thickness of a foam panel is of the order of one. The pressure difference occurrs only across the cell walls. The typical average distance between the cell walls is .3 mm so that gas molecules need to permeate through typicaly 50 cell walls to pass through one half thickness of a foam panel. Therefore, across one membrane,

$$(dp/p) = \text{order of}(1/50) = \text{order of}(10^{-2}) \tag{2.40}$$

On the other hand, a typical value of $(\Delta T/T)$ across one half of the foam thickness is 0.1 . The thermal conductivity of the solid polymer is higher then the conductivity of the gas mixture inside the cells, so that the temperature difference across a cell wall is very low. The heat flux through a foam panel is,

$$J_{e,foam} = (K_{eff}/t_{foam})\Delta T_{foam} \tag{2.41}$$

The heat flux passing normal to the surface of the cell walls, i.e., across the cell wall thickness has to be less then or equal to the flux through the foam panel since a fraction of the total flux is not conducted across the cell walls, but is conducted along the struts. Assuming that all of the heat flux passes normal to surface of the cell walls we can estimate the upper limit of the (dT/T),

$$J_{e,c.w.} = (K_{c.w.}/t)dT = (K_{eff}/t_{foam})\Delta T_{foam} \tag{2.42}$$

or,

$$(dT/T) = (\Delta T/T)_{foam}(t/t_{foam})(K_{eff}/K_{c.w.}) =$$

$$= \text{order of}[(10^{-1})(10^{-5})(10^{-1})] = \text{order of}(10^{-7}) \tag{2.43}$$

Since dT/T is so much smaller than dp/p, we can conclude that mass flux through cell walls due to temperature difference is neglegably small in polyurethane foams. Because of that, in the present analytical and experimental research on diffusion of gasses in

foams, only mass transfer due to partial pressure difference will be considered.

2.3 Permeation Through Cell Walls Under Partial Pressure Gradients

When a polymeric membrane such as a wall of a closed-cell foam is exposed to a gas, gas molecules are absorbed and desorbed at the membrane surface. The mass flow rate of one gas species as it diffuses across the membrane is according to equation (2.30),

$$J_m = -(Pe/t)\Delta p = (Pe/t)(p_2 - p_1) \tag{2.44}$$

where p_1 and p_2 are the low and the high partial pressure inposed on the two surfaces respectively, Pe is the permeability coefficient of the gas species through solid polymer, and t is the membrane thickness. The partial pressure of that gas species directly above the surface can be related to the concentration directly above the surface by Henry's Law,

$$C = Sp \tag{2.45}$$

where S is the solubility coefficient which can be assumed to be independent of pressure level [18]. Combining Henry's Law with Eq. (2.44), one gets

$$J_m = (Pe/S)/t\ (C_2 - C_1). \tag{2.46}$$

The diffusion coefficient of a gas throgh the membrane is defined as,

$$J_m = D/t\ (C_2 - C_1) \tag{2.47}$$

thus,

$$D = Pe/S. \tag{2.48}$$

Although molecules of the air components N_2, O_2 and CO_2 have roughly the same molecular size, experiments show that their permeation rates through a membrane vary substantially. Since the diffusion coefficients of the three gases are approximately equal [19]. then, according to Eq. (2.47) their diffusion rates under the same concentration gradient are also approximately equal. However, the air components have different solubilities [19] and therefore they have different concentration gradients, according to Eq. (2.45), Fig. 2.2. Consequently, their transport (permeation) rates defined in Equation (2.44) are quite different, even when the partial pressure differences of the gas across the membrane are same.

According to the Centimeter, Gram, Second, (CGS) system of units, the properties in the equations (2.44) to (2.48) have units,

t [cm]

p [bar] = 10^{+6} [dyn/cm^2] = 10^{+5} Pa

C [g/cm^3]

J_m [g/cm^2-s]

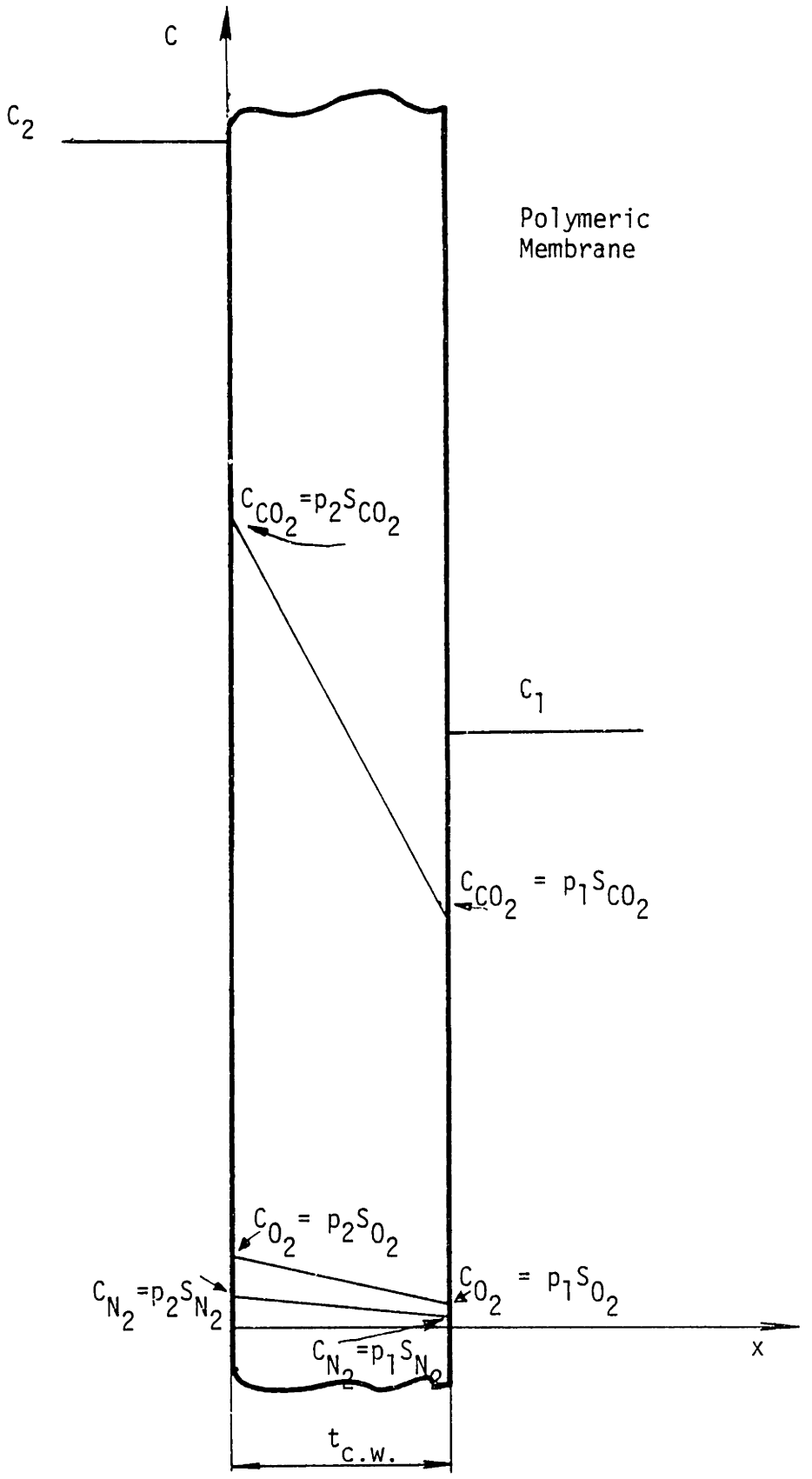

Fig. 2.2 CONCENTRATION GRADIENTS OF AIR COMPONENTS INSIDE A POLYMERIC MEMBRANE
(when each has equal partial pressures p_2= 1 atm at the high pressure side, and p_1=.5 atm at the low pressure side.)

S [g/cm^3-bar]

Pe [g/cm-s-bar]

D [cm^2/s] (2.49)

It is customary to use units cm^3_{STP} for the amount of gas in cm^3 at standard temperature and pressure [19] and atm as unit of pressure. Then,

t [cm]

p [atm]

C [cm^3_{STP}/cm^3]

J_m [cm^3_{STP}/cm^2-s]

S [cm^3_{STP}/cm^3-atm]

Pe [cm^3_{STP}/cm-s-bar]

D [cm^2/s] (2.50)

The units (2.50) are related to the CGS units, (2.49), and MKS units, (Meter, Kilogram, Second), in the Appendix I.

2.4 Diffusion of Gasses in Closed-Cell Foams

Figure 2.3 shows the one-dimensional mass transport process in foams. Due to partial pressure gradient gas molecules permeate through the cell walls which resist permeation. Some of the molecules are stored in the cell while the rest of the molecules are transported further. For gas diffusion, the cell walls are regarded as permeation

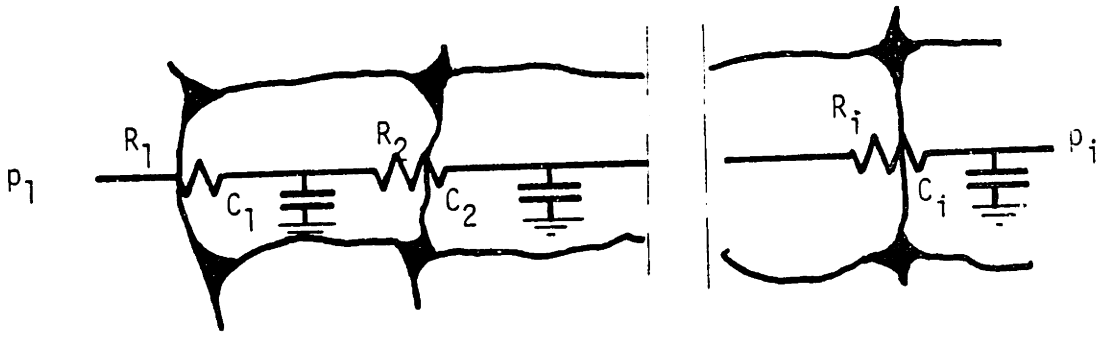

a) Diffusion of Gasses

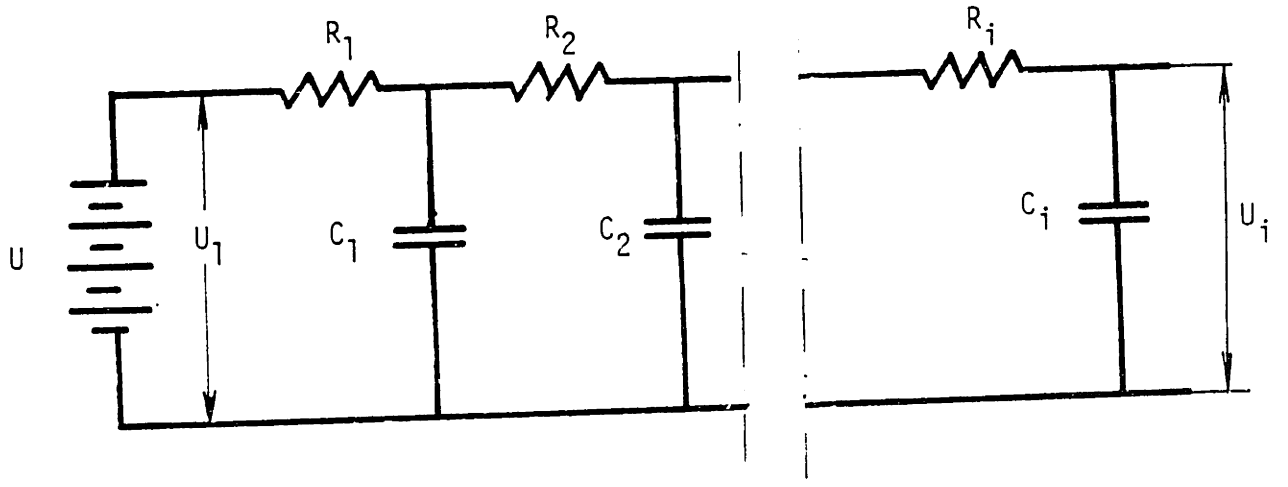

b) Transport of Electrical Charge

Fig. 2.3 ONE-DIMENSIONAL MASS TRANSFER PROCESS IN CLOSED CELL FOAMS, AND THE CORRESPONDING ELECTRICAL ANALOGY

resistors while the cells are the capacitors.

The same figure shows the analagous transport of electrical charge (i.e., the "electrical analogy"). The electrical charge is transported from the high potential, U_1, to the lower potentials, U_i. After passing through a resistor some of the charge is stored in the capacitors, while the rest of the charge is transported further.In Chapter 3 the analogy between mass transport and transport of electrical charge is used in to dewelope an electrical model of the gas diffusion in closed-cell foams.

In the next two sections of this Chapter, analytical models of the foam transport coefficients will be developed.

2.5 The Model of Gas Storage Capacity in Closed-Cell Foams

In closed cell foams the solid polymer and the voids store gases. According to Norton [9], the solubility of the solid polymer to air components is less than 0.1 [cm^3_{STP}/cm^3-atm]. By definition, $1cm^3$ of void space at standard temperature and pressure contains $1cm^3_{STP}$ of gas. For 35.2 kg/m^3 (2.2 lb/ft^3) foam, the solid polymer is 2.4% of the foam volume while pore space occupies 97.6%. This implies that the solid stores less than 1% of the gas. For practical applications, the solubility of the solid can be neglected. Consequently, the mass storage capacity of the foam (or the effective foam solubility) can be modeled as the storage capacity of the voids.

The ideal gas law can be used to determine the amount of matter that can be stored per unit of volume and unit of pressure in the

voids. The concentration of an ideal gas in voids is,

$$C = p/(RT) \tag{2.51}$$

At standard temperature and pressure, concentration is equal to,

$$C_{STP} = p_{STP}/(T_{STP}R) \tag{2.52}$$

By combining equations (2.51) and (2.52) we obtain,

$$C = C_{STP}(p/p_{STP})(T_{STP}/T) \tag{2.53}$$

Neglecting the concentration of gasses in the solid polymer, from the equation (2.53), the effctive concentration of a gas in a closed-cell foam is,

$$C_{eff} = C_{eff,STP}(p/p_{STP})(T_{STP}/T) \tag{2.54}$$

We can define an effective foam solubility by dividing equation (2.54) with p,

$$S_{eff} = C_{eff}/p = C_{eff,STP}/p_{STP}(T_{STP}/T) = S_{eff,STP}(T_{STP}/T) \tag{2.55}$$

Note that if cm^3_{STP} is used as a measure of mass in the concentration, and atm is used as an unit of pressure, the $S_{eff,STP}$ is equal to $1[cm^3_{STP}/cm^3\text{-atm}]$ for all the gasses. Then equation (2.55) takes the simple form,

$$S_{eff} = T_{STP}/T \tag{2.56}$$

where units of the effective solubility are $[cm^3_{STP}/cm^3\text{-atm}]$, as given in the (2.50).

Equation (2.55) or (2.56) models the effective foam solubility, (i.e., the foam storage capacity) with high accuracy as long as the gas follows the ideal gas law. No measurement is needed. It is important to note that foam mass storage capacity decreases linearly with 1/T.

Some types of fluorocarbons can condense inside of the closed cells. Equation (2.55) can not be used if any substantial condensation of the transported gas occurs.

2.6 The Successive Membranes Model For Permeability and Diffusion Coefficient in Foams

The measured polymer permeability can be combined with the measured foam geometry parameters to obtain an overall model of gas diffusion in foam insulation. For a typical foam application the thickness of a foam slab is much larger than the average cell diameter, so that a continuum model for the foam can be employed. The model includes the following assumptions:

- Each cell wall membrane is considered a resistance to gas diffusion. The diffusion resistance inside the cells is neglected because $D_{gas} = 1cm^2/s$, while $D_{solid} = 10^{-10}cm^2/s$.
- No pinholes or cracks exist in the cell walls.

- The gas flow lines are parallel to the concentration gradient.

As shown in Fig. 2.4, the cell walls can be modeled as successive membranes (SM). In this configuration, the most important geometric parameter characterizing the diffusion process in foams is the average distance between cell walls. This parameter is measured by drawing random lines parallel to the flow direction and counting the number of intersections with cell walls:

$$\langle l \rangle = L/n \tag{2.57}$$

where n is the total number of intersections and L is the total length of the lines.

Consider a volume of foam having cross-sectional area A_{x-s} perpendicular to the concentration gradient and having length L. For cells of equal wall thickness the resistance of successive membranes can be summed to give the effective foam resistance to permeation,

$$R_{foam} = n\, R_{c.w.} \tag{2.58}$$

The resistance of a single nonplanar successive membrane is defined as,

$$R_{c.w.} = t/(A_{SM}\, Pe_{c.w.}) \tag{2.59}$$

where A_{SM} is the membrane area with the cross-section A_{x-s}. If the membrane area is plane, parallel to A_{x-s}, then A_{SM} equals to A_{x-s}.

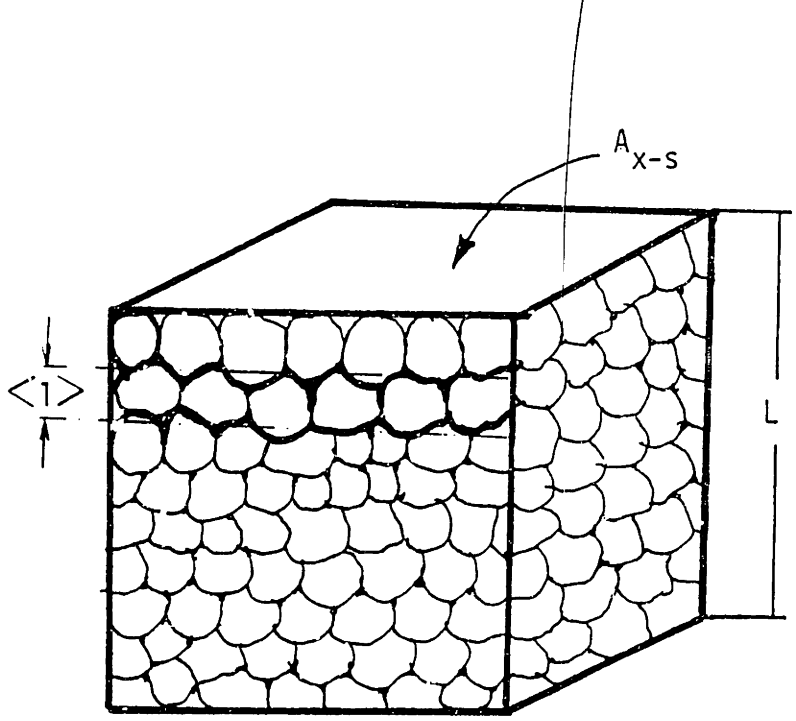

$$V = A_{x-s} L$$

$$S_v = A_T/V$$

$$A_{SM} = A_T/n = A_T/(L/\langle 1\rangle) = A_{x-s} S_v \langle 1\rangle$$

$$\varepsilon = A_{SM}/A_{x-s} = S_v \langle 1\rangle$$

Fig. 2.4 SUCCESSIVE MEMBRANE MODEL OF THE FOAM CELL STRUCTURE

Otherwise the membrane area will be larger than A_{x-s}.

Combined equations (2.58) and (2.59) yield,

$$R_{foam} = nt/(A_{SM}Pe_{c.w.}) \tag{2.60}$$

We can redefine the foam resistance to permeation in terms of the foam effective permeability,

$$R_{foam} = L/(A_{x-s}\ Pe_{eff}) \tag{2.61}$$

By equating (2.60) and (2.61) we get,

$$Pe_{eff} = (A_{SM}/A_{x-s})\ L/(nt)\ Pe_{c.w.} \tag{2.62}$$

or by using (2.57),

$$Pe_{eff} = (A_{SM}/A_{x-s})\ \langle l\rangle/t\ Pe_{c.w.} \tag{2.63}$$

We can deffine,

$$\varepsilon = A_{SM}/A_{x-s} \tag{2.64}$$

Then, the equation (2.61) can be rewritten as,

$$Pe_{eff} = \varepsilon\ \langle l\rangle/t\ Pe_{c.w.} \tag{2.65}$$

Equation (2.64) defines an important geometric parameter: the

ratio of the membrane area to the flow cross section. We will refer to parameter ε as the enhancement parameter. This parameter accounts for the fact that the cell walls are curved. The curved cell walls form non-plane membranes whose area is larger than the area of the membrane projected normally to the flow direction. According to equation (2.59) larger area of membranes results in less permeation resistance and the foam effective permeability coefficient increases.

To compute A_{SM}, let us consider a cubical volume V, Fig. 2.4. The total area of the cell walls is

$$A_T = V\ Sv \tag{2.66}$$

where Sv is the surface to volume ratio. Note that only one surface of a membrane is included for Sv, not both surfaces. Volume V is equal to A_{x-s} L. According to equation (2.57), the number of successive membranes inside the volume is,

$$n = L/\langle l \rangle \tag{2.67}$$

Therefore, the area of a single successive membrane is,

$$A_{SM} = A_T/n = A_{x-s}\ Sv\ \langle l \rangle \tag{2.68}$$

From the definition (2.64) we obtain,

$$\varepsilon = Sv\ \langle l \rangle \tag{2.69}$$

For a sphereical geometry of the cells,

$$Sv = Sv_{sphere}/2 = 3/d \tag{2.70}$$

where d is the average cell diameter. Sv ratio of a single sphere is divided by two because closely packed spheres share common cell walls. It shown, in Fig. 2.5 that for spherical geometry, if the location of the line segment cutting the sphere is random across the projected cross-section of the sphere,

$$\langle l \rangle = (2/3)\, d \tag{2.71}$$

or,

$$\langle l \rangle = 2/Sv \tag{2.72}$$

Consequently,

$$\varepsilon = 2 \, . \tag{2.73}$$

Note that $\varepsilon = 2$ can be obtained simply by dividing the area of one-half of a sphere with its projected area.

An alternative approach to compute ε assumes that cell walls forming successive membranes are randomly oriented planes. The ratio of area of randomly oriented planes and their projected area can be readily shown to be equal to 2.

Parameter ε is further analyzed in Chapter 3. It will be shown

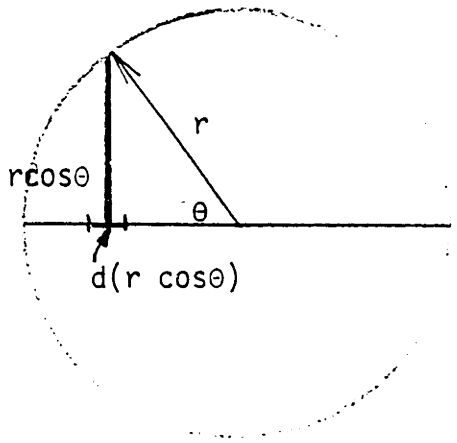

$$\frac{\langle l \rangle}{2} = 1/(2r) \int_0^{\pi} (r \sin\Theta) d(r \cos\Theta)$$

$$\langle l \rangle = (\pi/4) d_{circle}$$

a) Two-Dimensional Average Distance Between Cell Walls

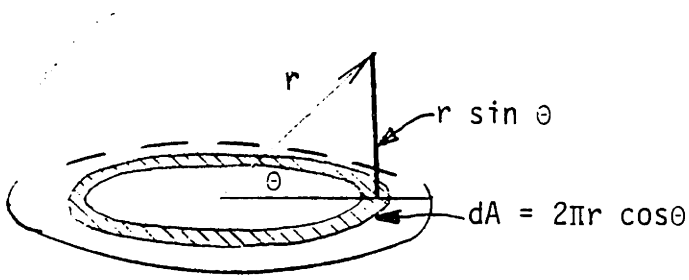

$$\frac{\langle l \rangle}{2} = 1/(r^2\pi) \int_{\pi/2}^{0} (r \sin\Theta)(2\pi r \cos\Theta)\, d(r \cos\Theta)$$

$$\langle l \rangle = (2/3)\, d_{sphere}$$

b) Three-Dimensional Average Distance Between Cell Walls

Fig. 2.5 RELATION BETWEEN $\langle l \rangle$ AND THE AVERAGE DIAMETER OF A CIRCLE AND A SPHERE

that the foam structure can be accurately modeled as closely packed elastic spheres.

The effective foam permeability coefficient can be now modified to account for the enhancement,

$$Pe_{eff} = 2 \langle 1 \rangle / t \; Pe_{c.w.} \tag{2.74}$$

The definition (2.48) can be rewritten in this form:

$$D_{eff} = Pe_{eff}/S_{eff} \cdot \tag{2.75}$$

By combining equations (2.72), (2.55) and (2.75) we finally obtain the model for the effective diffusion coefficient:

$$D_{eff} = 2 \langle 1 \rangle / t \; Pe_{c.w.} (T/T_{STP})/S_{eff,STP} \tag{2.76}$$

or by using the units given in (2.50),

$$D_{eff} = 2 \langle 1 \rangle / t \; Pe_{c.w.} (T/T_{STP}) \tag{2.77}$$

The units (2.50) are convivnient since $S_{eff,STP}$ is equal to $1[cm^3_{STP}/cm^3\text{-atm}]$ for all the gasses. Therefore, from equation (2.75), at standard temperature and pressure Deff and Pe have the same numerical value but different units.

Note that $Pe_{c.w.}$ is exponentialy temperature dependent, and follows an equation of Arrhenius type,

$$Pe_{c.w.} = Pe_0 \exp[-E/(RT)] \qquad (2.78)$$

where E is the activation energy of permeation, and Pe_0 is the exponential constant.

In Chapter 7, the results of the model will be compared with the measured foam diffusion coefficient.

3. ELECTRICAL ANALOGY OF THE MASS TRANSFER IN CLOSSED-CELL FOAMS

Given the measured value of the cell wall thickness and permeability, a prediction of the effective foam permeability requires treatment of the cell wall geometry. This includes the ratio of membrane area to flow cross sectional area developed in Section 2.5 and possible effects of the cell stagger. Since electrical quantities can be easily measured, an electrical analogy technique was developed to measure the geometry factors from cross-sectional photographs of actual foam.

3.1 The Electrical Analogy Technique

Cell walls are the only resistance to permeation and therefore they have to be represented by some finite resistance in the electrical circuit. The cells offer no resistance to permeation and therfore they were represented by zero resistance.

The resistance to permeation of a cell wall can be defined as:

$$R_{c.w.} = t/(Pe_{c.w.}A_{c.w.}) \qquad (3.1)$$

The actual two-dimensional geometry of the foam is found from cross-sectional photographs taken with the scaning electron

microscope. The geometry is duplicated from the SEM photographs to a printed cuircut (P.C.) board by means of a photo etching technique. A P.C. board consists of a copper layer deposited on a plastic board. The plastic board has very high electrical resistance, while the copper has effectively zero electrical resistance. When a negative photo-resist P.C. board is exposed to light and etched, the unexposed copper layer is removed leaving area of very high resistance while the exposed copper remains unetched leaving other area of very low resistance.

It was found convenient to use 100x magnification. The negatives obtained by the SEM were not used directly since cell walls were too thin at 100x magnification. Since the cell walls are approximately uniform in thickness, the foam cell structure was copied to a transparency by means of a drafting tape Fig. 3.1. The drafting tape gives uniform cell wall thickness with high black and white resolution. At 100x magnification the cells appear approximately 50 mm in diameter so that 1 or 2 mm thick drafting tape can be used. The strut geometry can be also copied to the transparency. On the bottom of the transparency, next to the cell structure, a line of drafting tape was applied, Fig. 3.1 . This straight line represents a single plane successive membrane.

After exposure to a special light source, developing, and etching, the cell structure is transfered to the P.C. board. The copper is removed from the unexposed parts below the cell walls, while the exposed copper remains on the plastic board covering the cell interior area geometry. To obtain the electrical analogy, we need to place material having a finite resistance (optimally in the kOhm

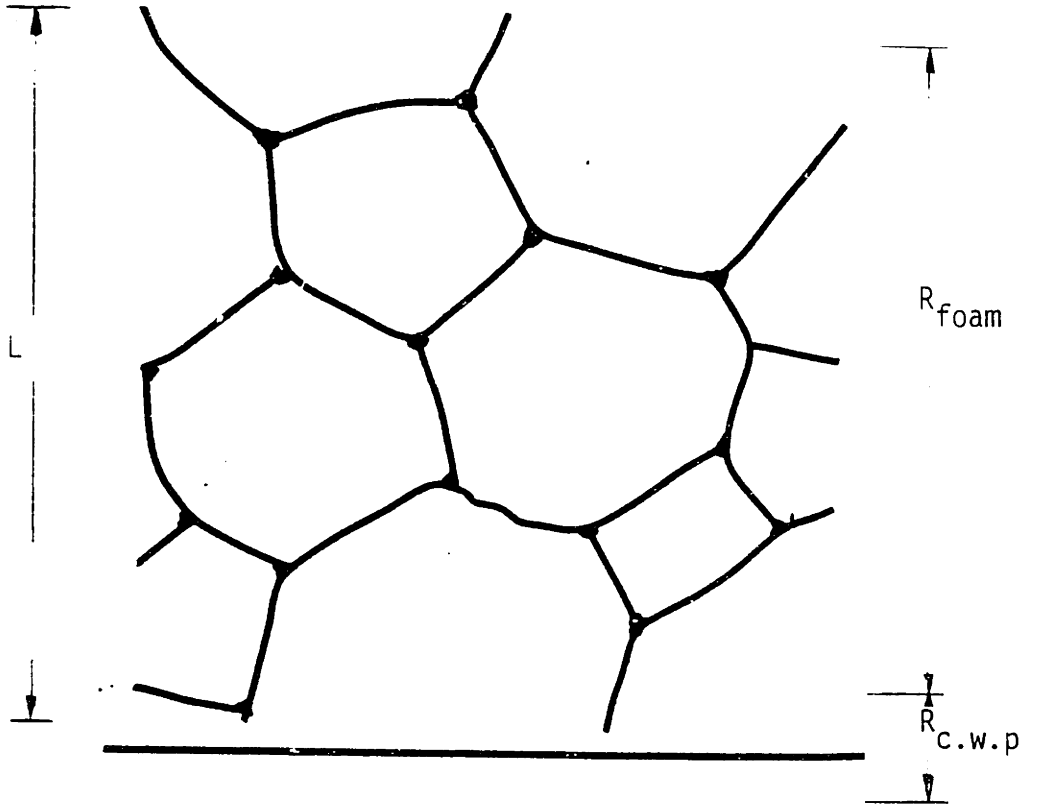

L [mm]

R_{foam} [Ohm]

$R_{c.w.p}$ [Ohm]

Fig. 3.1 STRUCTURE OF THE FOAM SAMPLE #1 COPIED TO A TRANSPARENCY BY MEANS OF 1 mm THICK DRAFTING TAPE

range) over the cell wall area. It is important also to apply an equal layer of the resistant material, in order to have an accurate representation of the cell wall resistance. Teledeltos paper* was used as an inexpensive and accurate cell wall resistor. The whole P.C. board was covered with a sheet of Teledeltos paper. Since there is some contact resistance between copper and the paper, the paper has to be pressed to the P.C. board by with a uniform pressure.

The board was placed into a rigid steel cylinder as shown on Fig. 3.2, and covered with the Teledeltos paper. A rubber bladder was placed into the cylinder, above the Teledeltos paper. The cylinder was closed and uniform pressure was obtained by pressurizing the bladder. Since current can flow freely through the copper in the cell interior, the only resistance is acrros the cell walls made of Teledeltos paper.

The resistance of the electrical network was measured by an accurate digital multimeter. The measured resistance can not be used directly in the foam model since the resistance of the Teledeltos paper and the thickness of the drafting tape were chosen arbitrarily. Instead, the measured resistance was compared to the resistance of the single plane membrane.

---

* Teledeltos paper is a product of General Electric Company, Schenectady, N.Y., and was used in an Analog Field Plotter, [20].

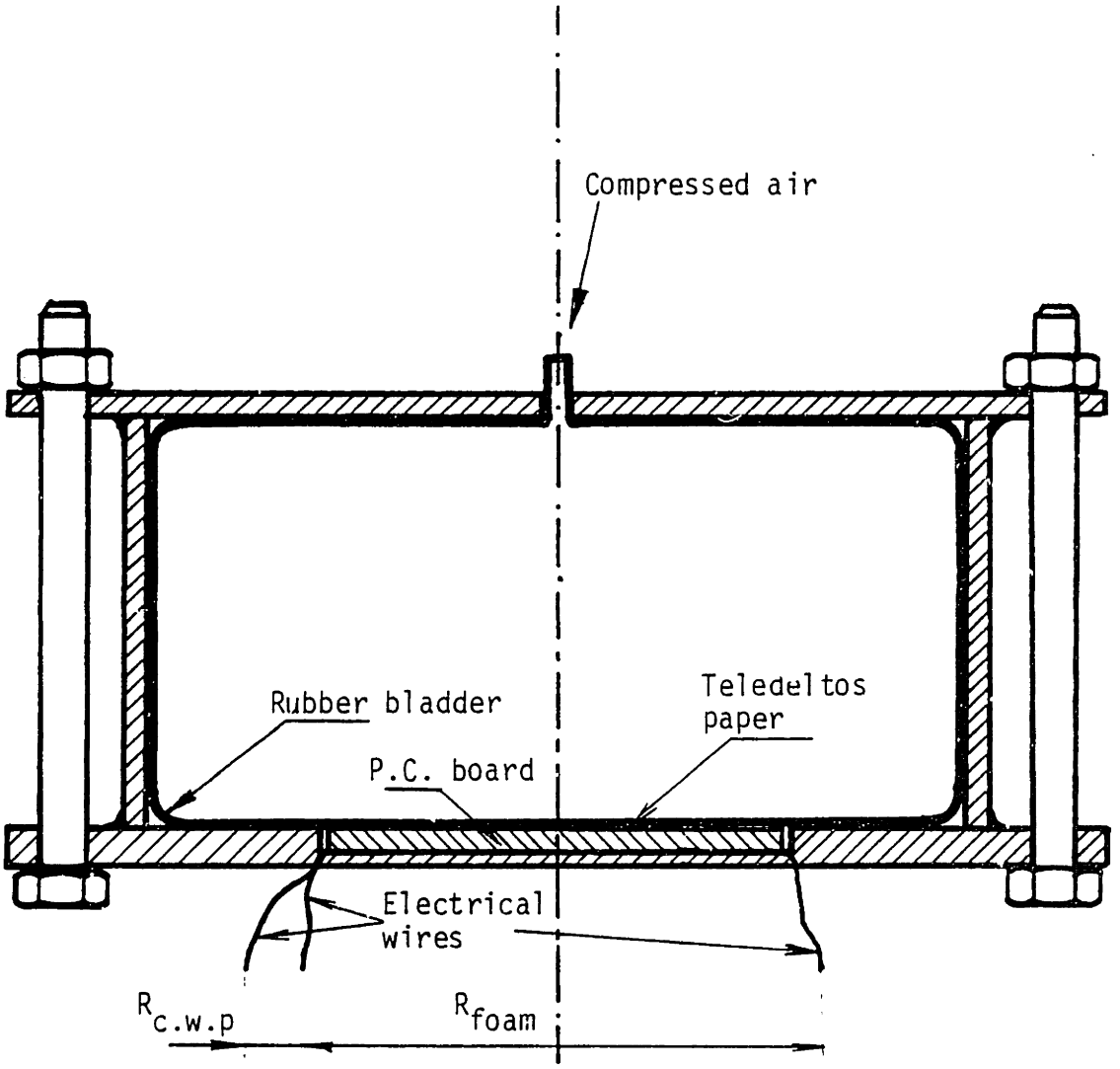

Fig. 3.2 AN APPARATUS USED TO MEASURE THE ELECTRICAL RESISTANCE OF P.C. BOARDS

At the low contact pressure, the resistance decreased as the pressure increased, although the ratio of the resistances between the foam geometry and the single cell wall remained constant within several percent. At higher pressure the ratio between foam resistance, R_{foam}, and resistance of the plane cell wall, $R_{c.w.p}$, was constant within 1% or better.

3.2 The Electrical Model of Permeability and Diffusion Coefficient

By analogy the ratio between the resistance of the foam structure and the resistance of the single membrane has to be the same both for transport of the electrical charge in the electrical netwark and for the transport of gas molecules in the real foam, i.e.,

$$(R_{foam}/R_{c.w.p})_{el} = (R_{foam}/R_{c.w.p})_{mass} \tag{3.2}$$

where $R_{c.w.p}$ is the resistance of a single plane cell wall (successive membrane). For a plane membrane, equation (2.58) yields,

$$R_{c.w.p} = t/(A_{x-s}Pe_{c.w.}) \tag{3.3}$$

The foam effective permeability coefficient can be obtained by substituting (2.61) and (3.3) into (3.2)

$$Pe_{eff} = (L/t)/(R_{foam}/R_{c.w.p})_{el}\ Pe_{c.w.} \tag{3.4}$$

where L is the length of the structure on the P.C. board measured in the direction of permeation.

By dividing the equation (3.4) with the foam effective solubility, equation (2.55), we obtain the electrical two-dimensional model of the foam effective diffusion coefficient,

$$D_{eff} = (L/t)/(R_{foam}/R_{c.w.p})_{el}\ Pe_{c.w.}(T_{STP}/T)/S_{eff,STP} \qquad (3.5)$$

The equation (3.5) was used to obtain the value of the foam effective diffusion coefficient. The structure of foam sample #1 was photographed and, using SEM, and then transfered to a P.C.board #1. The obtained data are given in Table 3.

The values of the permeability coefficient of the cell walls, $Pe_{c.w.}$ and the membrane thickness, t, for the foam sample #1 are given in the Table 4 and Table 8 respectively.

It is important to note that the effective permeability and effective diffusion coefficient measured by the electrical analogy include only two-dimensional enhancement effects (i.e., two-dimensional nonplanar membrane effect and staggering effect). It is was shown in the Chapter 2. that the enhancement parameter is equal to 2 in three-dimensions.

3.3 Measurement of the Two-Dimensional Enhancement Parameter

By substituting equations (2.60) and (3.3) into (3.2) we can write,

$$(R_{foam}/R_{c.w.p})_{el} = n(A_{x-s}/A_{SM}) = n/\varepsilon \qquad (3.6)$$

where n is the number of membranes in length L. By using equation (2.57) we obtain,

$$\varepsilon \langle l \rangle = L/(R_{foam}/R_{c.w.p})_{el} \qquad (3.7)$$

where again, L is the length of the structure at the P.C. board measured in the direction of permeation.

We can measure $\langle l \rangle$ or n by the geometric measurement described in the Section 2.6. The image of the foam structure on the P.C. board can be used directly instead of the two-dimensional SEM photographs. From the equation (3.7) the enhacement parameter is equal to,

$$\varepsilon = L/[\langle l \rangle (R_{foam}/R_{c.w.})_{el}] \qquad (3.8)$$

The data obtained by electrical and geometrical measurements on the P.C. board #1, are given in the Table 3.

The assumption that the foam cell structure can be modeled as closely packed spheres is equivalent to the assumption of closely packed circles in two-dimensions. Therefore ε can be obtained by dividing the one-half length of the circle, $r\pi$, by its projected area, circle diameter, 2 r. We obtain $\varepsilon = \pi/2 = 1.57$.

The same result can be obtained by assuming that cell walls are randomly oriented line segments. Then, ε is defined as the ratio of the length of a randomly oriented line segment and the projected line segment. The integration over all angles θ, which are equally

TABLE 3

RESULTS OBTAINED FROM THE ELECTRICAL RESISTANCE MEASUREMENT OF THE ELECTRICAL ANALOGY OF FOAM CELL STRUCTURE

	$[R_{foam}/R_{c.w.p}]_{el}$	L	$\langle l \rangle$	$\varepsilon\langle l \rangle$	ε	D_{eff,CO_2}
PC Board #1	2.160	.9	.274	.417	1.52	11.63
PC Board #2	3.384	1.07	.274	.3160	1.154	8.91
PC Board #3	2.960	1.247	.2373	.4216	1.776	11.99

PC Board #1 - Actual Foam Structure

PC Board #2 - Hexagonals stagered normally to concentration grad.

PC Board #3 - Hexagonals stagered paralelly to concentration grad.

$[R_{foam}/R_{c.w.p}]$- Measurement of the electrical resistance

L[mm] - Length of the foam structure on the P.C. board

$\langle l \rangle$ [mm] - Geometrical analysis (equ. (3.12 and (3.13))

$\varepsilon\langle l \rangle$ [mm] - Electrical measurement (equ. (3.7))

ε - Electrical and geometrical measurement (equ. (3.8))

$D_{eff}[cm^2/s]x10^{-7}$ Electrical measurement, $Pe_{c.w.}$ from Table 4, $t_{c.w.}$ from Table 8 and equation (3.5).

possible, yields:

$$\varepsilon = b/(b\langle\cos\Theta\rangle) = 1/\left(2/\Pi\int_0^{\Pi/2}\cos\Theta\, d\Theta\right) = \Pi/2. \qquad (3.9)$$

Note that the modeled value of the two-dimensional enhancement parameter $\varepsilon = \Pi/2 = 1.57$ is in excellent agreement with the measured value $\varepsilon = 1.52$.

3.4 Measurement of the Effect of the Direction of Staggerness on the Foam Effective Permeability and Diffusion Coefficient

The successive membrane model assumes that cells of the actual foam structure are staggered only in the direction normal to the concentration gradient. To check the effect of the direction of staggerness on the foam permeability coefficient (in two-dimensions), two electrical models (P.C. boards) were made, Fig. 3.3. The cell structure in both cases was closely packed hexagonals. This cell structure was selected because hexagonals, when closely packed, are staggered only in one direction. In addition, the average distance between successive membranes, $\langle l\rangle$, can be computed readily without a measurement.

To compute the size of the hexagonals, two-dimensional circular cross-section of the foam structure was assumed. It is shown in Fig. 2.5 that for a circle,

$$d_{circle} = 4/\Pi\langle l\rangle \qquad (3.10)$$

P.C. BOARD #2

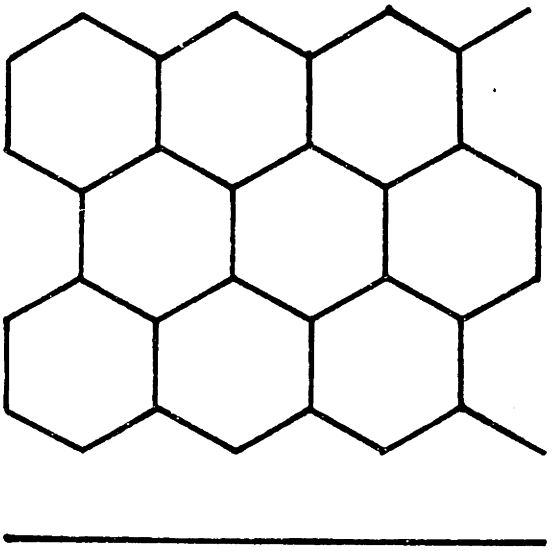

$\langle l \rangle = a + 2\,(a \cos 60)$

$\varepsilon = (2a)/(2a \cos 30) = 1.1555$

P.C. BOARD #3

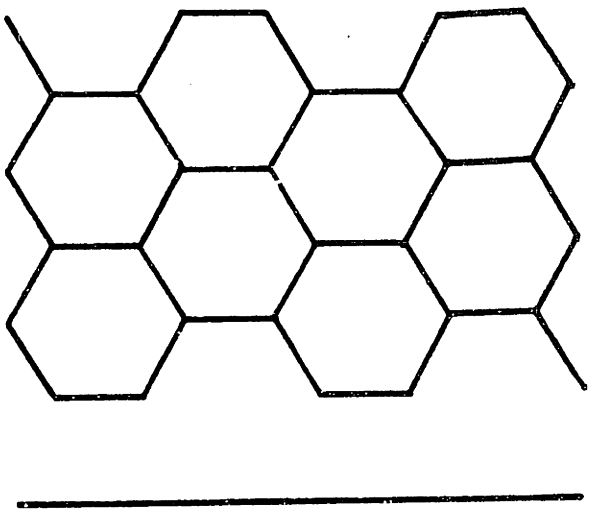

$\langle l \rangle = 1.5\ a \cos 30$

Fig. 3.3 GEOMETRY OF THE P.C. BOARDS #2 AND #3

Foam sample #1 was measured to have an average distance between the cell walls equal to .274 mm (Table 8.). Therefore, according to equation (3.10), the average circle diameter, d_{circle}, is equal to .3489 mm.

The length of the side of the hexagonals, a, was selected so that the perimeter of the hexagon, 6a, is equal to d_{circle}, where d_{circle} is the average circle diameter,

$$a = \Pi d_{circle}/6 = .1827mm \tag{3.11}$$

On the P.C. board #2, the hexagonals were staggered normally to the concentration gradien· It can be readily shown, that for this cell geometry, the average distance between the cell walls <l> is equal to:

$$<l> = a\ (1 + \cos 60) = .2740 \tag{3.12}$$

The data obtained by electrical and geometrical measurement on the P.C. board #2, are given in the Table 3.

Note that $\varepsilon = A_{SM}/A_{x-s}$ by definition. For the cell arrangement on the P.C. board #2, $\varepsilon = 1/\cos 30 = 1.155$ exactly. This is within .2% of the measured value given in Table 3. Therefore the electrical model is very accurate.

On the P.C. board #3, the cells were staggered in the direction parallel to the concentration gradient. For this geometry,

$$<l> = 1.5\ a \cos 30 = 1.2990\ a = .2373\ mm \tag{3.13}$$

The data obtained by electrical and geometrical measurement on the P.C. board #3, are given in the Table 3.

Note that hexagonals have different values of <l> depending on the direction of the measurement. The size of the hexagonals was selected by equating the perimeters of the hexagonals and the cells (i.e. tha area of permeation). To have equal <l>, we would have to have different sizes of hexagonals on P.C. boards #2 and #3.

The effective diffusion coefficients measured for P.C. boards #1, #2 and #3 are related as,

$$D_{eff,PC\#1} = 1.3\ D_{eff,PC\#2} = .970\ D_{eff,PC\#3} \tag{3.14}$$

Therefore, the hexagonal cell structure staggered in the direction normal to the concentration gradient has a diffusion coefficient 23% lower than the actual foam structure. The hexagonal cell structure staggered in the direction parallel to the direction of the concentration gradient has a diffusion coefficient 3% higher than the actual foam structure. Note that the enhancement parameter measured by the electrical analogy accounts for both for the nonplanar successive membranes and the cell staggerness effect. The analytical model is based on the assumption that the cells are staggered normally to the concentration gradient and the permeation is enhanced only by the nonplane successive membranes.

The actual foam structure is likely to be staggered in both directions. We can assume that an equal number of cells is staggered in both directions. Then by averaging we obtain,

$\varepsilon = 1.466$ (3.6% less than for P.C. board #1)

$\varepsilon \langle l \rangle = .255$ mm (6.7% less than for P.C. board #1)

$D_{eff} = 10.45 \times 10^{-7}$ cm^2/s (10.2% less than for P.C. board #1)

which is close to the measured values of the real foam structure, i.e., P.C. board #1.

3.5 The Corrected Electrical Model of Permeability and Diffusion Coefficient

The enhancement parameter was computed to be equal to 2 in three-dimensions and $\pi/2$ in two-dimensions according to the analytical model. We can appropriately correct the two-dimensional electrical model of the foam effective permeability and diffusion coefficient to account for the three-dimensional enhancement, by multipluing the equatios (3.5) and (3.6) by $\varepsilon_{3-D}/\varepsilon_{2-D} = 2/(\pi/2) = 4/\pi$

$$Pe_{eff} = 4/\pi\,(L/t)/(R_{foam}/R_{c.w.p})_{el}\; Pe_{c.w.} \tag{3.15}$$

$$D_{eff} = 4/\pi\,(L/t)/(R_{foam}/R_{c.w.p})_{el}\; Pe_{c.w.}\,(T_{STP}/T)/S_{eff,STP} \tag{3.16}$$

4. EXPERIMENTAL MEASUREMENT OF THE CELL WALL PERMEABILITY

The permeability of the membrane can be related to the measured flow as given by equation (2.44). To obtain cell walls for permeability measurements, samples were taken from large bubble-cells which are often created on the surface of free-rise foam. These bubbles have the same composition as the cell walls and a thickness which is the same order of magnitude (1 micron) as the walls of the normal size cell. They also have aproximately the same thermal history as other cell walls, a factor that could have had an important influence on the polymer permeability.

To measure the permeability of the membranes, a volumetric type apparatus was designed and built (Fig. 4.1). Since the membranes are very thin and fragile they are exposed to a concentration difference rather than a substantial pressure difference. One side of the membrane is exposed to the test gas at atmospheric pressure while the other side is exposed to fluorocarbon gas at atmospheric pressure. Fluorocarbon permeates much slower than any air component, so that its permeation can be neglected during tests of other gases. The test membrane is small, about 7mm in diameter, resulting in a very low volumetric flow of air through the membrane. Due to the low flow, any outgassing from other materials in the apparatus or temperature variation could seriously disturb the measurement. For that reason the whole cell was made from materials used in high vacuum applications. The membranes were fixed to a stainless steel mounting

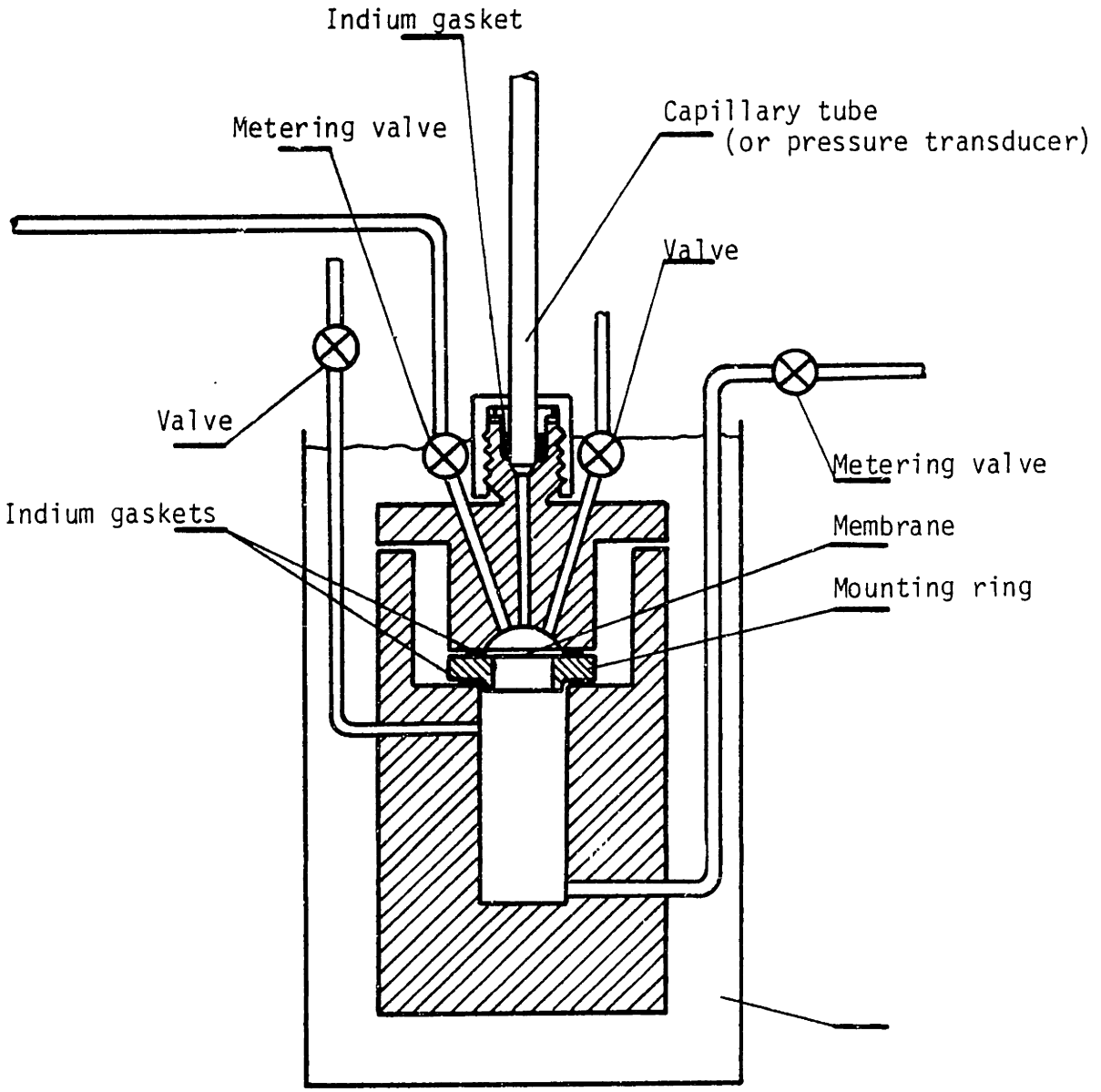

Fig. 4.1 APPARATUS FOR CELL WALL PERMEABILITY MEASUREMENT

ring by Sealstix cement. Seastix cement has a melting point at 140°C, vapor pressure 10^{-3}mmHg and is applied by a soldering iron. The cell was sealed by gaskets made out of indium. A high precision capillary tube having a 0.5 $\pm$ 0.005 mm diameter was also sealed by indium to the cell to measure the volume of the permeated gas. The volume was measured by recording the change of the position of a Methyl Isobutyl Ketone slug placed in the tube. The cell was placed in an ethyl alcohol constant temperature bath which was kept within $\pm$ 0.03°C. The temperature of the test gas and the freon was measured continuously. The room temperature was also maintained within $\pm$ 0.5°C since it was noticed that a temperature change of the valves partially outside the alcohol also disturbed the measurement.

To reduce the contamination of the surfaces in contact with gasses, the parts of the permeability cell were:

- rinsed with
  - trichloroethylene (C_2HCl_3)
  - acetone (CH_3COCH_3)
  - ethyl alchohol
- cleaned ultrasonicaly
- dried in an oven at about 100°C

The membrane samples were kept in vacuum when data were not taken.

While data were taken several drawbacks of the use of the capillary tube were noticed:

- Isobutyl Methyl Ketone has a 2000 Pa (15mmHg) vapor pressure at room temperature. The slug and the thin liquid film left behind the slug in the capillary tube evaporates creating

additional volumetric flow rate. This additional slug velocity was measured to be .1243 mm/min. Other liquids were tested. The ones with low vapor pressure were more viscous. Formamide was found to have somewhat better behavior than Isobutyl Methyl Ketone.

- The barometric pressure change (up to $\pm$ 2500 Pa or, 2.5% of the absolute pressure) disturbs the slug velocity in 12 hr long tests with nitrogen.

The capillary tube was replaced with an absolute pressure transducer (Validine AP10 with pressure range 140,000 Pa) so that change of pressure, rather than change of volume, was measured. AP 10 pressure transducer features all-welded costuction and very low internal volume (65 mm^3). The volumetric displacement is also very low which is esential because of the constant volume assumption. For full scale the vlolumetric displacement is les then 5 mm^3. During the measurement only about 100 Pa or .07% of the full scale pressure change is allowed. Therefore during the measurement the volume change due to diaphragm movement is only 3.6×10^{-3} mm^3.

To enshure the constant volume the mounting ring was somewhat changed to give better support to the membrane (Fig. 4.2). To take data, the pressure in the upper plenum containing the test gas is increased about 400 Pa (3mm Hg) above the atmospheric pressure pushing the membrane towards the mounting ring in a stable position. Therefore only 3 mmHg of total pressure differential was applied to the membrane. As the test gas permeates through the membrane into fluorocarbon, the pressure in the upper plenum decreases. Since the membrane is very thin, the steady state flow through the membrane is

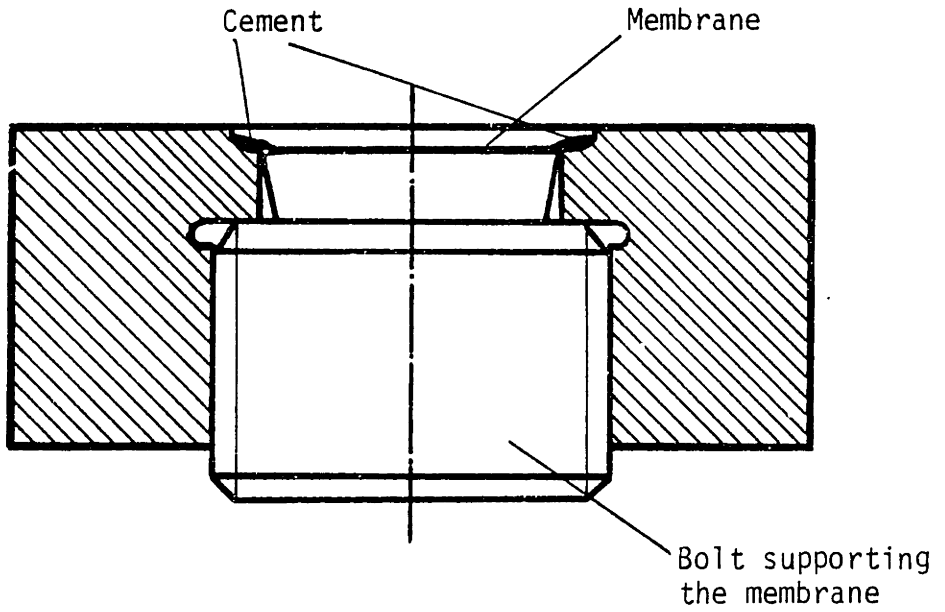

Fig. 4.2 MEMBRANE MOUNTING RING

established in one to several minutes. Because of the short transient time we were not able to separately measure the diffusion coefficient or the solubility coefficient. We could only measure their product which is permeability. The total pressure change needed to take data is 133 Pa (1mm Hg) or less.

The Fig. 4.3 shows the pressure decrease in the upper plenum for CO_2, O_2, and N_2 as function of time.

To calibrate the pressure transducer, both capillary tube and pressure transducer are mounted to the low pressure plenum of the cell. A slug is next placed into the capillary tube while it is positioned vertically. The slug moves under the gravity force causing volumetric inflow into the completely sealed low pressure plenum. This volumetric inflow is easy to measure from the slug displacement. At the same time the change of voltage of the transducer is recorded. The evaporation of the liquid slug is negligablle because of the rapidity of the calibration test. The needed calibration constant is thr volumetric change per unit of voltage change.

Special care has to be devoted to membrane selection. Membranes having pores or microbubbles could not be used. Defects are much more likely to occur in the walls of these comparatively large membranes than in much smaller membranes forming the cell walls.

The membrane thickness was measured on a scanning electron microscope at 2,000x to 10,000x magnification, Fig 4.4. The measured membrane thickness at different membrane locations varies tupicaly +-30% form some average value. Note that the inverse value of the membrane thickness has to be averaged, i.e. $\langle 1/t \rangle$, not the thickness, $\langle t \rangle$.

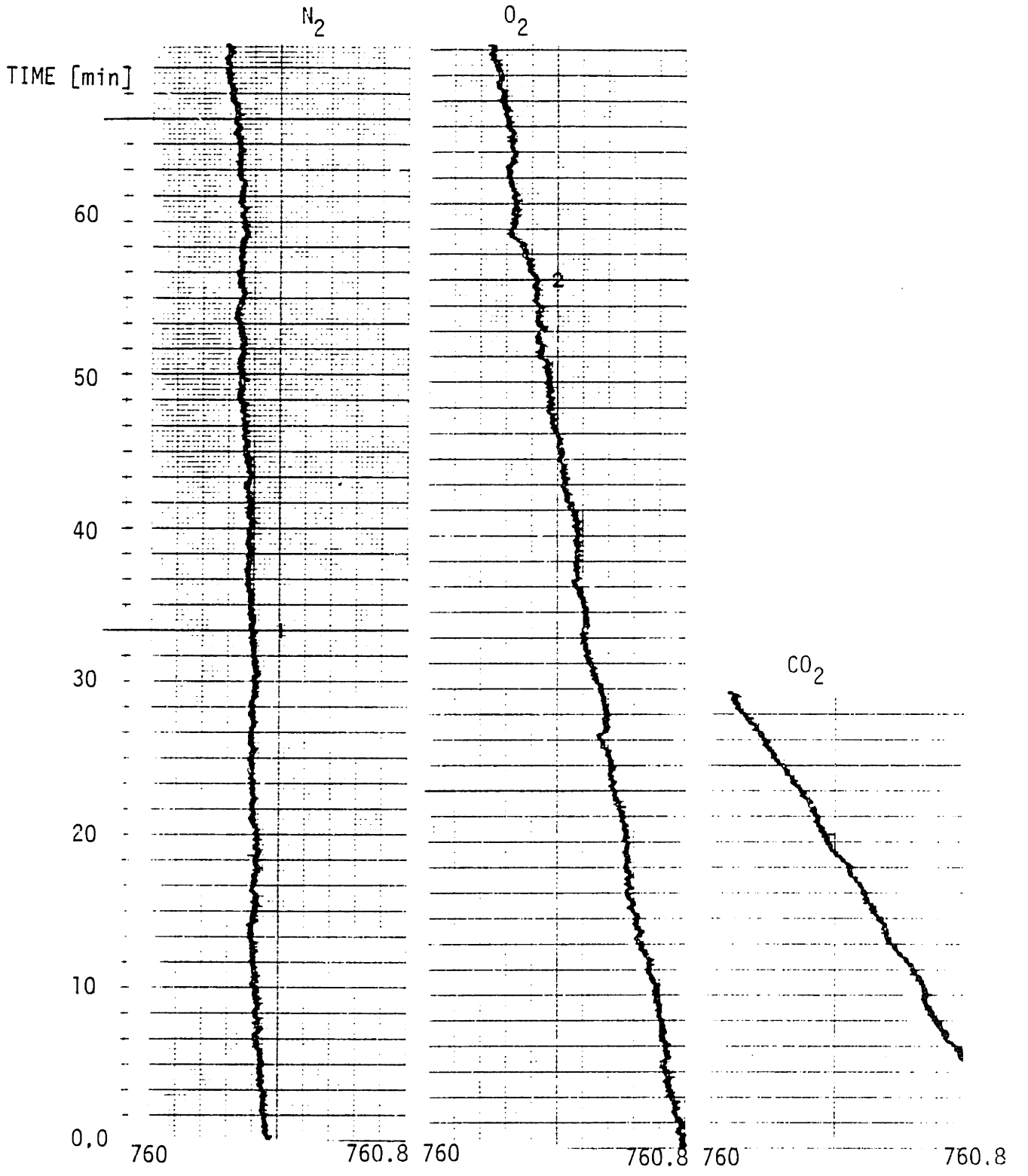

Fig. 4.3 PRESSURE DECREASE IN THE UPPER PLENUM DUE TO PERMEATION OF N_2, O_2 AND CO_2 THROUGH A CELL WALL MEMBRANE (Membrane #3, T=25 ^{o}C)

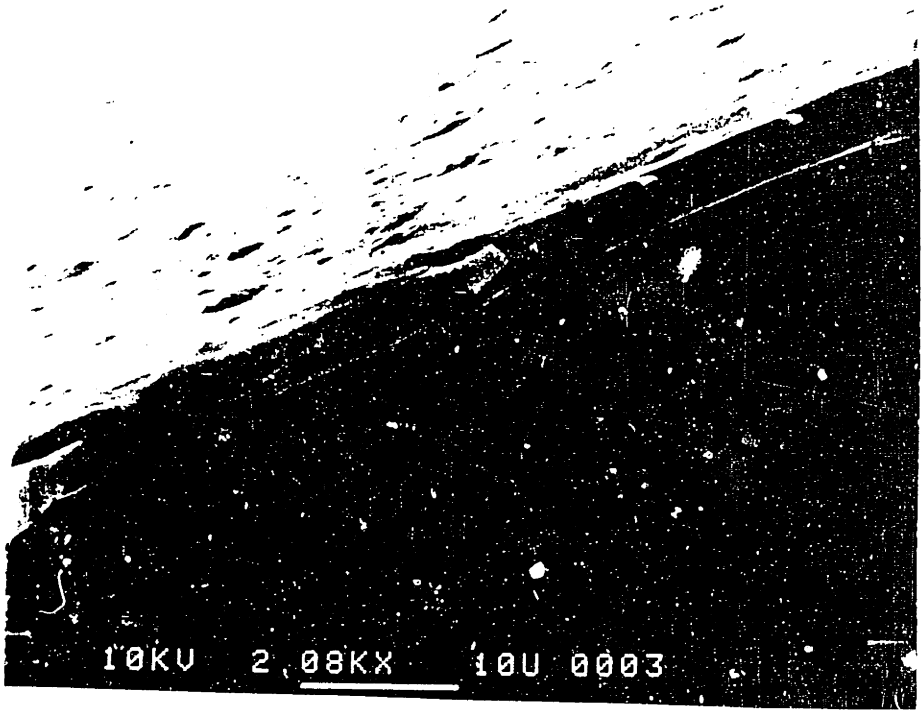

Fig. 4.4 LARGE BUBBLE-CELL MEMBRANE
(Membrane #3, $t = 3.84 \times 10^{-3}$ mm, magnification 2080 x)

All tested membranes had a thickness of 2.8×10^{-3} mm to 5×10^{-3} mm. The cross-sectional area of the membrane taking part in the permeation process was measured from enlarged photographs of the membrane mounted in the ring. Once the membrane thickness and the area are known, the permeability coefficient can be computed from the volumetric flow or pressure increase in the upper plenum, the concentration difference, and the membrane geometry.

About twenty methane diisocyanate (MDI) and tolylene diisocyanate (TDI) membranes were tested. Only three MDI membranes did not have defects such as microbubbles or pores. Microbubbles were easy to detect under a microscope. The walls of the microbubbles are much thinner than the membrane, so that artificially high permiation rate was measured in membranes having microbubbles.

Membranes having large pores compared to the mean free path of air molecules were easy to detect. Under pressure difference created by the weight af the slug in the capillary tube, bulk flow much higher than the expected permiation rate was always observed. If the diameter af the pores is smaller than the mean free paths of the air molecules, the so-called Knudsen diffusion occurs [18]. Molecules of N_2, O_2 and CO_2 have approximately same thermal velocity and diffuse with approximately the same rate through the pores. For that reason the measured permeability coefficients of N_2, O_2 and CO_2 do not have the ratio found for sound films,

$$Pe_{CO2}/Pe_{O2} = 4 \tag{4.1}$$

$$Pe_{O2}/Pe_{N2} = 6 \tag{4.2}$$

The obtained data are given in the Table 4 of the Chapter 9.

5. EXPERIMENTAL MEASUREMENT OF THE FOAM PERMEABILITY AND DIFFUSION COEFFICIENTS

5.1 Motivation for the Use of the Steady State Transmission Method

When two out of the three transport properties, the solubility, the permeability and the diffusion coefficient are known the third transport property can be computed from the definition (2.48). It has been shown in Section 2.5 that a foam effective solubility coefficient (i.e., the capacity to store gasses per unit of foam volume and unit of pressure) can be computed by making use of the ideal gas law. Consequently, one needs to measure only one more transport property: the foam permeability coefficient or the foam diffusion coefficient.

Measurements of mass transport properties are carried out by two basic methods [21]: transmission methods and sorption-desorption methods. In the sorption-desorption methods the solubility coefficient is usually obtained from the equilibrium sorption value. For example, the change of weight of the sample is often measured. The transient sorption or desorption rate gives the diffusion coefficient.

In the transmission methods a partial pressure gradient is applied across the sample. The gradient can be applied with or without a total pressure difference across the sample. The permeation rate can be measured by different methods, such as a volumetric measurement, a pressure measurement, gas chromatography, mass spectroscopy or others

[21]. From the transient permeation rate the diffusion coefficient can be computed.

Transient measurements are faster then steady state measurements, which is an advantage since gas diffusion is a very slow process. Generally, transient methods are considered to be less accurate. They have several disadvantages when applied to closed-cell foams:

- Only a relatively thin surface layer of foam takes part in the transient proces. It is unclear how well the continuum assumption can be applied to one or two cell layers.
- The surface of a foam sample is usually damaged by cutting and has many open cells. The open cells change the solid-to-gas ratio inside of the surface layer and increases the sorption/desorption area. This area is difficult to determine.
- It is difficult to change the boundary conditions in a short time. When the capillary tube is used to measure the permeation rate the slug motion is not continuous. The capillary tube is difficult to flush.
- The pressure transducer and its connecting tubes have some non-zero volume (.1 to 1 cm^3). Therefore, point or line source methods cannot be used.
- It is much more dificult to mantain thermal equilibrium during a transient measurement then during a steady-state measurement.

Accurate, reference data are needed to test the models of the foam effective diffusion coefficient. The large spread of the reported foam data obtained by transient or indirect measurement (Table 1) implies that closed-cell foams require much more accurate measuring

methods. The measurement of steady state permeation rates was selected as the most accurate method for foam effective coefficient measurement.

5.2 Description of the Apparatus for Measurement of the Foam Effective Permeability Coefficient

A volumetric type apparatus, similar to those widely used for film tests, was first considered. Several disadvantages of of this test for the closed-cell foams compared to films were noticed. To measure the effective permeability of the foam, the foam sample has to be at least 20 cell diameters (10 mm) thick to eliminate surface effects. Besides that closed-cell foams can not withstand pressure higher then approximately 5 to 10 atm. If the foam sample is kept under high pressure for long periods of time, or if it is kept at elevated temperature, foam starts to creep and is compressed. The pressure inside the compressed cells increases so that gasses inside the cells diffuse out. Therefore during long steady-state measurement the foam should be exposed to a much lower pressure - not more than 1 atm.

The thick sample and low pressure differential result in a permeation rate which is lower by several orders of magnitude than that for films. The low permeation rate substantially complicates the measurement: any evaporation or outgassing becomes important and acts as a volumetric source. Every surface in contact with gas acts as a semi-infinite medium absorbing or releasing gases under concentration

gradients. To avoid this, only materials having low vapor pressures and diffusion coefficients much lower than the foam D_{eff} can be used in the apparatus. The cleanliness of the apparatus is also essential.

Measurements should not be made until steady state conditions are acheived within the foam sample. This requires not only a linear concentration gradient of the test gas but also elimination of other gas components from the sample whose diffusion can lead to erroneous test results. Thus when CO_2, which rapidly reaches steady state, is tested, data cannot be taken until N_2 is exhausted from the sample; a process which takes about ten times longer than CO_2. Since freon has such a low diffusion rate, it will not contribute significant errors to the test of other gases. Until steady-state concentration profile of the tested gas is acheived and all other air components are exhausted from the sample, the sample must be constantly flushed by a gas on both sides while a pressure difference, typically 5.5×10^4 Pa (8 psi), is maintained across the sample.

The whole apparatus shown in Fig. 5.1., was made out of materials used in high vacuum applications. The foam sample 75 mm in diameter, usually 10mm thick, was fixed to a stainless steel mounting ring by DER 331 epoxy (Allied Resin Corporation), which has very low vapor pressure. The mounting ring was sealed to the permeability cell with indium gaskets. The permeability cell was made out of solid stainless steel rods to minimize welding. The connecting tubes were welded to the cell from the gas side, to eliminate the surfacs which can trapp gasses and ease the cell cleaning. The parts of the cell in contact with the gasses were cleaned by using the cleaning procedure described in the Chapter 4.

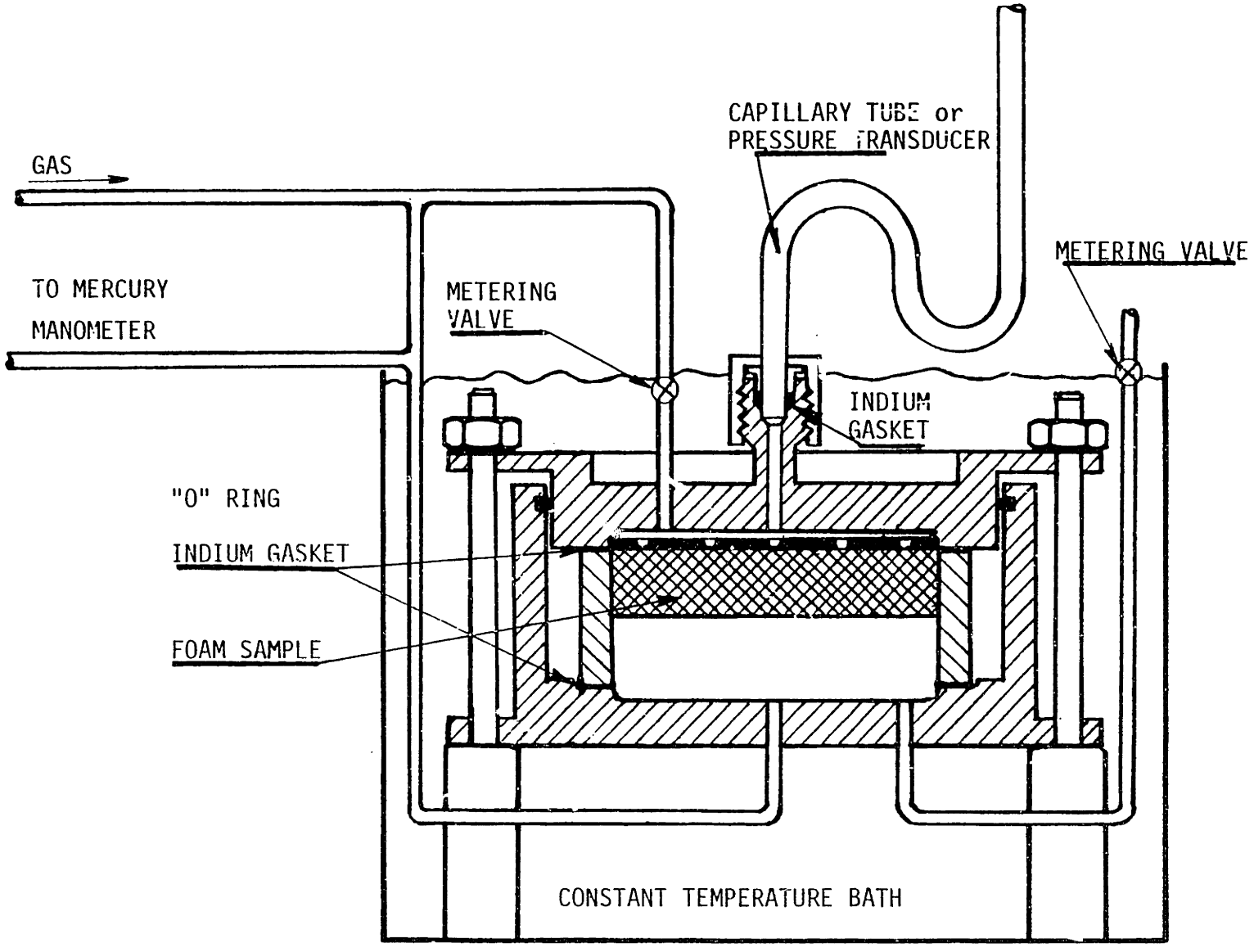

Fig. 5.1 APPARATUS FOR FOAM EFFECTIVE PERMEABILITY COEFFICIENT MEASUREMENT

To ensure thermal equilibrium the cell was submerged in a constant temperature water bath.The temperature of the water bath was controlled to within $\pm$ 0.03°C while the temperature in the room was controlled within $\pm$ 0.1°C.

The gas volume on the low pressure side was minimized to reduce the influence of temperature and pressure variations. Through the capillary tube the foam sample is exposed to barometric pressure variations. Two modes of experimental error due to barometric pressure variations were noticed (Fig.5.2). As the pressure, changes the slug in the capillary tube moves so that the pressure in the upper plenuum remains equal to the room pressure. In Fig.5.3 a typical barometric pressure variation in Cambridge is also shown. The pressure oscillations have an amplitude up to 0.03 atm and a wavelength of 1 to several days. A change of pressure up to several mmHg/hr is quite frequent. In the .5 mm diameter capillary tube the slug moves 2.45 cm per mmHg of barometric pressure change. If there is no permeation through the foam sample, the change of the barometric pressure can move the slug more than 10 cm/hr. At room temperature, the volumetric inflow of N_2 due to permeation through a typical 10 cm thick sample moves the slug only 3 cm/hr. On several occasions when the barometric pressure was increasing faster then 1 mmHg/hr, a reverse slug flow was observed.

Although the error resulting from the barometric pressure change is very high, it has not been reported previously. It is interesting to note that the reported temperature control is usually .1% or better. The room pressure is not controlled although for an ideal gas temperature and pressure variations cause equal experimental error

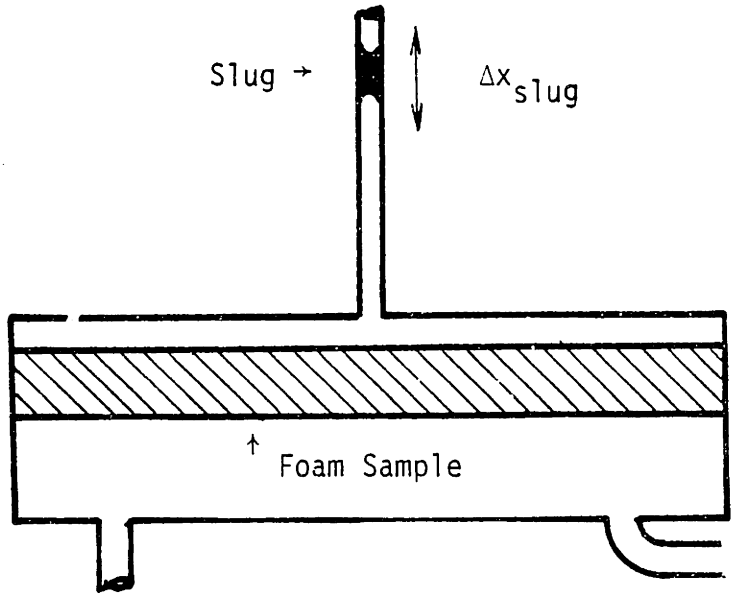

a) Slug movement due to barometric pressure change

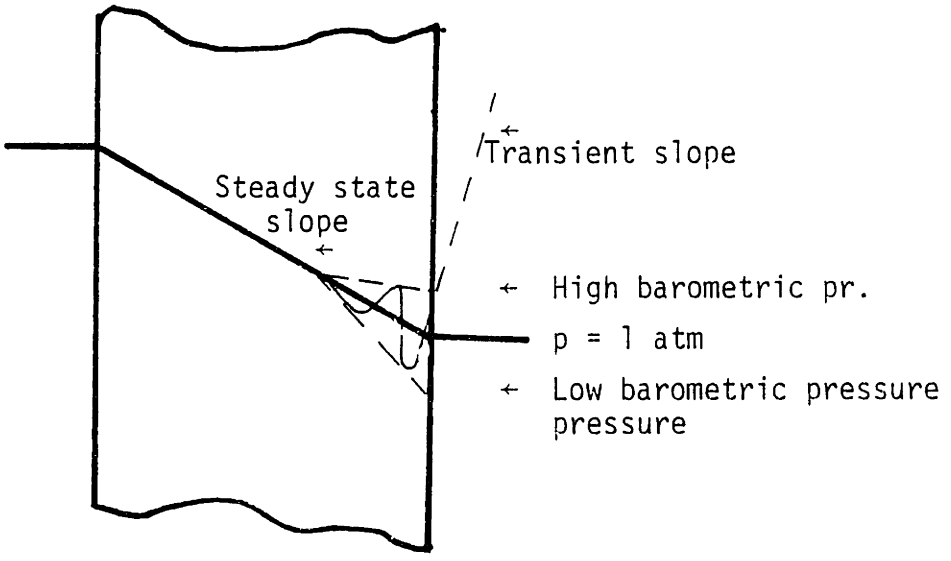

b) Transient slope of the partial pressure gradient due to barometric pressure oscilations

Fig. 5.2 MODES OF EXPERIMENTAL ERROR DUE TO BAROMETRIC PRESSURE VARIATIONS

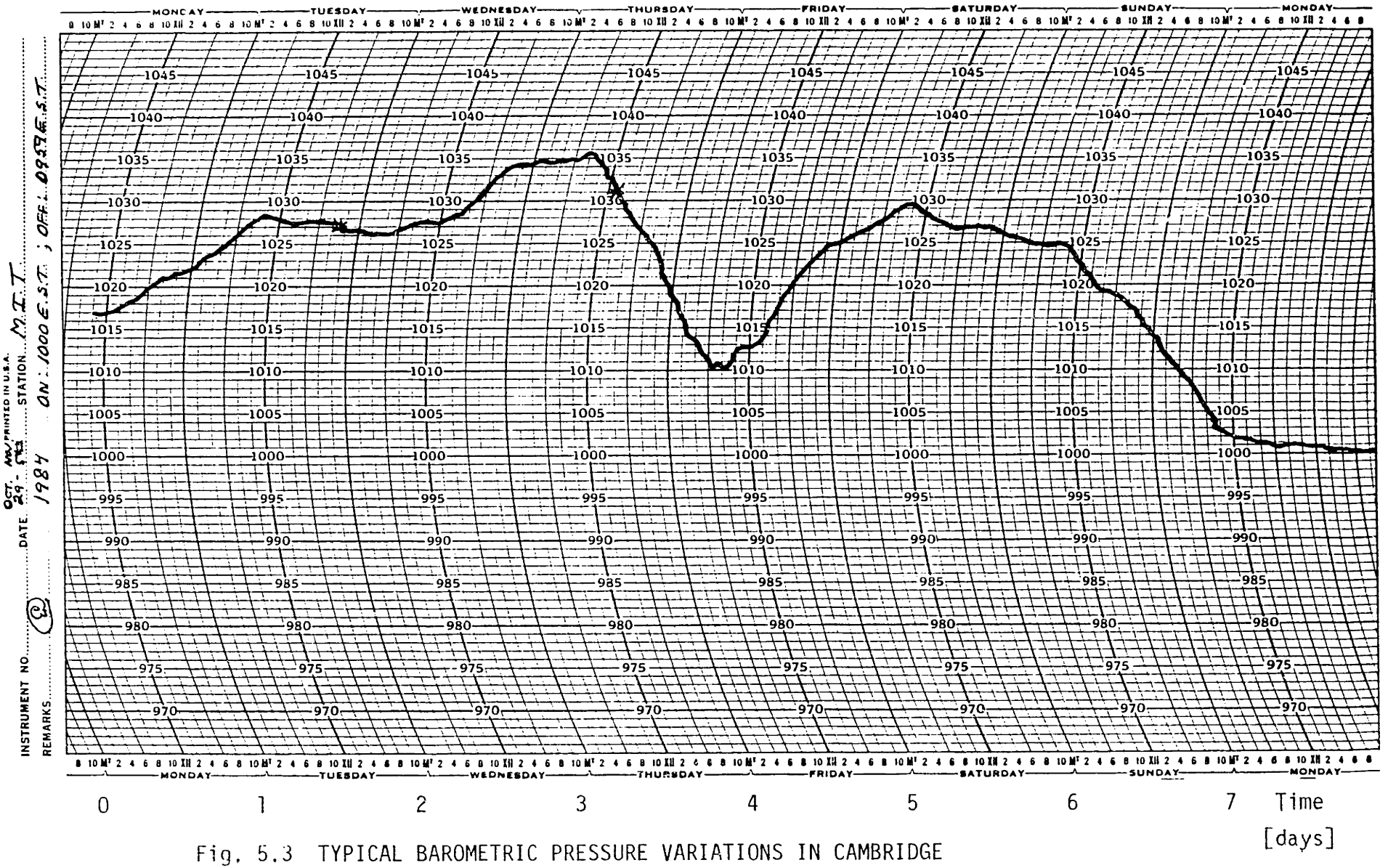

Fig. 5.3 TYPICAL BAROMETRIC PRESSURE VARIATIONS IN CAMBRIDGE

(i.e., same change of volume).

The second kind of experimental error was caused by the oscillatory boundary conditions. The foam sample is flushed on both sides with the tested gas to obtain the steady state linear partial pressure profile. The barometric pressure oscillations propagate into the sample, Fig.5.2. If data are taken when the barometric pressure is low, the partial pressure gradient is steeper than the imposed average pressure gradient. A higher transient permiation rate occurs and the computed permeability coefficient is erroneous. If barometric pressure is higher than the average, the partial pressure gradient is less steep. The error due to the oscillatory boundary conditions before the measurement is much lower than the error due to the pressure change during the measuerment, but not negligeable. Before this effect was understood, permeation rates up to 30% higher or lower than the permeation rate with complete steady state were observed.

The evaporation of the slug liquid is also a source of experimental error. As the slug moves a thin liquid film remains on the capillary tube and evaporates. At the room temperature Isobutyl Methyl Ketone has a vapor pressure equal to 15 mmHg. Up to 1 cm/hr additional slug motion due to evaporation was measured. To minimize the evaporation rate Formamide was used instead of Isobutyl Methyl Ketone. The slug motion is less continuous since Formamide ($HCONH_2$) is more viscous.

Attempts were made to reduce the influence of barometric pressure oscillations. The pressure was controlled on the high and low pressure sides to compensate for the barometric pressure changes.

Finally, the capillary tube was replaced with the Valedyne AP 10

absolute pressure transducer that was used for the cell wall permeability tests. The pressure transducer enabled faster and much more accurate measurements than the capillary tube. No open contact with the atmosphere is made so that the transducer output is independent of barometric pressure. As shown on Fig. 5.4, the steady-state volumetric inflow into the low-pressure volume results in a linear pressure increase. Only 1 hr is needed to obtain a pressure increase of N_2 at 25 °C, sufficient to accurately measure the slope of the pressure increase (20 min are needed at 50 °C). With the present cell design we are able to reproduce the permeability coefficient of N_2 with $\pm$ 2% accuracy or better. With a capillary tube, at least 10 hours are needed to obtain sufficient displacement of the slug due to permeation of nitrogen at 25 °C to be able to perform accurate volumetric measurement.

5.2 The Method and the Apparatus for Rapid Steady State Measurement

The steady-state permeability measurement requires a linear concentration profile of a specific gas species under test. By presently used methods, it takes several months to establish a steady-state concentration profile of N_2 in a 1 cm thick sample at room temperature. Concentration of O_2 becomes linear in several weeks, while fluorocarbon 11 is estimated to require several years.

The diffusion coefficient of gasses in the closed cell polyurethane foams are strongly temperature dependent. The foam permeability coefficient follows an Arrhenius-type equation while the effective solubility has an inverse linear temperature dependence

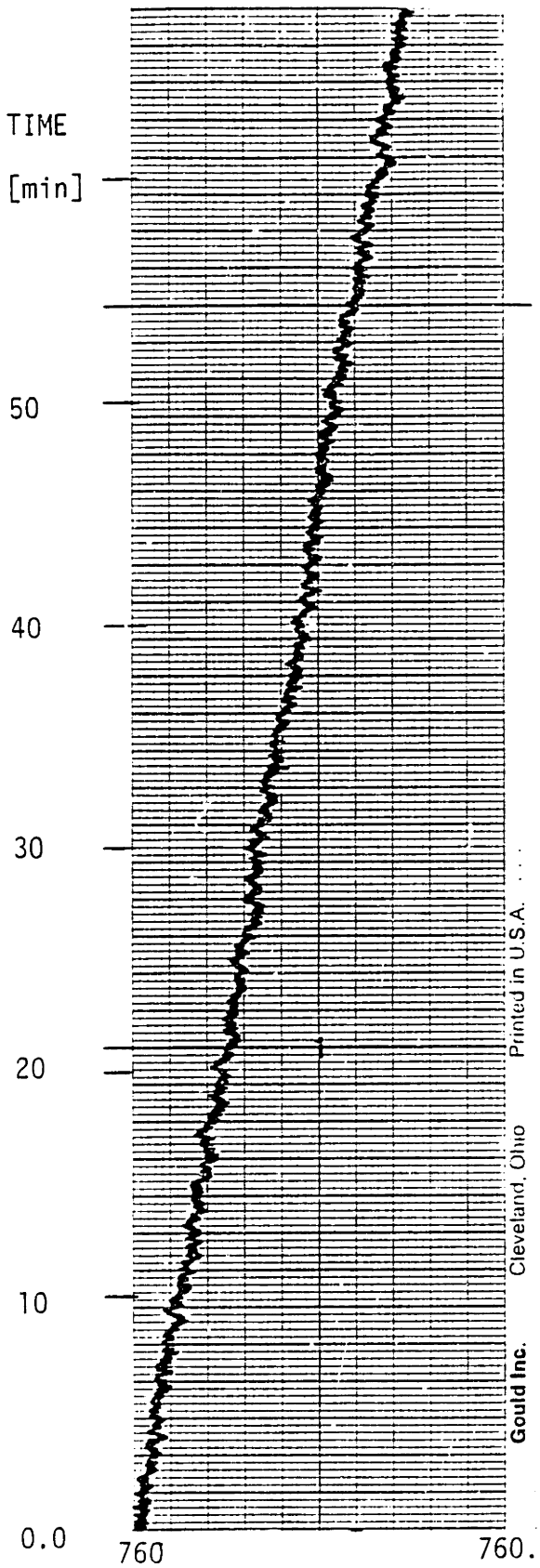

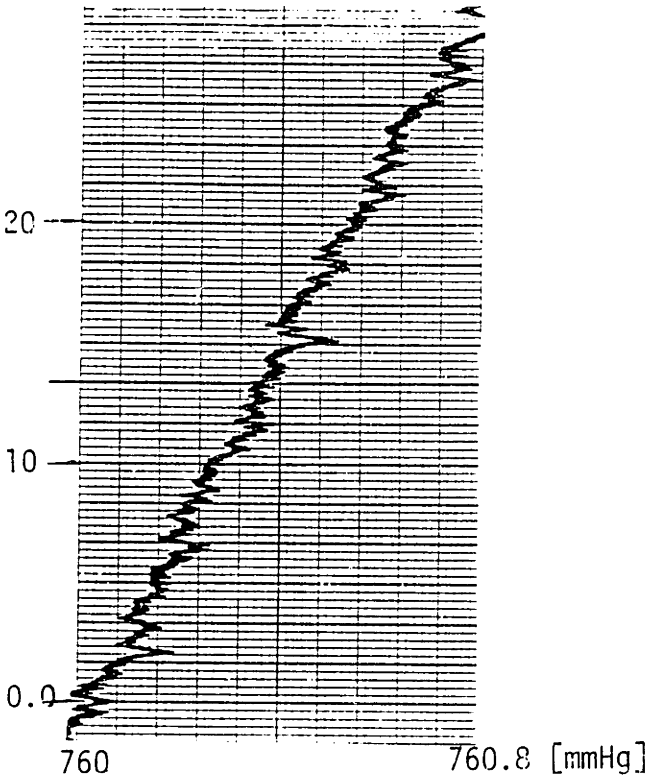

Fig. 5.4 PRESSURE INCREASE IN THE UPPER PLENUM AS A FUNCTION OF TIME

(Gas : N_2)

which comes from the ideal gas law. Consequently,

$$D_{eff} = Pe_0 \exp(-E/RT)\ (T/T_{STP}) \qquad (5.1)$$

The diffusion coefficient of the air components, measured in the present study, increases by a factor of 10 when the temperature increases by 50 °C. The increase of the freon effective diffusion coefficient is even greater. Consequently, the linear concentration profile of a specific gas species can be obtained much faster at elevated temperatures than at room temperature.

The experimental apparatus which makes use of the high value of the diffusion coefficient at elevated temperatures is shown on Fig. 5.5. The low and the high pressure plenums of the cell were each conected to a large volume chamber.

The following measuring method was used:

- Impose a partial pressure difference of a gas species on the boundaries of the tested foam sample.
- Increase the temperature and obtain a steady state linear concentration profile inside the foam sample. At 75 °C the linear steady-state profile is established 10 times faster than at room temperature (25 °C), while at 125 °C it is established 100 times faster than at the room temperature. When the linear steady state profile is established valves 2 and 3 are closed (Fig. 5.5) and the foam sample is isolated from the environment.
- To preserve the linear concentration profile, one must change the partial pressure imposed on the boundaries simultaneously with the temperature change. By doing so, equality

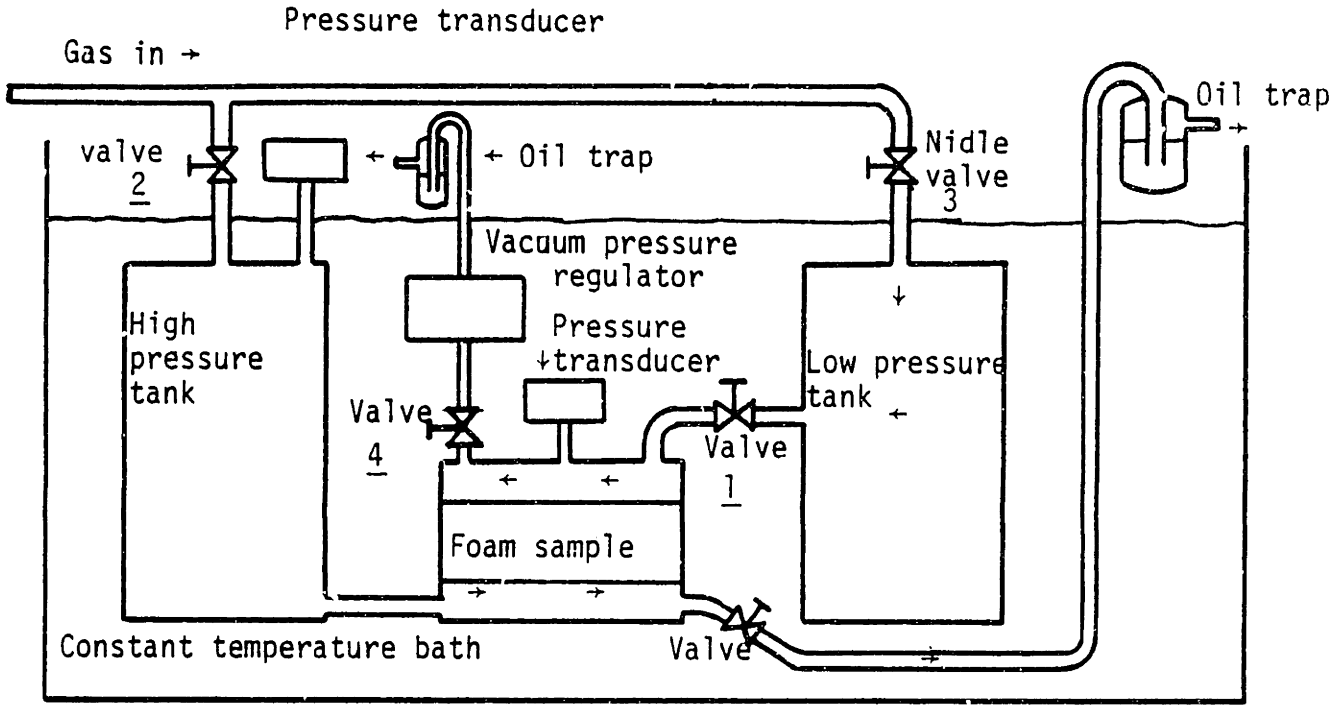

Fig. 5.5 SCHEMATIC DIAGRAM OF THE RAPID STEADY-STATE PERMEABILITY TEST

of partial pressure is preserved across the foam surface, between the gas within the foam, and gas outside the surface. When the temperature changes in the low and high pressure reservoir and the plenums, the pressure also changes according to the ideal gas law. The gas partial pressure in the foam cells changes in the same way so that the partial pressure profile is continuous at the foam-gas interface. The volume of the high and low pressure tank has to be high enough so that the volume of the permeated gas causes negligible pressure change in the tanks.

- When valve 1 is closed the plenum is isolated from the reservoir.The pressure increase in the low pressure plenum is due to the volumetric inflow from the foam sample and is related to the permeability and diffusion coefficients.

- Valve 1 is opened to connect the plenum and the reservoir. The temperature is changed to another level at which the diffusion coefficient is to be measured. Again, due to this specific design of the diffusion cell, the linear steady-state concentration profile will not be perturbed by the temperature change, so that data can be taken as soon as thermal equilibrium is cheived.

When the rapid method, i.e., using elevated temperatures to reach steady state concentrations, was not used, about 120 days were needed to obtain steady state linear profile with N_2 at 25 °C, while about 40 days were needed at 50 °C, Fig. 5.6. The measurement of the Pe_{eff} was repeated with the rapid steady state method, Fig 5.7. Steady state was obtained in 13 days at 75 °C. After that the the temperature was changed within several hours to 50, 25 and 90 °C respectively and

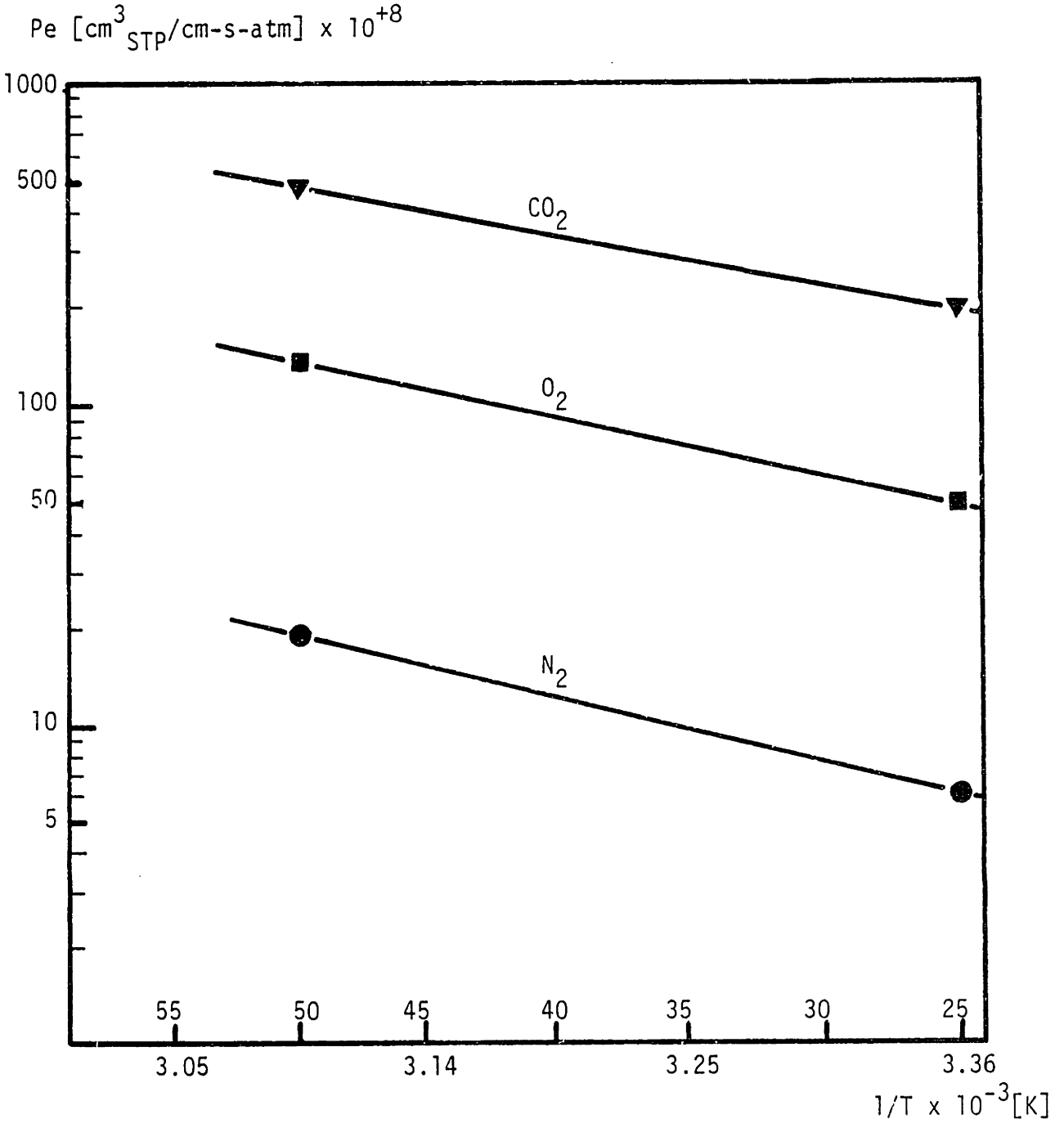

Fig. 5.6 PERMEABILITY COEFFICIENT OF N_2, O_2 AND CO_2 IN THE FOAM SAMPLE # 1

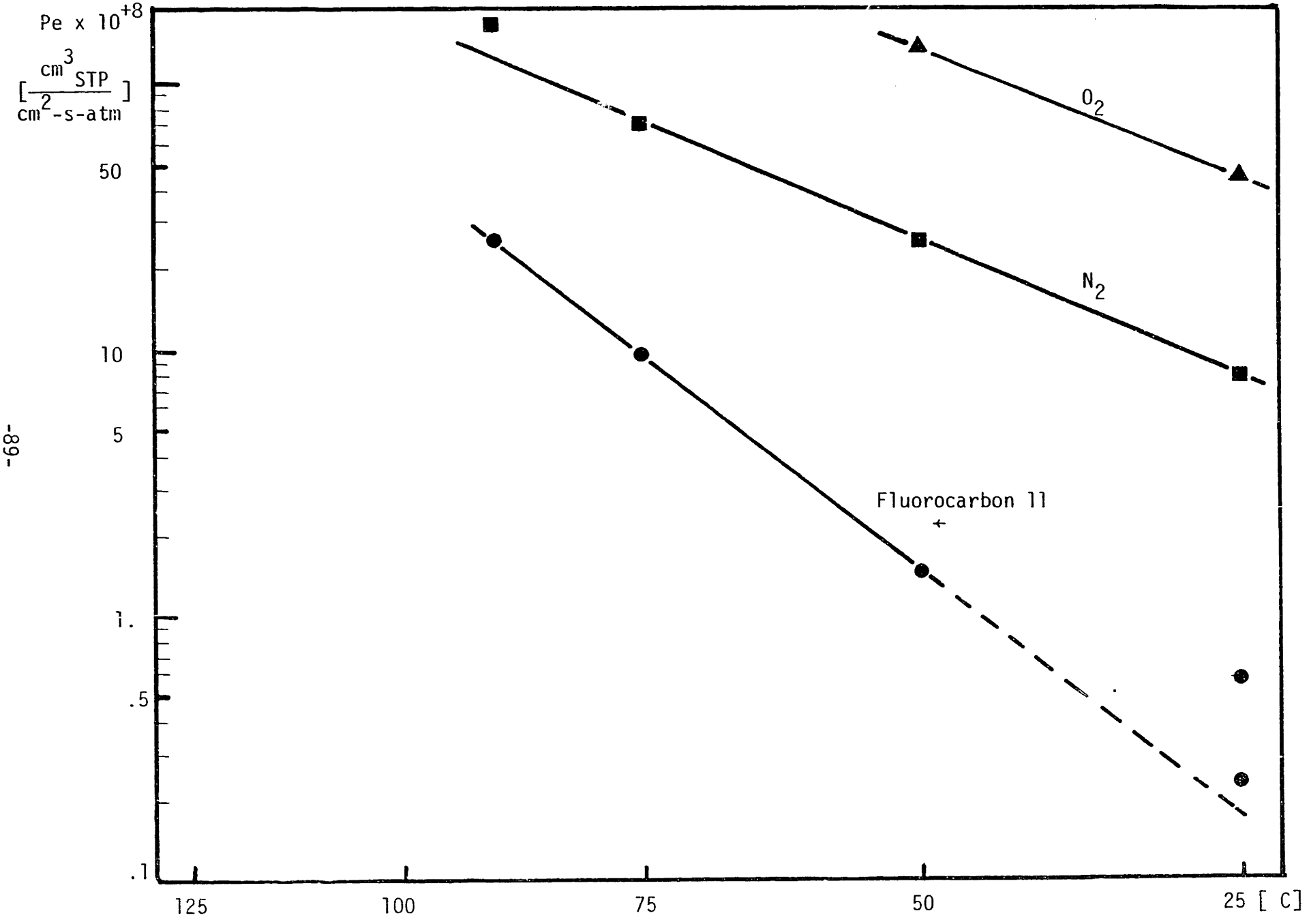

Fig. 5.7 PERMEABILITY COEFICIENT OF O_2, N_2 AND FLUOROCARBON 11 IN THE FOAM SAMPLE # 1 MEASURED BY THE RAPID STEADY STATE TECHNIQUE

Pe_{eff} was measured at each temperature level. Note that the data obtained with the rapid steady state technique follow the Arrhenius-type temperature dependance, and are in an excellent agreement with the data on Fig 5.6.

The rapid steady state method has enabled data with fluorocarbon 11 to be obtained. A 1 cm thick foam sample was kept for 90 days at 90 °C, which is equivalent to about 3,000 days at room temperature. The measured flowrate of fluorocarbon was very low at 35 and 25 °C, and the data could be only reproduced to within +-50%, possibly because of the temperature regulation which was inadequate considering the very low flow rate. To obtain more accurate data, measurements were repeated at different temperatures for about thirty days. The curve shown on of Fig. 5.7 is the best fit to the data obtained.

6. CHARTS FOR 1-D UNSTEADY DIFFUSION IN FOAM SAMPLES

Linear rate equations equations are used with steady-state transmission measurements to compute the effective permeability and diffusion cefficient. The linear equations (2.44) and (2.47), are valid only for steady state procesess. If steady state is not reached in the test, the measured mass flux is equal to,

$$J_m = Pe_{eff} \left[\partial p_i / \partial x\right]_{x=0} \tag{6.1}$$

where $\left[\partial p_i / \partial x\right]_{x=0}$ is the transient slope of the partial pressure, at the low pressure side of the foam surface. Since this slope is not equal to the steady state slope, equations (2.44) and (2.47) give an erroneus transport coefficient.

Diffusion of gasses in closed-cell foams is a very slow process. For instance, the diffusion constant of the fluorocarbon 11 in polyurethane foam, at room temperature was found to be 0.2×10^{-8} cm^2/s. A transient diffusion process in a solid approaches steady-state when Fo number based on the thickness of the solid, $D_{eff}t/L^2$, approaches unity. Based on the diffusion constant for fluorocarbon 11, steady state can be reached in $5 \times 10^{+8}$ s or 15 years for a 1 cm thick sample.

Foam samples used in the foam permeability measurement apparatus are described in the Chapter 5. The samples have the shape of a circular plate. The flat sides of the plate are exposed to constant

partial pressures p_1 and p_2 respectively; the circular area is impermeable. Therefore the sample can be modeled as an infinite slab (Fig. 6.1).

To determine if steady state is reached in the foam samples during a foam permeability measurement, special charts were developed. These charts, similar to the Heisler Charts, are valid for nonhomogenous boundary conditions. Two types of charts have been developed: partial pressure charts and flux charts.

6.1 The Partial Pressure Charts

Concentration or partial pressure of a gas species inside of a closed-cell foam is not affected by the presence of other gasses (i.e., the driving potential for diffusion is unaffected). Gas molecules present neglegible resistance to diffusion of other gas molecules compared to the diffusion resistance of the molecules of the solid polymer. Consequently, different gas species diffuse independently.

We wish to find the unsteady partial pressure in the sample when the initial partial pressure inside the foam sample is taken to be constant or equal to zero. At $t > 0$, unequal partial pressure is imposed on the boundaries. The formulation of the problem in terms of partial pressures relative to the initial partial pressure is,

$$\partial p/\partial t = D\partial^2 p/\partial x^2 = (Pe/S)\partial^2 p/\partial x^2 \qquad (6.2)$$

$$p(x,0) = 0,$$

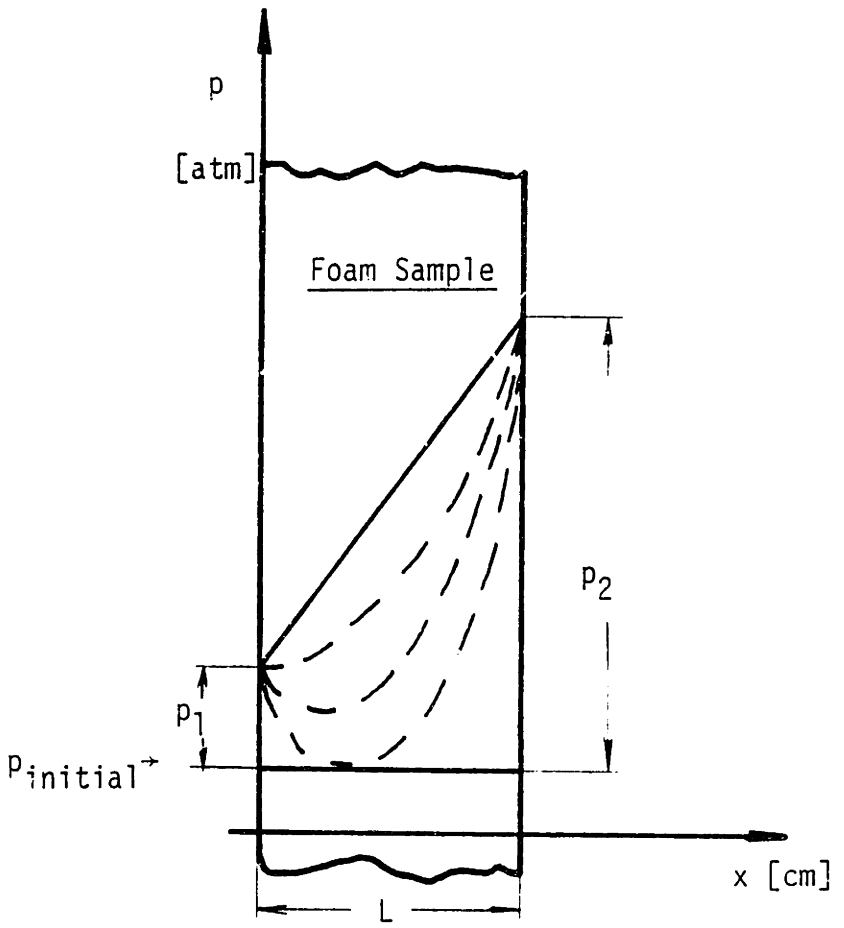

Fig. 6.1 INITIAL AND BOUNDARY CONDITIONS IMPOSED ON A FOAM SAMPLE INSIDE THE PERMEABILITY CELL

$$p(0,t) = p_1,$$

$$p(L,t) = p_2$$

From the solution to equation (6.1), the transient partial pressure is equal to [22],

$$p(x,t) = p_1+(p_2-p_1)x/L+$$

$$+ 2/\Pi \sum_{n=1}^{\infty} [(p_2\cos(n\Pi)-p_1)/n \sin(n\Pi x/L)\exp(-n^2\Pi^2 Dt/L)] \quad (6.3)$$

By using the dimensionless coordinate $x^* = x/L$, the dimensiomless time $Fo = D_{eff}t/L^2 = Pe_{eff}t/(SL^2)$, the dimensionless ratio of the pressures at the sample boundaries, $p^* = p_1/p_2$, and by rearranging the equation (6.3), we can obtain the dimensionless partial pressure inside the foam sample, defined as $U^*=p/p_{ss}$,

$$U^* = 1+2/\Pi \sum_{n=1}^{\infty} [(\cos(n\Pi)-p^*)/n \sin(n\Pi x^*)\exp(-n^2\Pi^2 Fo)]/[p^*+(1-p^*)x^*] \quad (6.4)$$

The steady state partial pressure, p_{ss} is equal to

$$p_{ss} = p_1 + (p_2-p_1)x^* \quad (6.5)$$

U^* is the ratio of the transient partial pressure to the steady state partial pressure for different positions x^* and time (Fo). When steady state is achieved, this ratio becomes one. To evaluate equation (6.4) a computer program was developed. In Fig. 6.2., U^* is plotted

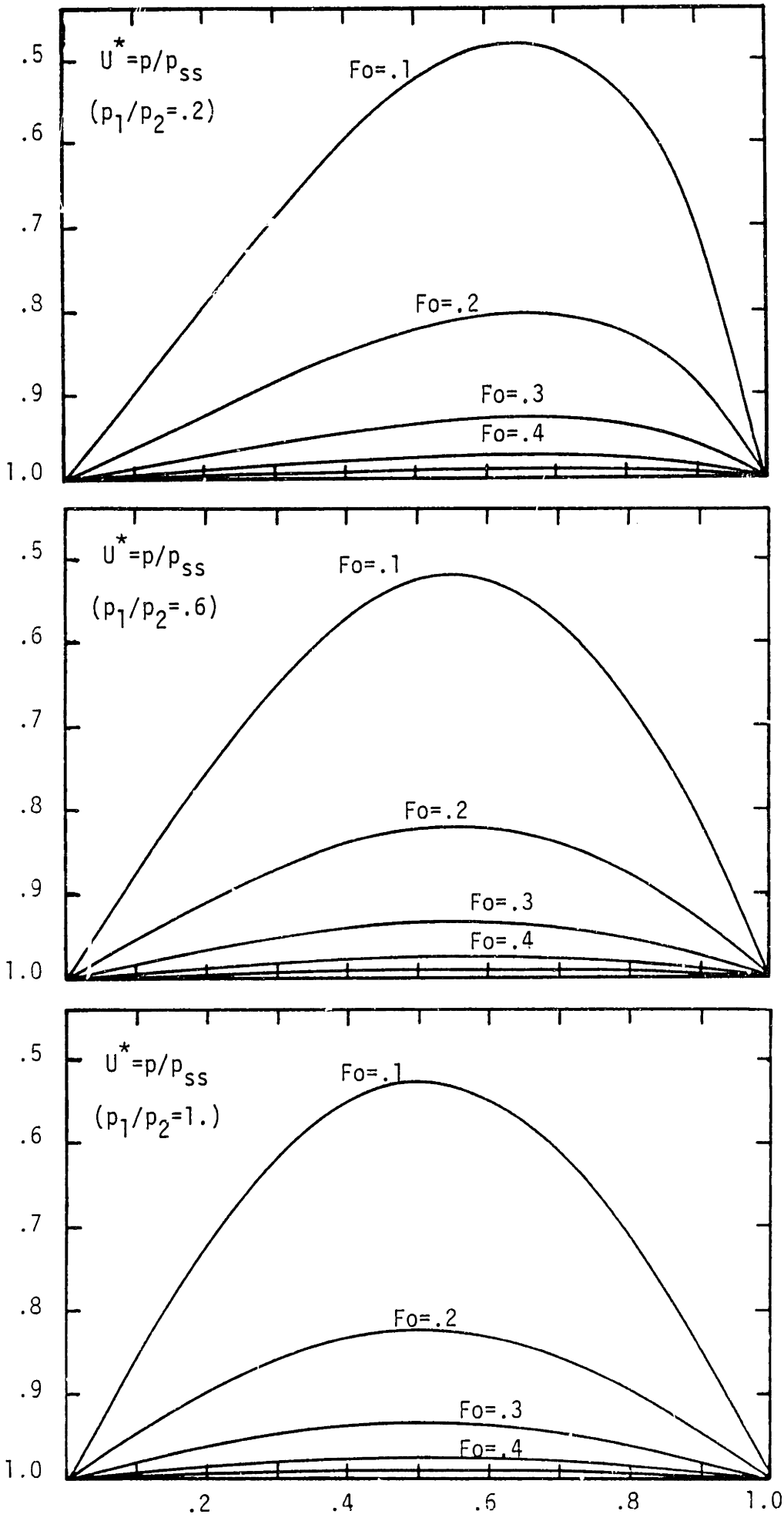

Fig. 6.2 PARTIAL PRESSURE HISTORY IN AN INFINITE FOAM SLAB EXPOSED TO PARTIAL PRESSURE DIFFERENCE

against x^* for p^* = .2, .6, and 1. with Fo as parameter. The results having p^* equal to 1. corresponds to the Heisler chart with an infinite Biot number. The figures indicate that U* does not differ significantly with different values of p^*.

6.2 The Unsteady Flux Charts

The transport coefficients are computed based on the mass flux measured for the foam sample. Theoretically, infinite time is needed to obtain a linear steady state partial pressure profile. To have confidence in the measured value of the permeability coefficient it is important to determine if the measured mass flux, equation (6.1), is equal to the steady state flux, equation (2.44).

The mass flux at any position x can be obtained by combining (6.1) and (6.3), using nondimensional properties and rearranging,

$$J_m = (Pe/L)(p_2-p_1)+ \\ + 2(Pe/L)p_2/L \sum_{n=1}^{\infty} [(\cos(n\Pi)-p^*)\cos(n\Pi x^*)\exp(-n^2\Pi^2 Fo)] \qquad (6.6)$$

To simplify the equations, the subscript "eff" shall be omitted up to the end of this chapter. Again the problem can be formulated in terms of a dimensionless flux which is the ratio of the local transient flux to the steady state flux, $J_m^*=Jm/J_{m,ss}$, where,

$$J_{m,ss} = Pe/L\ (p_2-p_1) \qquad (6.7)$$

$$J_m^* = 1+2/L \sum_{n=1}^{\infty} [(\cos(n\pi)-p^*)\cos(n\pi x^*)\ \exp(-n^2\pi^2 Fo)]/(1-p^*) \quad (6.8)$$

In Figure 6.3. The dimensionless flux, equation (6.8) is computed and plotted against x^*, for p^* = .2, .4, .6 and .8 with Fo as a parameter.

The graphs show that there is a strong dependence between the parameter p^* (boundary conditions) and J_m^* at x^*=0, i.e., at the foam suface where the flux is measured. For p^* = .2, J_m^* becomes equal to 0.84 if Fo = 0.3. For p^* = 0.8, q^* is equal to 0.07 if Fo = 0.3. This indicates that it is advantageous to have p^* as small as possible during the measurement. As p^* approaches 1, it takes a much longer time to approach the steady state. Also the mass flux is small and difficult to measure.

6.3 Transient Measurement of Permeability and Diffusion Coefficient

Shirtliffe has analyzed the settling time needed for heat transfer measurements [23]. He computed and plotted the error due to neglect of the remaining transient effect.

It is possible, however, to obtain data before the steady state profile is completely developed without introducing an error by using the analytical solution of the transient transfer process. Since the transient solution is implicit, and contains an infinite series, graphs were made relating the unknown property, permeability, to measured transient mass flux on the low pressure side of the sample as a function of time.

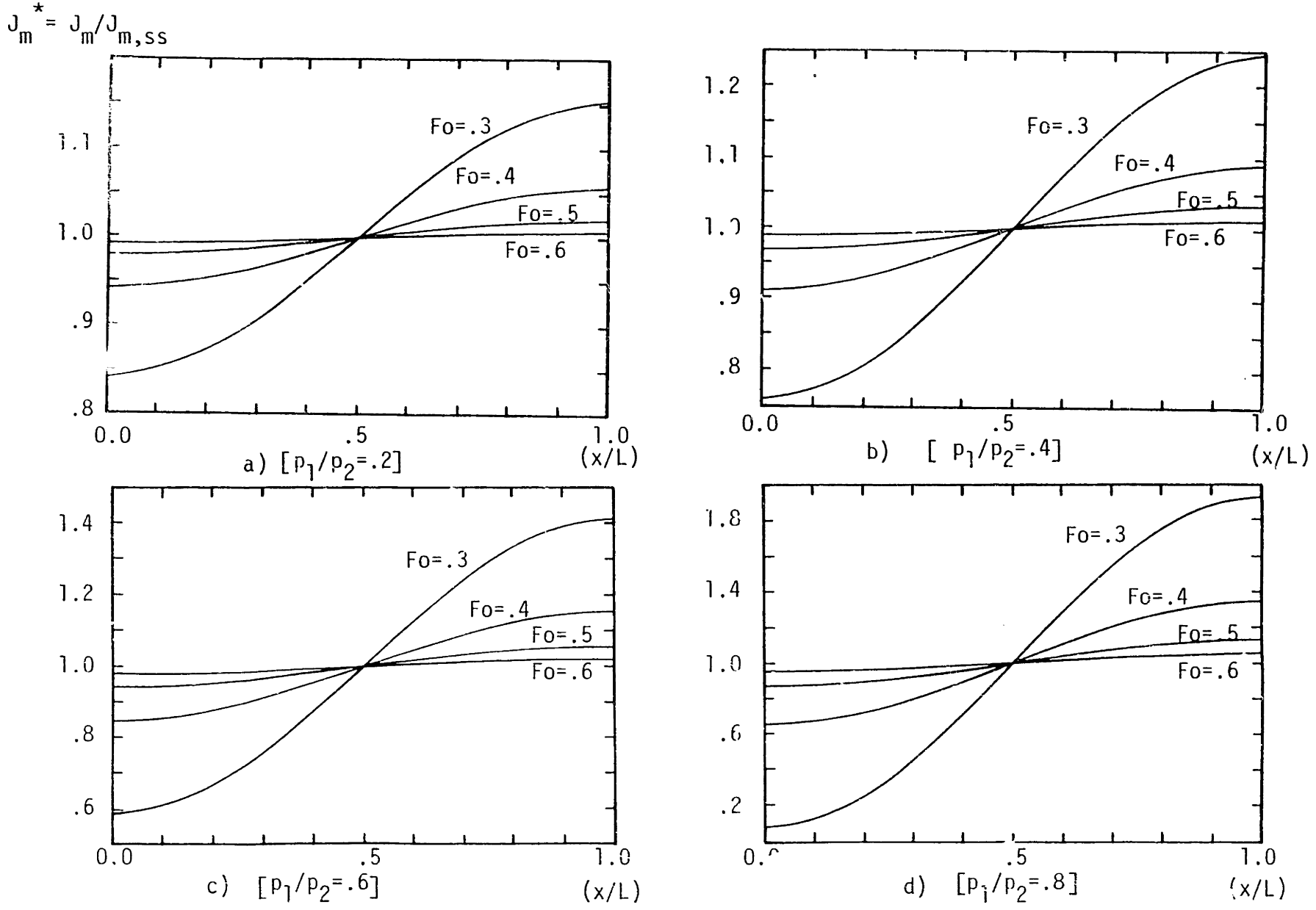

Fig. 6.3 MASS FLUX HISTORY IN AN INFINITE SLAB EXPOSED TO PARTIAL PRESSURE DIFFERENCE AT THE BOUNDARIES

Assuming initial and boundary conditions as in the section 6.1 (i.e., $p(x,0)=0$, $p(0,t)=p_1$, $p(L,t)=p_2$), the distribution of the driving potential as function of time and x, is given by equation (6.3). The flux inside the sample, J_m, is given by equation (6.6). The measured flux at x=0, has to be equal to

$$J_m = (Pe/L)(p_2-p_1)[1 + 2/L \sum_{n=1}^{\infty} (p_2\cos(n\Pi)-p_1)\exp(-n^2\Pi^2 Fo)/(p_2-p_1)] \quad (6.9)$$

We wish to find the unknown permeability Pe by measuring J_m at x=0. The known (measured) quantities in equation (6.9) are: transient flux, time, solubility S and partial pressures p_1 and p_2. These 6 quantities can be rearranged in three nondimensional groups, p^*, Fo and $J_{m,Fo=1}$, where,

$$J_{m,Fo} = Pe/L(p_2-p_1) = Fo\ S\ L(p_2-p_1)/t \quad (6.10)$$

and,

$$J_{m,Fo=1} = S\ L/t(p_2-p_1) \quad (6.11)$$

$J_{m,ss}$ is not known at the time of the measurement since the steady state has not been established. Instead, $J_{m,Fo=1}$ can be used to nondimensionalise the flux,

$$J_{m,Fo=1}^{*} = J_m/J_{m,Fo=1} \quad (6.12)$$

Physically $J_{m,Fo=1}$ is the flux that would be measured at the time when Fo = 1, (i.e., at t = Fo L^2/D time of the transient).

The equations (6.9),(6.11) and (6.12) give the nondimensionalised transient measured flux,

$$J_{m,Fo=1}^{*} = Fo[1 + 2/L \sum_{n=1}^{\infty} (\cos(n\pi)-p^{*})\exp(-n^2\pi^2 Fo)/(1-p^{*})] \quad (6.13)$$

where Fo contains the unknown transport coefficients, D and Pe.

Equation (6.13) relates Fo to p^* and $J_{m,Fo=1}^{*}$ implicitly. $J_{m,Fo=1}^{*}$ is plotted in Figure 6.4 against Fo with p^* as parameter. To use the chart in Figure 6.4, one has to measure J_m, t, p_1, p_2, L, and compute the solubility S from Equation (2.55). Next from equation (6.11) we compute $J_{m,Fo=1}$ and $p^*=p_1/p_2$. Next, from equation (6.12) we compute $J_{m,Fo=1}^{*}$ and from the graph we obtain the Fo. Then,

$$Pe = Fo\ S\ L^2/t \quad (6.14)$$

or,

$$D = Fo\ L^2/t \quad (6.15)$$

From these equations permeability and diffusion cefficient are computed.

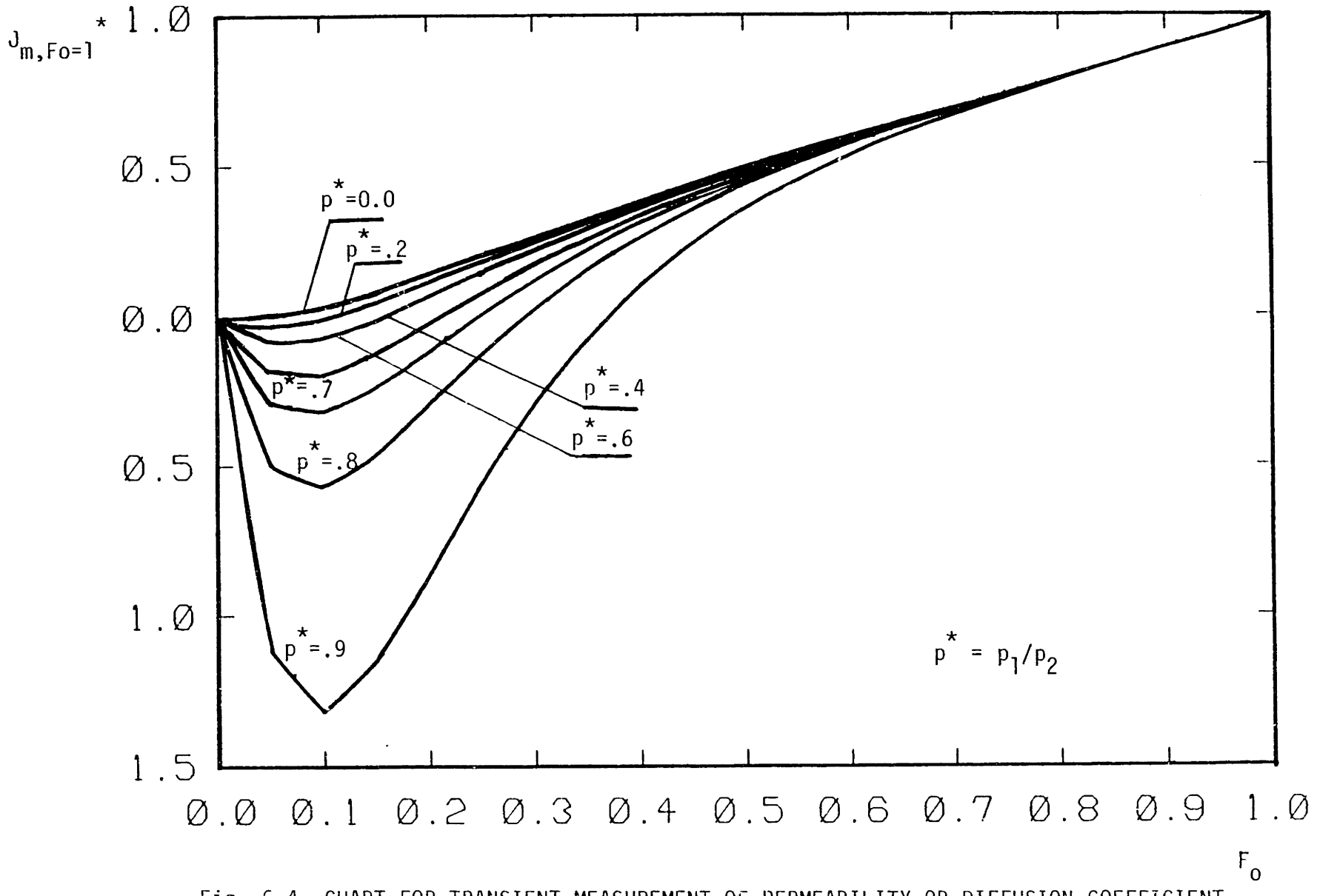

Fig. 6.4 CHART FOR TRANSIENT MEASUREMENT OF PERMEABILITY OR DIFFUSION COEFFICIENT

7. MODEL OF THE CHANGE IN FOAM EFFECTIVE THERMAL CONDUCTIVITY OVER TIME

The effective thermal conductivity coefficient of the foam panels can be computed based on a prediction of the thermal conductivity of the gas mixture inside the foam, the thermal conductivity of the solid and the apparent conductivity due to radiation. The thermal conductivity of the gas mixture is dependent on the gas composition.

In this chapter, the equations governing the gas composition and the thermal conductivity of the gas mixture inside the foam panels are presented. The system of equations along with data for solid conduction and radiation form a model for the effective thermal coefficient of foam panels. To solve the system of equations, a computer code called ECVA (Effective Conductivity Versus Age) was developed.

7.1 Model for the Effective Thermal Conductivity Coefficient of Foam Panels

The one-dimensional transient diffusion of air components and fluorocarbon 11 inside foam panels is described by the set of partial differential equations equating acumulation to net transport for each gas component,

$$\partial p_i/\partial t = (\partial/\partial x)(D_{eff,i}\,\partial p_i/\partial x) \qquad (i = 1, 2, 3, 4) \qquad (7.1)$$

The initial conditions are,

$p_i(x,0) = 0$ for i = 1,2,3, the air components,

$p_i(x,1) = 1$ for i = 4, the gas used to blow the foam.

The boundary conditions are,

$$p_i(0,t) = p_i(L,t) = .7808 \quad \text{for } i = 1$$
$$p_i(0,t) = p_i(L,t) = .2095 \quad \text{for } i = 2$$
$$p_i(0,t) = p_i(L,t) = .000314 \quad \text{for } i = 3$$
$$p_i(0,t) = p_i(L,t) = 0.0 \quad \text{for } i = 4$$

where subscript i = 1, 2, 3, denotes the air components N_2, O_2 and CO_2 i=4 denotes the fluorocarbon 11. The equations (7.1) are uncoupled; i.e., the transient diffusion of one gas does not affect the transient diffusion of the other gasses.

In most situations of practical interest, foam panels are exposed to a temperature gradient. To be able to compute the values of the temperature dependent properties, like the effective diffusion coefficient or the conductivity of gasses, the temperature profile has to be known at different locations inside the foam. Since the thermal diffusivity is much larger then the effective diffusivity for mass transfer, it can be assumed that the temperature profile inside the foam develops instantaneously according to the equation,

$$T(x,t) = T(0,t) + [T(0,t) - T(L,t)](x/L) \qquad (7.2)$$

where $T(0,t)$ and $T(L,t)$ are temperatures imposed on the foam boundaries. $T(0,t)$ and $T(L,t)$ can vary in time.

The values of the effective diffusion coefficient can be obtained from equation (2.76) or from measurement. The data obtained for foam in Chapter 5 indicate that the effective diffusion coefficient follows the temperature dependence given by equation (5.1). The foam effective diffusion coefficient is recalculated whenever the temperature imposed on the foam boundaries changes.

Equations (7.1), (7.2) and (2.76) together with the initial and boundary conditions, determine the one-dimensional distribution of the gas partial pressure. From the partial pressures, the mixture composition inside foam panels is computed. Based on the mixture composition, the mixture conductivity is modeled next.

A review of thermal conductivity equations modeling the gas mixtures is given in reference [24] by N.V. Tsederberg. An equation with empirical corrections proposed by Lindsay and Bromley was selected as the most accurate to be used in the model. The equation has the form,

$$K_{mix} = \sum_{i=1}^{4} Ki/(1 + 1/x_j \sum_{\substack{j=1 \\ i \neq j}}^{4} A_{ij}x_j) \qquad (7.3)$$

where K_i are the thermal conductivities of the gasses in the mixture, and the x_i are the molar fractions of the gasses. The coefficients A_{ij}

are computed as,

$$A_{ij} = .25([1+[(\mu_i/\mu_j)(M_j/M_i)^{.75}(T+s_i)/(T+s_j)]^{.5})^2(T+s_{ij})/(T+s_i) \quad (7.4)$$

where μ_i are the dynamic viscosities of the components and M_i are the molar masses. The constants s_i and s_{ij} are computed from the equations,

$$s_i = 1.5\ T_{bi} \quad (7.5)$$

and

$$s_{ij} = (s_i s_j)^{.5} \quad (7.6)$$

where Tb_i is the absolute boiling temperature of the gas component i at atmospheric pressure. When the molecules of one of the gasses are strongly polar, the geometric average (7.6) is multiplied by 0.773 .

Besides the conduction through the gas mixture, heat is transfered through closed-cell foam by conduction through solid and by radiation. However, conductivity of the solid and the amount of heat transfered by radiation do not change with time. These two components of heat transfer can be modeled or measured separately and added to the mixture conductivty computed from equation (7.3).

$$K_{eff} = K_{mix} + K_{solid} + K_{rad} \quad (7.7)$$

7.2 Description of the ECVA Code

A computer code called ECVA was developed to solve the set of equations (7.1) to (7.7) and compute the change of the gas composition and conductivity of the gas mixture inside the foam panels. The configuration of the code is given in Figure 7.1. The code consists of six subprograms: MAIN, PPRESS, KMIX, FBACK, LUDE and M.DAT. The listing of the ECVA code is given in the Appendix II.

Subprogram MAIN

Subprogram MAIN takes the input data from the input data file M.DAT. A number of quantities that do not change with time are computed next. These quantities include the partial pressure of the air components at standard pressure, S(I), S(I,J).

The initial temperature profile inside the foam is computed from the boundary conditions and equation (7.2). It is assumed that initial pressure of the gas mixture (usually only R 11) inside the foam cells is equal to 1 atm at 25°C. If temperature inside the foam changes, the partial pressure of the mixture components also changes. From the computed initial temperature distribution, the initial partial pressure of the gas inside the axial nodes is computed, by using the ideal gas law.

At each time step, subprogram PPRES is called to compute the partial pressure of the air components and fluorocarbon 11 inside the axial nodes.

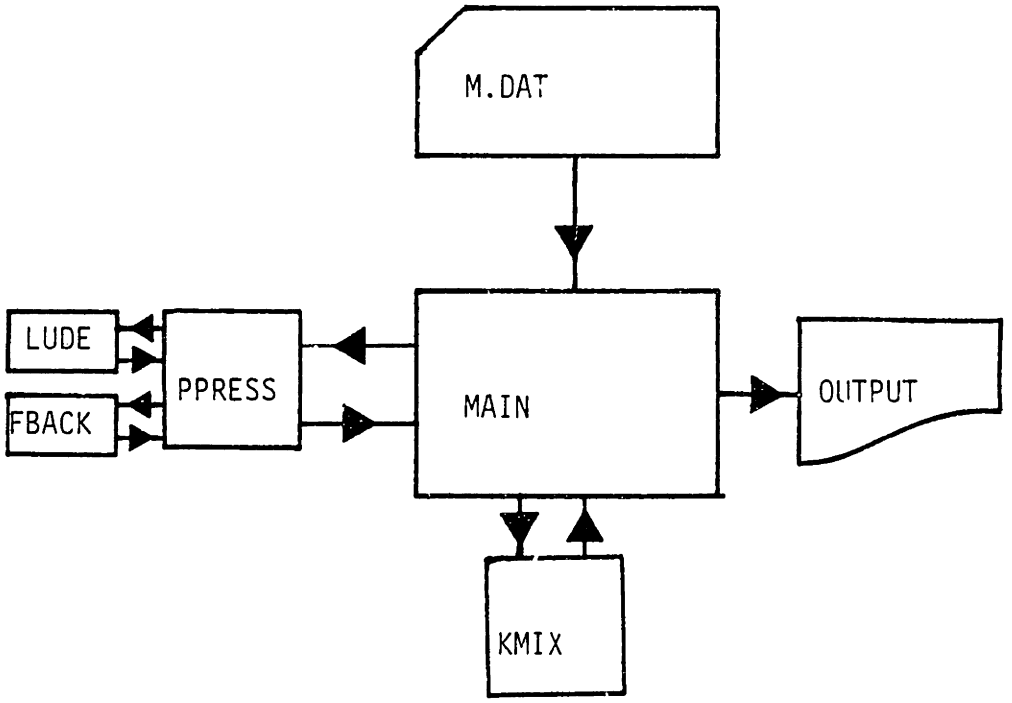

Fig. 7.1 CONFIGURATION OF THE ECVA CODE

Each time step, subprogram KMIX is called to compute the value of the thermal conductivity of the gas mixture in the axial nodes.

The conductivity of the mixture is averaged to obtain an average conductivity of the gas mixture in the foam panel.

The thermal conductivity of the solid and the apparent conductivity due to radiation are added to the average conductivity of the gas mixture in the foam panel.

Results are then printed and plotted.

Subprograme PPRESS

Subprogram PPRES is called from the subprogram MAIN to compute the partial pressure of the air components and R11.

Diffusion coefficients of the N_2, O_2, CO_2 and R 11 are computed for all axial nodes as a function of temperature.

The equations (7.1) were approximated by the Crank-Nicolson finite difference scheme. In an explicit scheme the time step would have been limited by the speed of the fastest diffusing gas ($t \sim D_{eff} / \Delta x^2$). To avoid the stability limits on the time step, the Crank-Nicolson (C-N) finite difference scheme was used. The C-N scheme is an implicite one level - one step scheme, with second order accuracy. The selected time steping scheme is,

$$\partial p_i / \partial t = [p^{n+1}_l - p^n_l]_i / \Delta t \qquad (i=1 \text{ to } 4) \qquad (7.8)$$

where subscript i denotes that the equation is valid for the air components and R 11, n is the time level and l is the node number.

To simplify the numerical scheme, the term $(\partial D_{eff}/\partial x)(\partial p_i/\partial x)$ was neglected in the equations (7.1). The space discretisation of the C-N scheme is,

$$D_{eff}(\partial^2 p_i/\partial x^2) = (D_{eff}/\Delta x^2)[.5(p^{n+1}_{l-1} - 2p^{n+1}_{l} + p^{n+1}_{l+1}) + .5(p^{n}_{l-1} - 2p^{n}_{l} + p^{n}_{l+1})]_i \quad (i=1 \text{ to } 4) \qquad (7.9)$$

Combined equations (7.8) and (7.9) yield,

$$[p^{n+1}_{l} - p^{n}_{l}]_i/\ t = (D_{eff}/\Delta x^2)[.5(p^{n+1}_{l-1} - 2p^{n+1}_{l} + p^{n+1}_{l+1}) + .5(p^{n}_{l-1} - 2p^{n}_{l} + p^{n}_{l+1})]_i \quad (i=1 \text{ to } 4) \qquad (7.10)$$

After rearranging, equation (7.1) becomes,

$$[p^{n+1}_{l-1} - (2+C)p^{n+1}_{l} + p^{n+1}_{l+1}]_i = [p^{n}_{l-1} - (2-C)p^{n}_{l} + p^{n}_{l+1}]_i \quad (i=1 \text{ to } 4) \qquad (7.11)$$

where $C = \Delta x^2/(.5\Delta t D_{eff})$,

or in matrix form,

$$[A]_i[p^{n+1}]_i = [Q]_i \quad (i=1 \text{ to } 4) \qquad (7.12)$$

where $[A]_i$ are the four tridiagonal matrixes that contain the coefficients of the left-hand side of equation (7.11), $[p^{n+1}]_i$ are the four solution vectors, (i.e., the partial pressures of N_2, O_2, CO_2 and R11 in the nodes at the new time level), and the four vectors $[Q]_i$, called forcing functions, have coefficients equal to the right-hand

side of equation (7.11). The solution vectors are obtained from equations (7.12) by calling the subprograms LUDE and FBACK.

According to the ideal gas law partial pressure of the gasses inside of the foam cells change linearly with temperature. Because of that the partial pressures have to be recalculated after every temperature change.

Subprogram KMIX

At each time step, subprogram KMIX is called from the MAIN subprogram to compute the new value of the thermal conductivity of the gas mixture in the axial nodes.

The molar fractions are computed first from the partial pressures of the gasses. Next, temperature dependant properties like viscosity and conductivity of the gasses are computed as a function of the local temperature in the axial nodes.

The conductivity of the mixture is computed from the equations (7.3) and (7.4)

Subprogram LUDE

Subprogram LUDE is called from the subprogram PPRES.

Subprogram LUDE decomposes a tridiagonal matrix [A] to lower and upper diagonal matrixes [L] and [U].

Subprogram FBACK

Subprogram FBACK is called from the subprogram PPRES.

Subprogram FBACK uses matrixes [L] and [U] and the forcing function [Q] to compute the solution vector $[p^{n+1}]$, by the so-called forward - backward procedure.

Subprogram M.DAT

Subprogram M.DAT contains the input data file. The input data specification is given in the Appendix II.

8. RAPID LABORATORY TESTS OF THE EFFECTIVENESS OF DIFFUSION BARRIERS

Closed cell foams are often faced with various materials such as aluminum, steel or felt foils, bonded to the surface. The facings protect the foam from damage and act as diffusion barriers. The foils are usually quite thin compared to the foam panel thickness. To be able to substantially slow down the diffusion process, a diffusion barrier has to have a diffusion coefficient many orders of magnitude lower than the foam. For faced foams, the aging rate becomes a function of both the internal diffusion resistance of the foam and the diffusion resistance of the diffusion barriers.

8.1 The One-Dimensional Approximation of the Diffusion in Foam Panels

It was shown in the Chapter 6 that air components and fluorocarbon 11 diffuse independently under partial pressure gradients. Therefore the three-dimensional transient diffusion of any of the air components or fluorocarbon 11 in foam slabs is described by the diffusion equation,

$$\partial p/\partial t = D_{eff}(\partial^2 p/\partial x_1^2 + \partial^2 p/\partial x_2^2 + \partial^2 p/\partial x_3^2) , \qquad (8.1)$$

along with initial and boundary conditions. The air components have equal partial pressure outside the sample while the initial partial pressure of fluorocarbon 11 throughout the sample is uniform. For

these initial and boundary conditions the three-dimensional diffusion of gasses in foam panels can be expressed in terms of the three separate one-dimensional problems, [25],

$$\partial p_i / \partial t = D_{eff}(\partial^2 p / \partial x_i^2) \quad (i = 1,2,3) \tag{8.2}$$

where,

$$p(x,y,z,t)=p_1(x_1,t)p_2(x_2,t)p_3(x_3,t) \tag{8.3}$$

The time scale of a one-dimensional transient diffusion process in a solid is given by the Fourier number,

$$Fo= Dt/L_i^2 \tag{8.4}$$

where D [cm^2/s] is the diffusion coefficient, t [s] is the transient time, and L_i is the characteristic length of the solid in the direction of diffusion. According to the definition (8.4), the time of the diffusion process is proportional to the squre of the thickness of the solid.

The thickness of the foam panels is much smaller than their length or width. Therefore, diffusion in the direction of the thickness is going to be much faster then the diffusion in the other directions, exept near the edges. The partial pressure within the panel is going to be approximately equal to the result of one dimensional diffusion in the direction of the thickness. The change of the partial pressure due to diffusion in other two dimensions will be

neglegable. Therefore, for an unfaced foam, only diffusion in the direction of the thickness is important.

8.2 Permeability Measurement of Diffusion Bariers

The resistance to diffusion of a diffusion barrier can be defined as,

$$R_{barr} = t_{barr}/(A_{x-s}Pe_{barr}) \tag{8.5}$$

while the resistance of the foam is,

$$R_{foam} = t_{foam}/(A_{x-s}Pe_{foam}) \tag{8.6}$$

where t_{foam} is one half the thickness of the foam panel.

By combining (8.5) and (8.6) we obtain,

$$R_{barr}/R_{foam} = (t_{barr}/t_{foam})(Pe_{foam}/Pe_{barr}). \tag{8.7}$$

To have an efficient diffusion barrier, the resistance of the barrier has to be much higher than the resistance of the foam, i.e.,

$$(t_{barr}/t_{foam})(Pe_{foam}/Pe_{barr}) >> 1 \tag{8.8}$$

or,

$$(t_{barr}/t_{foam}) >> (Pe_{barr}/Pe_{foam}) \tag{8.9}$$

If equation (8.9) is satisfied the diffusion through the diffusion barrier can be neglected and diffusion from the edge to the center of the foam becomes inportant.

Materials used for facing were tested separately from the foam. Aluminum and felt facings were peeled from foam slabs and placed into the permeability cell for the foam tests. The volumetric flowrate was measured by a capillary tube. When a pressure difference was applied across the felt, very high permeation rate with no time lag was observed, indicating that the felt is porous (a porous material has interconected voids or pores inside the solid). The flow rate was too high to be measured with a capillary tube. If the pores are much bigger than the mean free path of the air molecules, molecule-to-molecule collisions are important while molecule-to-solid collisions have no effect on diffusion. In this case pressure gradient causes bulk flow, so that the permeation rate through the large pores can not be related to a permeability or diffusion coefficient.

The effective diffusion coefficient in a porous solid can be modeled as [18],

$$D_{A,eff} = \alpha/k_t^2 \, D_{AB} \tag{8.10}$$

where α is the open void fraction, D_{AB} is the diffusion coefficient of the gas A through the gas B, and k_t is a geometry correction factor which corrects for the fact that many of the surface pores are at an angle with the surface. The experimental value of k_t vary from 1.2 to 2.5 [18]. At atmospheric pressure, D_{AB} is typically equal to .1 to 1 cm^2/s.

According to equation (8.10), the diffusion coefficient of a gas through felt, $D_{A,eff}$ is not much lower than the diffusion coefficient of a gas through gas. Therefore, the thin felt facing does not offer any diffusion resistance to the molecules diffusing into and outside the foam.

The permeation rate through the tested aluminum foils was found to be zero within the precision of the apparatus. This measurement was made in the early stage of this project, so that cappilary tube was used to measure the flowrate. Although the capillary tube was later found to cause substantial experimental error, it is certain, that aluminum foils represents much higher premeation resistance than a foam slab 1 cm thick.

The permeability of metals at the low temperatures is very low. For N_2, at the room temperature, practicly no data are available. By extrapolating the high temperature data given in the reference [26] to the room temperature, we can estimated that the permeability of aluminum to H_2 is in the order of 10^{-15} to 10^{-20} [cm^3_{STP}/cm-s-at]. The permeability of aluminum to N_2 is even lower then to H_2, and therefore it was not posible to measure any volumetric flow through 2.5×10^{-3} mm thick, aluminum foil having cross-section equal to 45 cm^2 assuming that there are no pinholes or pores in the aluminum.

The aluminum foils usually have thickness $t_{Al} = 1 \times 10^{-3}$ mm to 2.54×10^{-3} mm. Equation (8.9) implies that even 1×10^{-3} mm thick foil presents infinite permeation resistance compared to the resistance of the foam panels,

$$(Pe_{Al}/Pe_{foam})\ \ 10^{-7} \text{ to } 10^{-15} \gg (t_{Al}/t_{foam})\ \ 10^{-4} \qquad (8.11)$$

8.3 The Leak Test of the Foam/Facing Interface

The analysis and the measurements given in the previous section, indicate that neglegable ammount of gas molecules permeate through aluminum foils. As an alternative explanation of the failure of diffusion barriers to substantially slow down the aging process, existance of inhomogenieties in foam panels, specificly in the form of longitudinal open leak paths was considered. The paths could apper at the foil-foam interface due to pure adhesion between the solid polymer and the metal facing.

To quantify the diffusion resistance of the foam/facing interface a special permeability cell was designed, Figure 8.1, samples 22 cm in diameter were cut out from 2.54 cm thick faced foam panel. The facing was removed from the one side of the foam and a groove having outside diameter equal to 5 cm was cut into the sample. The sample was next glued to a supporting plate. A layer of epoxy was applied to the facing at the opposite side of the groove to prevent leaks that could appear due to possible damage to the facing while the groove was made.

Samples were next placed in the cell and a small overpressure, up to 13,600 Pa, was applied. The leak rate from the high pressure side to the groove (through the interface) was measured by a capillary tube.

Most of the samples had open paths between the groove and the high pressure plenum of the cell. A high flowrate, usually several mm^3/s, was measured with time lag equal to several seconds. The low

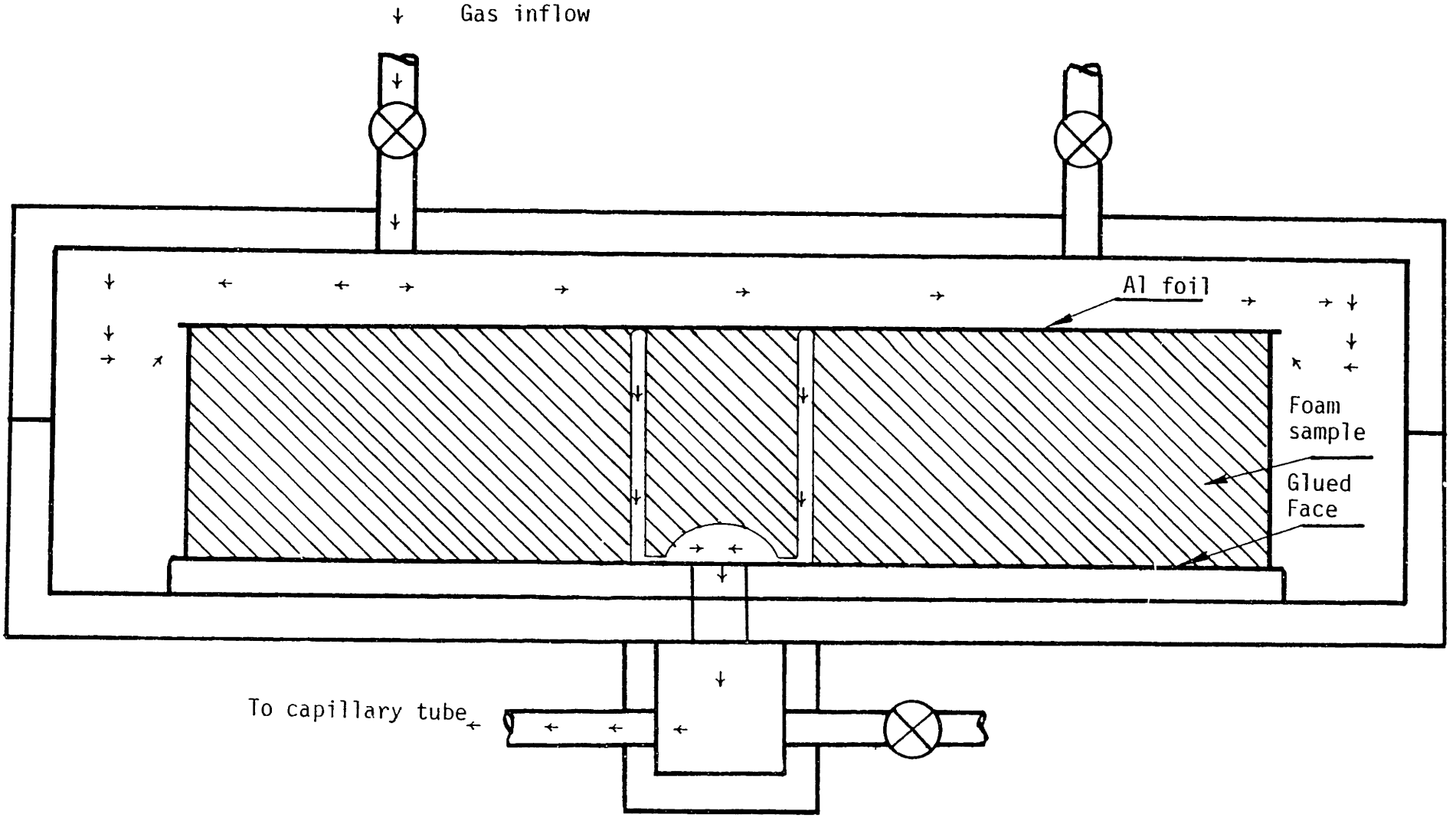

Fig. 8.1 THE INTERFACE LEAK CELL

pressure side of the cell has volume equal to approximatelly 5 cm^3, so that it takes several seconds to build up enough pressure to move the slug in the capillary tube. The flowrate of CO_2 and N_2 was approximately the same, while the volumetric flowrate had a square dependance on the pressure difference, which is typical for a bulk flow of fluids, Fig 8.2

The precision of the apparatus was not high due to the fact that temperature of the cell was not controlled. Besides, the slug moved very fast, approximatelly 5 cm/s leaving liquid-film trail in the capillary tube, so that the displacement of volume was not measured precisely.

If molecules were diffusing through the cell walls the meassured permeation rate would have been several orders of magnitude lower, CO_2 would have a permeation rate approximately 25 times higher than N_2 and a time lag in establishing steady state equal to at least several months, would have been observed.

It was concluded that open interconected paths must exist at the foam/foil interface.

The only tested sample having zero leak rate was the one with heavy steel facing. Steady state permeation rate through that foam sample was not measured since it was estimated, based on the measured value of the diffusion coefficient of CO_2 and N_2, that the time needed to establish steady state is t_{CO2} = 1 year and t_{N2} = 25 years respectively.

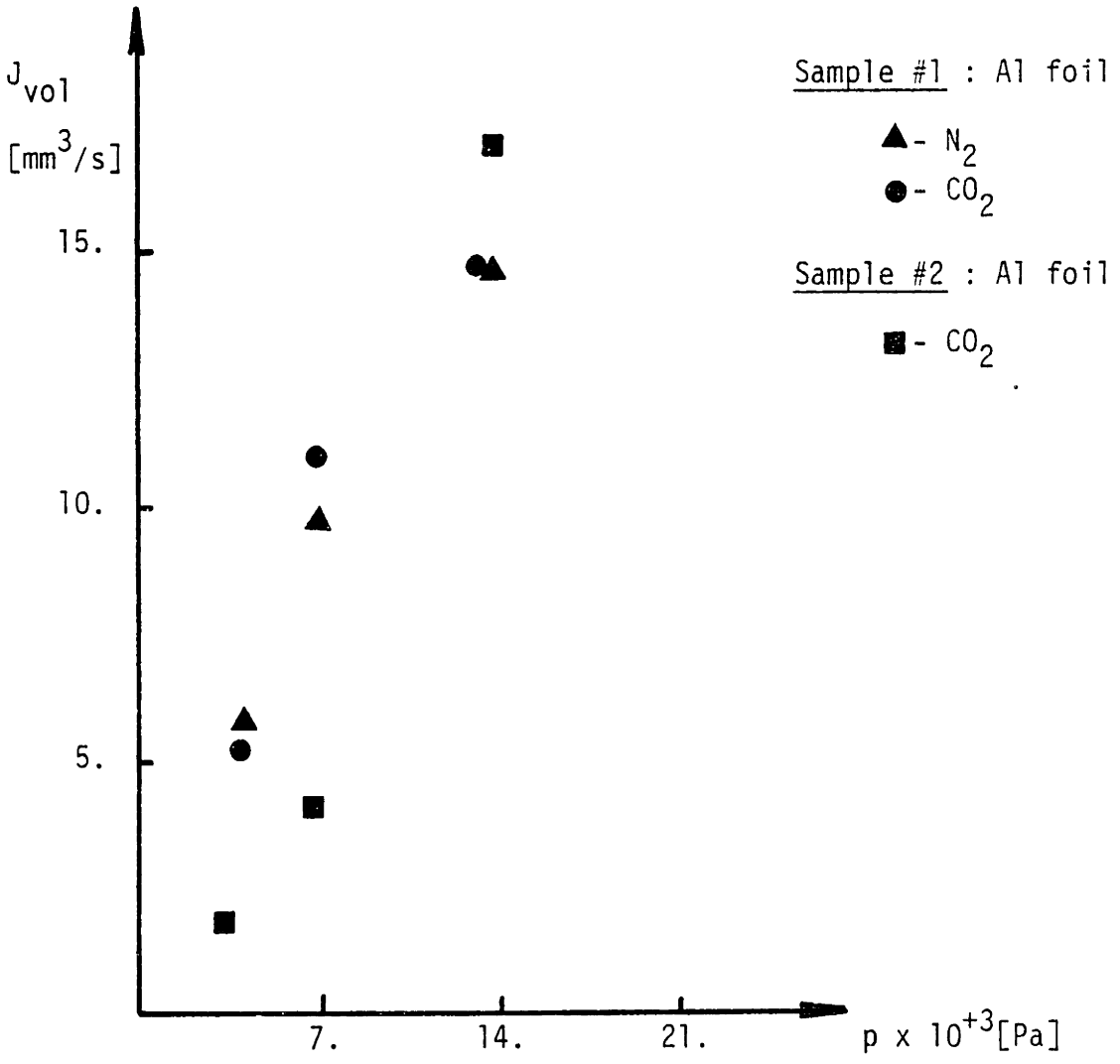

Fig. 8.2 MEASURED VOLUMETRIC LEAK RATE AT THE INTERFACE OF ALUMINUM FACED FOAM AS A FUNCTION OF APPLIED PRESSURE DIFFERENCE

8.4 The Dye Technique

To be able to visualise the open paths allowing bulk flow and estimate the porosity of the foam/foil interface, a rapid and simple dye test was developed. A faced sample, usually 15 x 15 x 2.54 cm, is submerged into a bath of ethylalchohcl mixed with dye, Figure 8.3. Vacuum is next applied to the submerged sample to remove the air from the open paths. Because of the presence of the alcohol in the desiccator, the pressure in the paths can not be reduced below the vapor pressure of the alcohol. When atmospheric pressure is reestablished, it forces the dyed liquid freely enters the empty paths. The sample is immediately removed from the alchohol bath and desiccator and dried to evaporate the alcohol and create colored trails in the open paths wetted by the alcohol.

After drying, the facing is peeled from the sample and the sample can be examined. The ratio of the dyed to undyed area defines the two-dimenional open voids fraction of the interface,

$$\alpha_{2D} = A_{dyed}/A_{facing} \tag{8.12}$$

Cuts through the sample can be made to check for the open paths that are not near the interface. All areas of the foam which exibit discoloration due to the dye are areas exposed to the air; i.e., areas not protected by the facing.

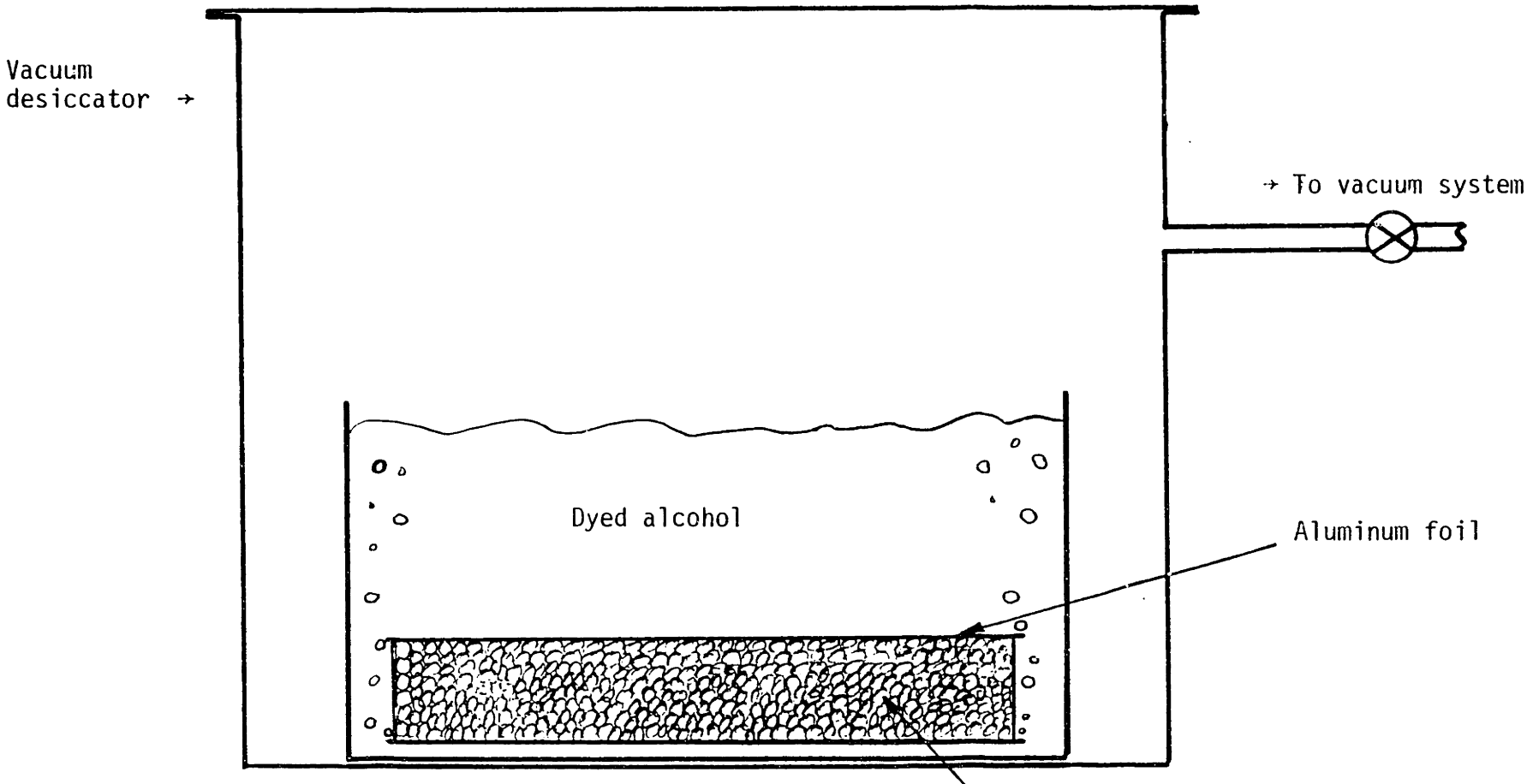

Fig. 8.3 THE DYE TEST

9. RESULTS

9.1 Cell Wall Permeability Coefficient

An experimental technique was developed to measure the permeability of the cell walls. The permeability data for the cell walls are given in the Table 4. Permeability of membranes #1 and #2 was measured with a capillary tube. For these membranes consistent data were not obtained with N_2 since at least 24 hours were needed to obtain substantial slug displacement. During that period of time, barometric pressure changed, causing errors in the measured permeability. Membrane #3 was tested with an absolute pressure transducer. Therefore data obtained from this membrane are believed to be the most accurate. Membranes #1 and #3 were obtained from the surface of the foam #1, Table 8.

The ratio between the permeability coefficients in foams and in sound films is given in Table 5. The ratio is not quite the same for foam samples and films probably because a few micropores existed even in the membranes that were belived to have no pores.

The permeability coefficient of CO_2, can be measured more accurately then the permeability coefficients of other air components, because of the high permeation rate of CO_2. By dividing the permeability coefficient of CO_2 with the ratios of the foam permeability coefficients, we obtained $Pe_{02} = 3.89 \times 10^{-10}$ and $Pe_{N2} = .634 \times 10^{-10}$ $[cc_{STP}/cm\text{-}s\text{-}atm]$.

TABLE 4

MEASURED PERMEABILITY OF POLYURETHANE CELL WALLS

$[cm^3_{STP}/cm\text{-}s\text{-}atm]$

Membrane	Density kg/m^3	Pe_{CO2}	Pe_{O2}	Pe_{N2}
#1, MDI	28.35	16.9×10^{-10}	4.26×10^{-10}	-
#2, MDI	25.15	17.5×10^{-10}	4.33×10^{-10}	-
#3, MDI	25.15	16.74×10^{-10}	4.46×10^{-10}	$.798 \times 10^{-10}$

MDI = methane diisocyanate

TABLE 5

RATIO BETWEEN FOAM PERMEABILITY COEFFICIENTS

AND CELL WALL PERMEABILITY COEFFICIENTS

	FOAM DATA	CELL WALL DATA
Pe_{CO2}/Pe_{N2}	26.4	21.0
Pe_{CO2}/Pe_{O2}	4.3	3.75
Pe_{O2}/Pe_{N2}	6.14	5.6

The measured value of the permeability coefficients of O_2 and N_2 in the Table 4, are higher by 14% and 25% respectively than the computed permeability coefficients based on the ratio of the foam data. The permeation rate through pores is approximately the same for all air components. Therefore, the permeability coefficient of CO_2 is affected by the permeation through the pores approximatelly 6 times less then the permeability coefficient of O_2, or 25 times less then the permeability coefficient of N_2 (i.e., about 2% or less).

The data in Table 4 indicate that permeability of the cell walls does not depend on the formation history of the two different foam samples. However, it is not proven that the permeability of the cell walls having different chemical composition (TDI polymer for example), is constant.

If the diffusion coefficient of one air component is known, Table 5 can be used to compute the diffusion coefficents for the other components.

9.2 Measurement of the Foam Permeability and Diffusion Coefficient

The foam permeability and diffusion coefficients were measured by steady-state transmission technique. Several sources of experimental errors were identified. The main sources of errors are: outgassing from the foam sample not fully in the steady state, outgassing form contaminated surfaces, transient diffusion in materials used in the permeability cell and effects of the barometric pressure variations. These effects cause much larger error if transient measuring

These effects cause much larger error if transient measuring techniques are used. The large spread of the published foam data (Table 2 in the Chapter 1) is possibly caused by these effects.

Three foam samples having different density were tested. Figure 9.1 shows data taken on the foam sample #2. These data show that mass flux through a foam sample (i.e., permeation rate) is proportional to the applied pressure difference. The permeability coefficients are independent of pressure difference at each temperature level. The data show some uncertainty at each temperature level since they were taken by a capillary tube.

A rapid technique was developed to measure the foam permeability and diffusion coefficient. Compared to long term steady-state technique, the rapid steady-state technique is 10 to 30 times faster for the polyurethane closed cell foams. Compared to the accelerated aging tests it is faster for another factor of 5 to 25, because the foam sample in the permeability cell is only 1 cm thick, compared to 1 or 2 inch (2.54 or 5.1 cm) thick foam panels used in the accelerated aging tests. The aging rate is inversly proportional to the square of the sample thickness.

To test the Rapid Steady-State Technique, the N_2 data shown on Fig. 5.5, which were obtained in 6 months by long-term steady-state tecnique, were reproduced in 13 days, Fig 5.6. Note that in the same time data with N_2 at 75°C and 90°C were also obtained.

The rapid staedy-state technique can be used as an accurate and reliable technique to measure the foam effective diffusion coefficient and from it predict the change of the foam effective conductivity with time. It is more accurate and reliable than the analytical model since

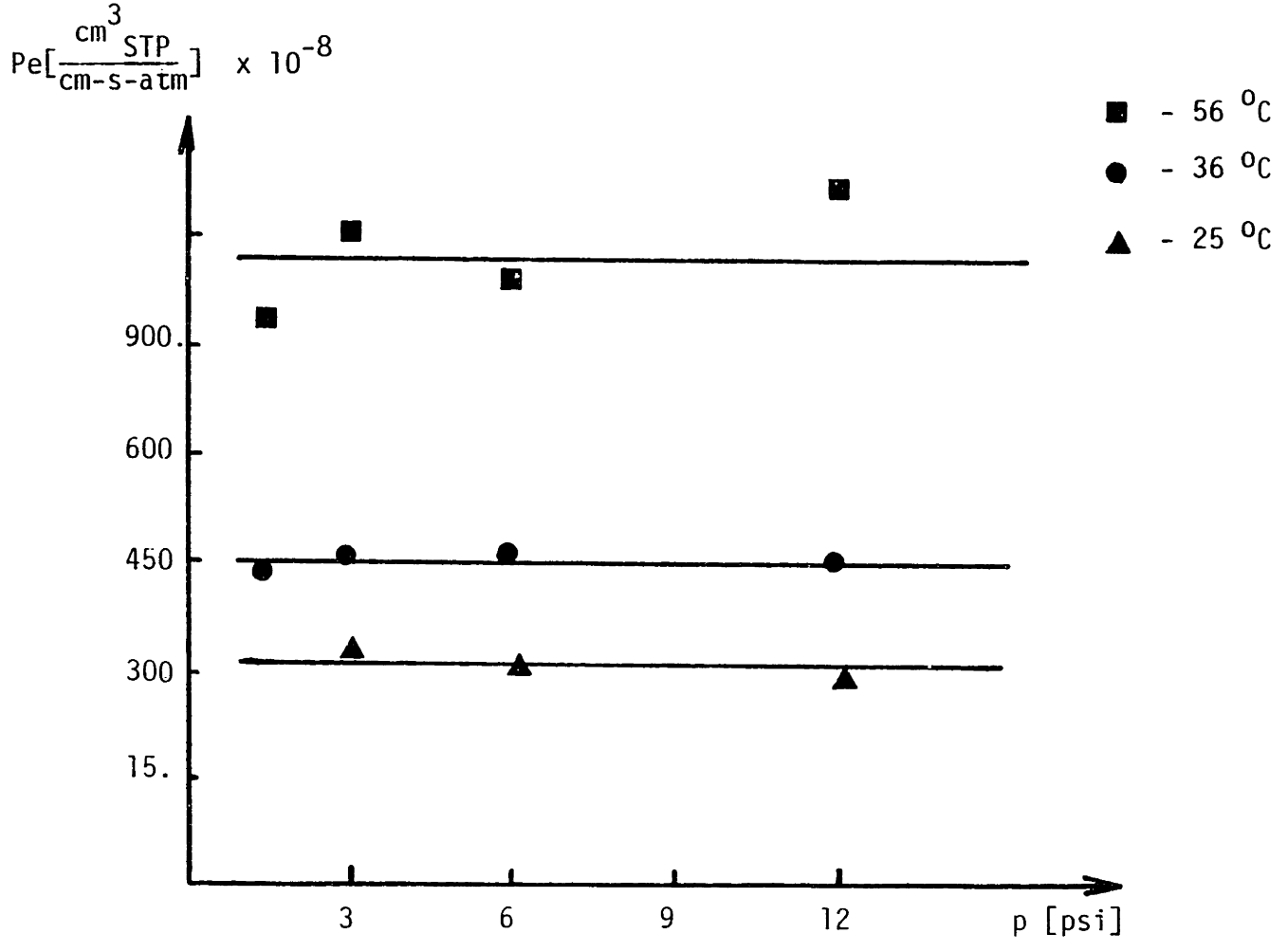

Fig. 9.1 FOAM PERMEABILITY TO CO_2 AS A FUNCTION OF TEMPERATURE MEASURED AT FOUR DIFFERENT PRESSURE DIFFERENCES (Foam sample #2)

it does not rely on a model of the foam geometry and does not require the measurement of the foam geometrical parameters. Although it was developed for the testing of the polyurethane foam, it can be used for variety of closed-cell foams.

The highest temperature that foam can be exposed to limits the time gain obtained at elevated temperatures. After the foam sample #1 was kept at 90°C for 100 days, exposed to pressure difference of 60,500 Pa (8.5 psid) of fluorocarbon 11, its thickness decreased to 1/2 of the initial value although the cell walls were not demaged. Under the pressure load, fluorocarbon diffused out from the cells and the foam was compressed. Since the number of the cell walls, not the distance between them determines the resistance to permeation (equation (2.62)), the steady state results obtained are still valid. However, the effective diffusion coefficient should be based on the original foam thickness.

Values of the measured permeability and diffusion coefficients for the foam sample #1, #2 and #3, are given in Table 6 and Table 7 respectively. The foam sample #1 was tested at different temperatures, with N_2, O_2, CO_2 and fluorocarbon 11. Foam samples #2 and #3 were tested with CO_2 only, at 25 °C.

Figure 6.3 was frequently used during foam tests to determine if steady state profile was reached in a sample. For example, when a sample whose sides were exposed for 90 days to nitrogen with partial pressure ratio $p^* = .6$ was tested, chart (c) on the Figure 6.3 was used. The diffusion coefficient was measured to be 7.6×10^{-8} cm^2/s assuming steady state. For 1 cm thick sample Fo = 0.59. From Fig. 6.3

TABLE 6

MEASURED FOAM PERMEABILITY COEFFICIENT, $[cm^3_{STP}/cm\text{-}s\text{-}atm]$

Foam	Temp.	Pe_{CO2}	Pe_{O2}	Pe_{N2}	Pe_{R11}
#1	25°C	$202.\times10^{-8}$	46.8×10^{-8}	7.6×10^{-8}	.23 to $.57\times10^{-8}$*
	50°C	$488.\times10^{-8}$	$134.\times10^{-8}$	24.3×10^{-8}	1.6×10^{-8}
	75°C	-	-	70.8×10^{-8}	9.6×10^{-8}
	90°C			$166.\times10^{-8}$	24.3×10^{-8}
#2	25°C	$317.\times10^{-8}$	-	-	-
	36°C	$450.\times10^{-8}$	-	-	-
	56°C	$1100.\times10^{-8}$	-	-	-
#3	25°C	$1083.\times10^{-8}$	-	-	-

* Extrapolation of data at 50°C and 90°C gives $.20\times10^{-8}$

Foam sample #1: MDI, Density = 25.2 kg/m^3

Foam sample #2: MDI, Density = 28.3 kg/m^3

Foam sample #3: MDI, Density = 22.2 kg/m^3

TABLE 7

MEASURED FOAM DIFFUSION COEFFICIENT, [cm^2/s]

Foam	Temp.	Pe_{CO2}	Pe_{O2}	Pe_{N2}	Pe_{R11}
#1	25°C	$202.x10^{-8}$	$46.8x10^{-8}$	$7.6x10^{-8}$	.23 to. $57x10^{-8}$*
	50°C	$529.x10^{-8}$	$145. x10^{-8}$	$26.3x10^{-8}$	$1.7x10^{-8}$
	75°C	-	-	$82.7x10^{-8}$	$11.2x10^{-8}$
	90°C	-	-	$202. x10^{-8}$	$29.6x10^{-8}$
#2	25°C	$317.x10^{-8}$	-	-	-
	36°C	$467.x10^{-8}$	-	-	-
	56°C	$1214.x10^{-8}$	-	-	-
#3	25°C	$1083.x10^{-8}$	-	-	-

* Extrapolation of data at 50°C and 90°C gives $=.20x10^{-8}$

Foam sample #1: MDI, Density = 25.2 kg/m^3

Foam sample #2: MDI, Density = 28.3 kg/m^3

Foam sample #3: MDI, Density = 22.2 kg/m^3

we obtain $J_m^* = 0.98$, i.e the measured flux is approximately 98% of the steady state flux and the steady state assumption is justified.

9.3 The Successive Membrane Model

Table 8 presents a comparison of the effective diffusion coefficient predicted by the model (Equation (2.76)) and the measured effective diffusion coefficient for foam #1, #2, and #3 at 25°C. Since the effects of the open cells is not included in the model, the model somewhat underpredicts the foam effective diffusion coefficient.

One would expect that permeability of a foam to decrease as the foam density increases. However, foam #1 has smaller cells and thicker cell walls than foam #2 and therefore is less permeable. The model correctly predicts that the less dense foam #1 has lower diffusion coefficient than the more dense foam #2.

Foam #3 was specially fabricated to have the lowest density, 22.5 kg/m^3. At the same time, it has the largest average distance between the successive membranes, the thinnest cell walls, and a high percentage of open cells. The percent age of open cells for this foam was measured to be 26.9 %, while the closed cell polyurethane foams usually have 5 to 10% of open cells*. The model correctly predicts that this results in a very low permeation resistance, i.e., a very high diffusion coefficient. The model underpredicts the foam effective

---

* The measurement was done at Owens Cornning Fiberglas Technical Center, Granville, Ohio 43023.

TABLE 8

COMPARISON BETWEEN THE ANALYTICAL MODEL AND THE FOAM DATA

FOAM	GAS	SUCCESSIVE MEMBRANE MODEL $D_{eff}[cm^2/s]$	FOAM DATA $D_{eff}[cm^2/s]$	ERROR %
#1.,MDI type ρ=25.2kg/m^3 d=.412 mm t=.60x10^{-3}mm <l>=.274mm <l>/t=458	CO_2	15.33x10^{-7}	20.1 x10^{-7}	-23.7
	O_2	4.08x10^{-7}	4.68x10^{-7}	-12.8
	N_2	.73x10^{-7}	.76x10^{-7}	- 3.9
#2.,MDI type ρ=28.35kg/m^3 d=.51 mm t=.37x10^{-3}mm <l>=.34 mm <l>/t=919	CO_2	30.8 x10^{-7}	31.7 x10^{-7}	- .3
#3 ρ=22.5kg/m^3 d=.795 to 1.08mm <l>=.53 to .722 t=.28x10^{-3}mm <l>/t=1906 to 2597 open cells= 26.9 %	CO_2	66.5 to 87.x10^{-7}	108.3 x10^{-7}	-19.7 to -38.6

diffusion coefficient by 19.7 to 38.6 %, partially because the model does not account for the existance of the open cells. Unequal cells size was also observed in the SEM photographs of this foam. Because of that, the average distance between the cell walls in different photographs varied. Concequently, the modelled effective diffusion coefficient also varied, as shown in the Table 7.

9.4 The Electrical Analogy

The electrical analogy was used to measure: the resistance of the foam cell structure to permeation, the two-dimensional enhancement parameter, and the effect of the direction of staggereness on the effective diffusion coefficient.

It was shown in the Chapter 3 that the electrical model is very accurate. For P.C. board #2, (cosely packed hexagonals stagered normally to the concentration gradient),the enhancement parameter obtained by the electrical model was within .2% of the exact value obtained analyticaly for the hexagonal geometry.

The two-dimensional enhancement parameter for the foam sample #1 was measured to be $\varepsilon = 1.52$. This is in a very good agreement with the prediction of the analytical model for the two-dimensional geometry, $\varepsilon = \Pi/2$.

The electrical model combined with the cell wall thickness and permeability data was used to predict the foam effective diffusion

coefficient. In Table 9, the effective diffusion coefficients obtained by the electricsl model are compared to the foam data. The uncorrected electrical model, equation (3.5), underpredicts the foam data more than the analytical model, i.e., for 26% to 42%. The model was corrected to account for three-dimensional enhancement of permeation, i.e., equation (3.5) multiplied by $\varepsilon_{3-D}/\varepsilon_{2-D}$. The corrected electrical model, equation (3.16) gives a more accurate prediction of the effective diffusion coefficient, a prediction almost identical to the analytical model. The corrected electrical model also underpredicts the effective diffusion coefficient of CO_2, partially because the effect of the open cells was not included. The open cells represent zero resistance to diffusion, and should be modeled by zero electrical resistance. To account for the effect of the open cells, the same percent of the cell walls on a P.C. board should be randomlly selected and shortcuted, for example by painting them over with a line of silver paint. By doing this, we can adequately model the open cell walls like zero electrical resistance, while the total resistance of the circuit decreases.

9.5 The Computer Code

Figures 9.2 to 9.4 show the comparison between the effective thermal conductivity as predicted by the ECVA code and the data [11] obtained in long-term tests. The foam samples were aged under three different thermal environments:

TABLE 9

COMPARISON BETWEEN THE ELECTRICAL MODEL AND THE FOAM DATA

FOAM	GAS	ELECTRICAL MODEL, 2-D $D_{eff}[cm^2/s]$	ELECTRICAL MODEL, Corrected* $D_{eff}[cm^2/s]$	FOAM DATA $D_{eff}[cm^2/s]$
#1.,MDI type				
ρ =25.2kg/m^3	CO_2	11.66x10^{-7}	14.85x10^{-7}	20.1 x10^{-7}
d=.412 mm				
t=.60x10^{-3}mm	O_2	3.10x10^{-7}	3.95x10^{-7}	4.68x10^{-7}
<l>=.274mm				
<l>/t=458	N_2	.56x10^{-7}	.71x10^{-7}	.76x10^{-7}

* multiplied with 4/Π.

Values of the used cell wall permeabilty coefficients are given in the Table 4

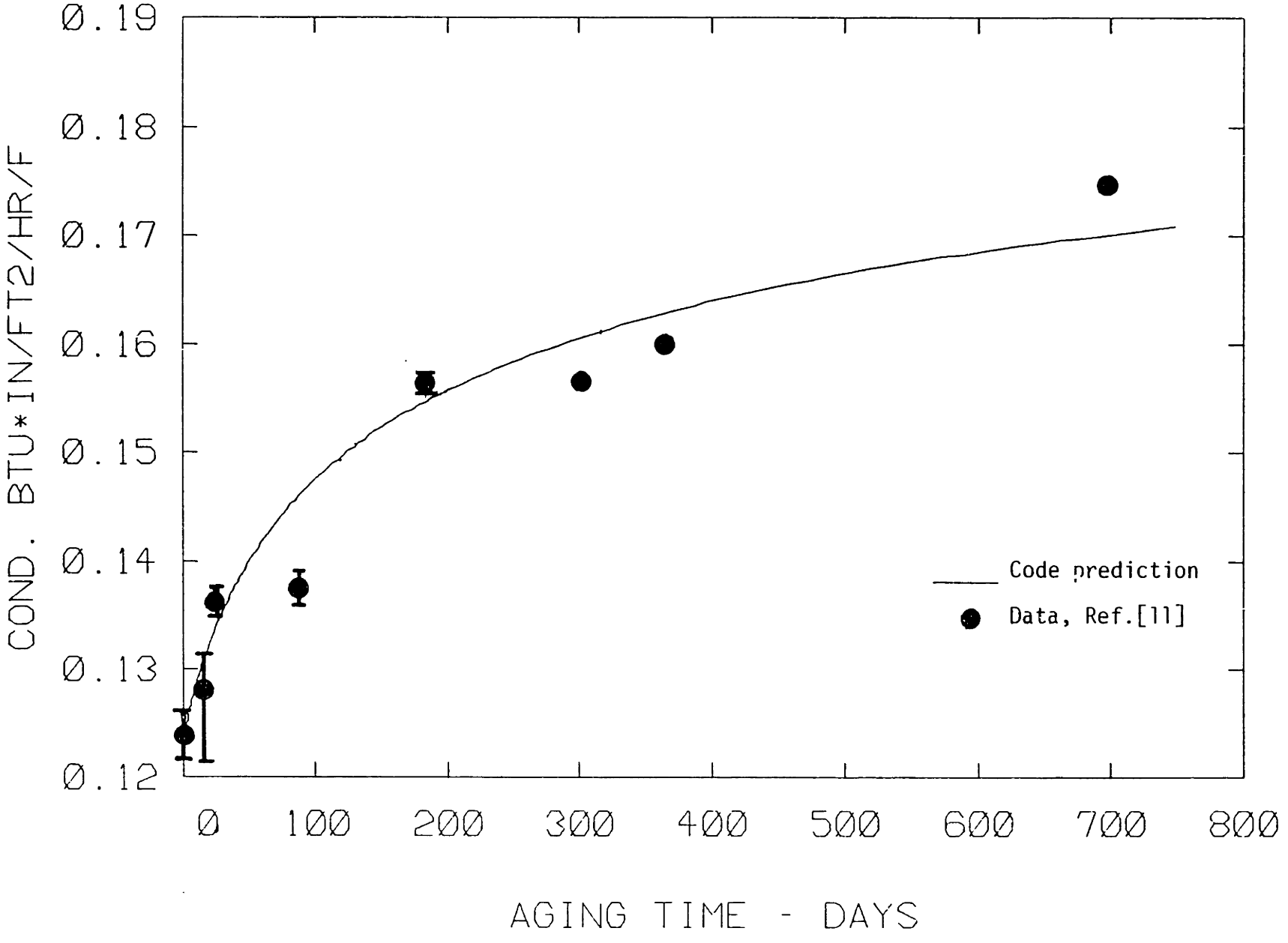

Fig. 9.2 EFFECTIVE THERMAL CONDUCTIVITY OF CLOSED CELL POLYURETHANE FOAM AS A FUNCTION OF AGING TIME
($T_1 = T_2 = 24\ ^{o}C$; $\rho = 28.35\ kg/m^3$; Specimen thickness = 5.1 cm)

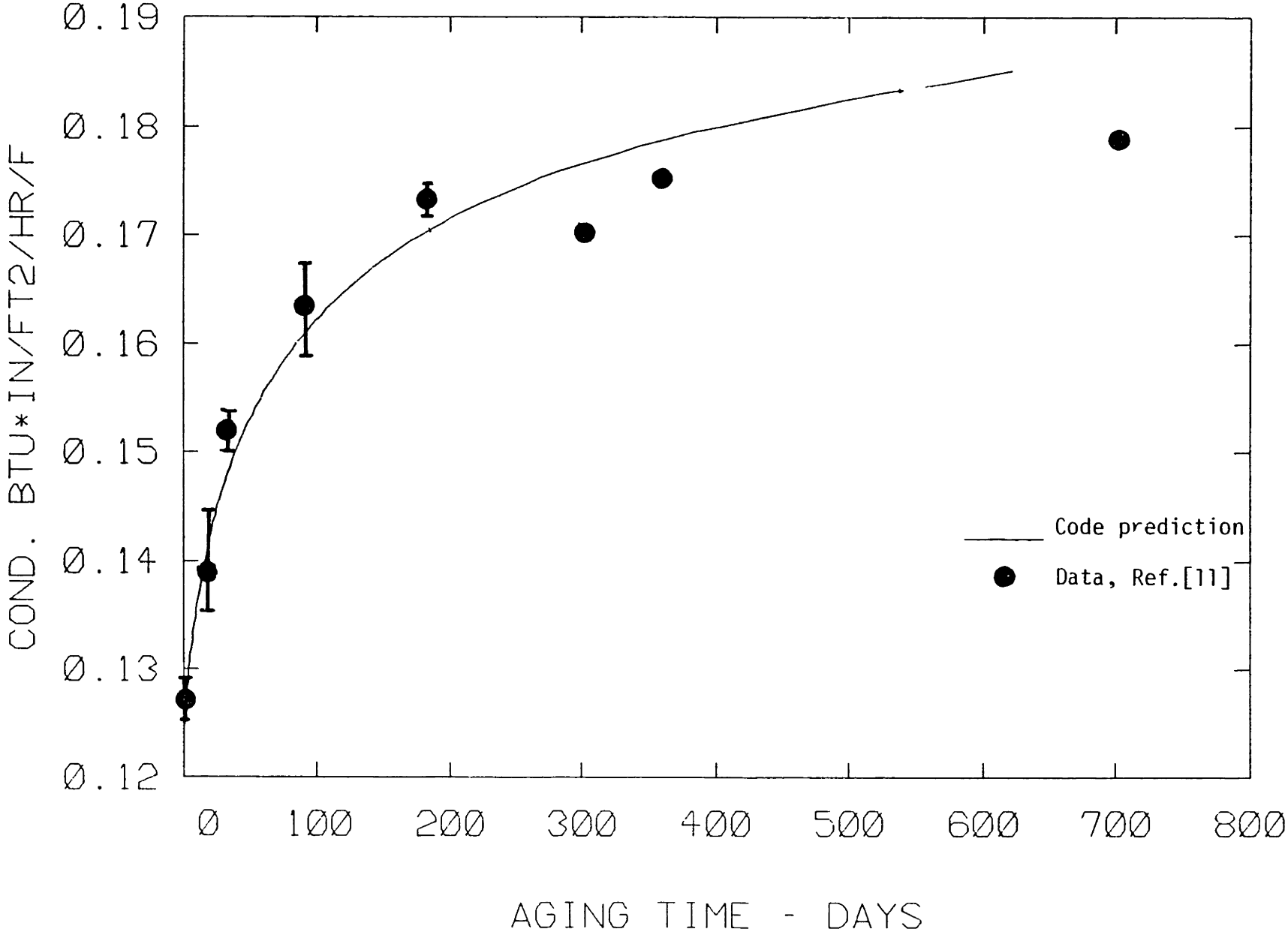

Fig. 9.3 EFFECTIVE THERMAL CONDUCTIVITY OF CLOSED CELL POLYURETHANE FOAM AS A FUNCTION OF AGING TIME
($T_1 = T_2 = 60\ ^{o}C$; $\rho = 28.83\ kg/m^3$; Specimen thickness = 5.1 cm)

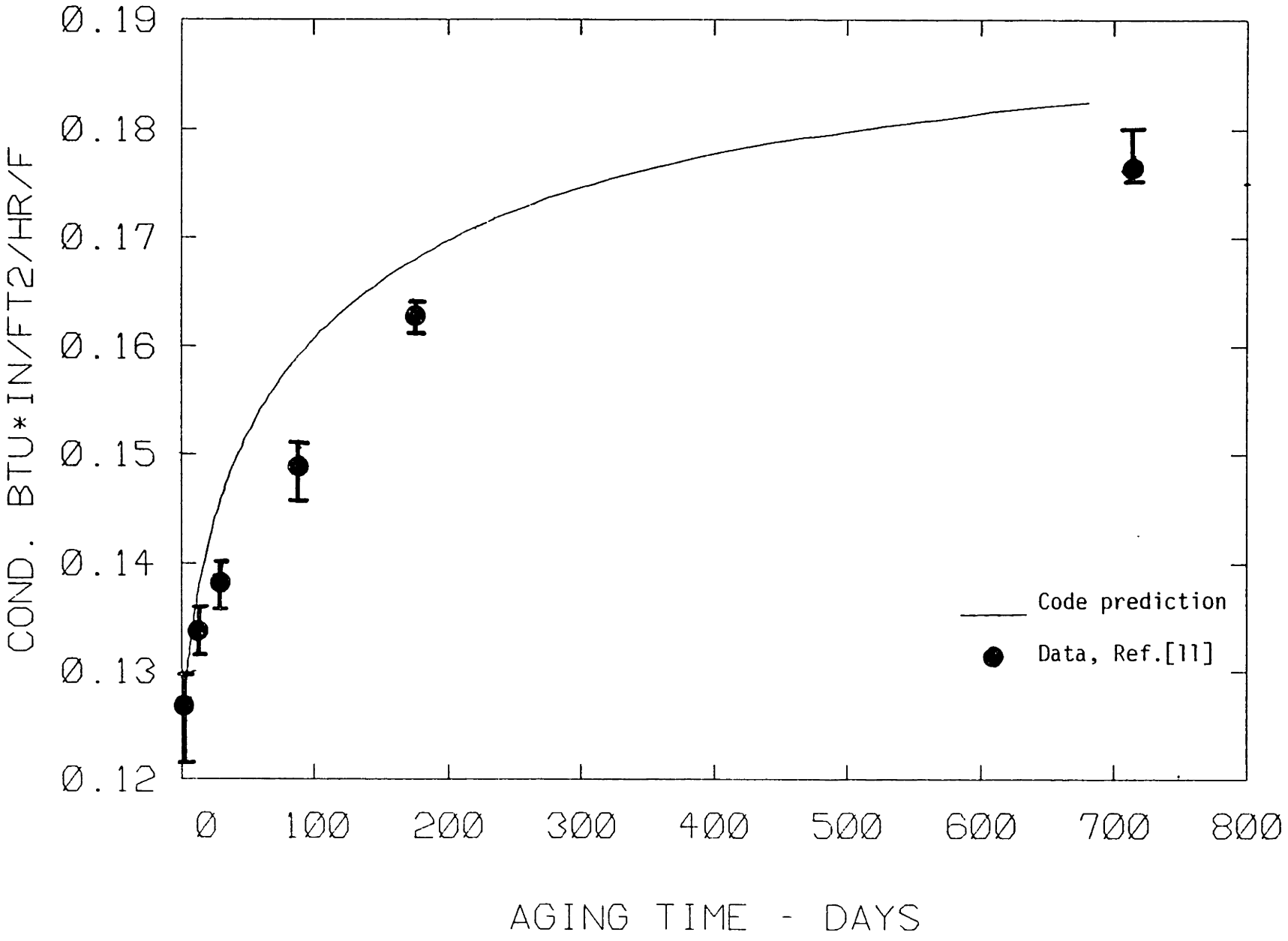

Fig. 9.4 EFFECTIVE THERMAL CONDUCTIVITY OF CLOSED CELL POLYURETHANE FOAM AS A FUNCTION OF AGING TIME
(T_1 = 24 ^{o}C, T_2 = 60 ^{o}C; ρ = 28.20 kg/m^3; Specimen thickness = 5.1 cm)

a) T_1 = 24 °C, T_2 = 24 °C; 4 samples tested.

b) T_1 = 60 °C, T_2 = 60 °C; 4 samples tested.

c) T_1 = 24 °C, T_2 = 60 °C; 4 samples tested,

where T_1 and T_2 are the temperatures imposed on the sides of the foam specimens.

The temperatures, T_1 and T_2, were given together with the sample thickness as an input to the computer program. The data given in Fig. 5.7 and Table 6 show that the effective foam permeability coefficient exhibits an exponential temperature dependance. Therefore, the data in Table 6 were interpolated by exponential curves and entered into the code in the form of coefficients of exponential equations. The coefficients of the exponential equations for N_2, O_2, CO_2 and fluorocarbon 11 are given in the Table 10.

The data on Figures 9.2 to 9.4 represent the average values of measurements performed on the four tested samples. The code prediction is within 6 % of the data, or better.

Fig. 9.5 and 9.6 show the code prediction of the change of the partial pressure of N_2, O_2, CO_2 and fluorocarbon 11 with the aging time at the center line and at the surface of 2.54 cm thick sample exposed to room temperature. It can be seen that the partial pressures change much faster in the surface node than in the node at the center line. After 10^{+4} days only a small amount of fluorocarbon 11 is left in the foam sample.

Fig. 9.7 shows the change of the effective conductivity of 2.54 cm thick foam panel exposed to room temperature for 10^{+4} days.

Fig. 9.8 shows the code predictions for the change of the

TABLE 10

COEFFICIENTS FOR THE EQUATION $Pe_{eff} = Pe_0 \exp(-E/RT)$

(computed from the data in TABLE 5)

GAS	PeO [cm^3_{STP}/cm-s-atm]	E/R [°K]
CO2	.1797	3396.
O2	.3737	4050.
N2	.2535	4476.
R11	842.715	7974.

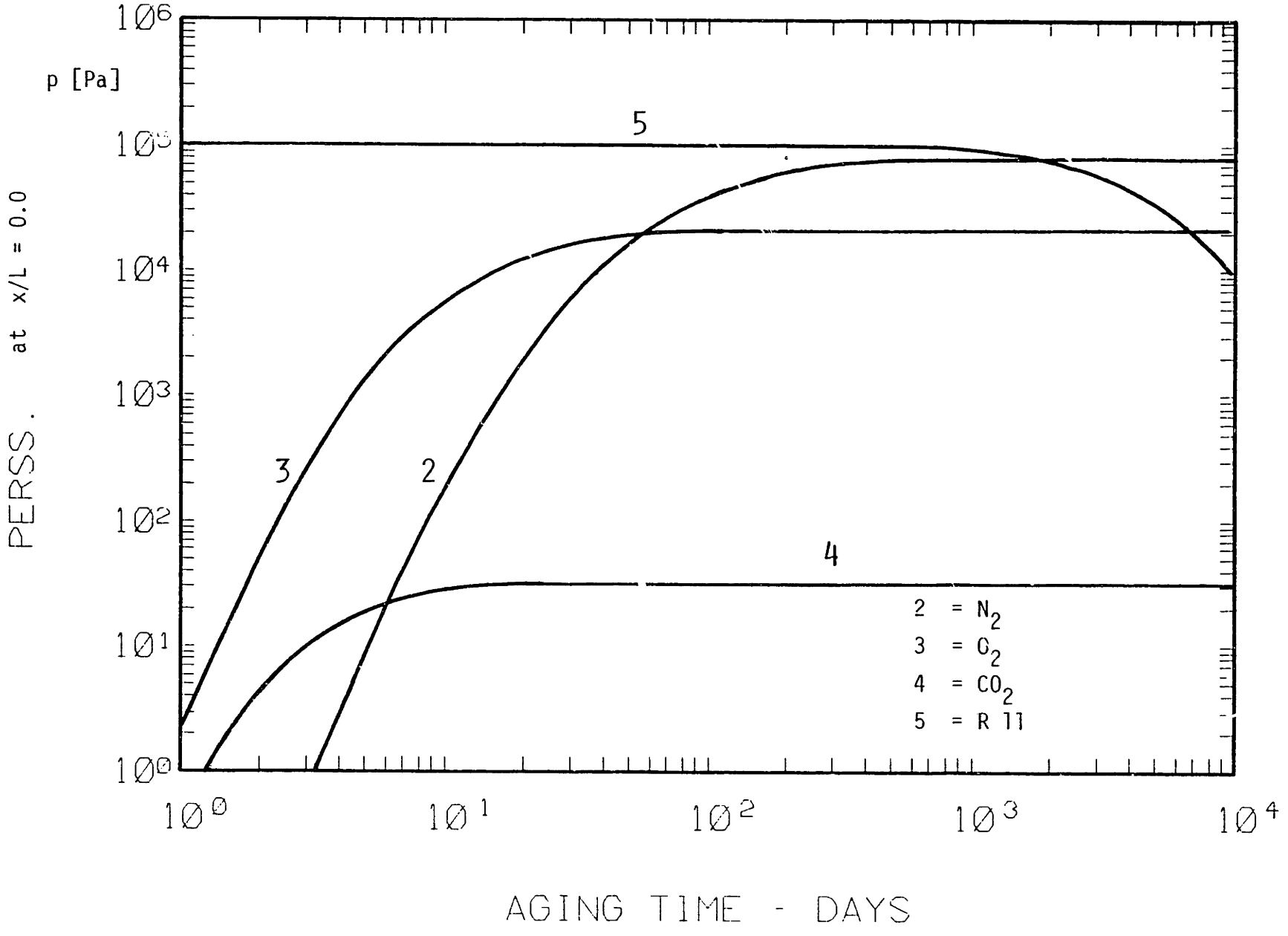

Fig. 9.5 PARTIAL PRESSURE OF N_2, O_2, CO_2, AND FLUOROCARBON 11 AS A FUNCTION OF THE AGING TIME ($T_1 = T_2 = 25^{o}C$; Specimen thickness = 2.54 cm; Center line node)

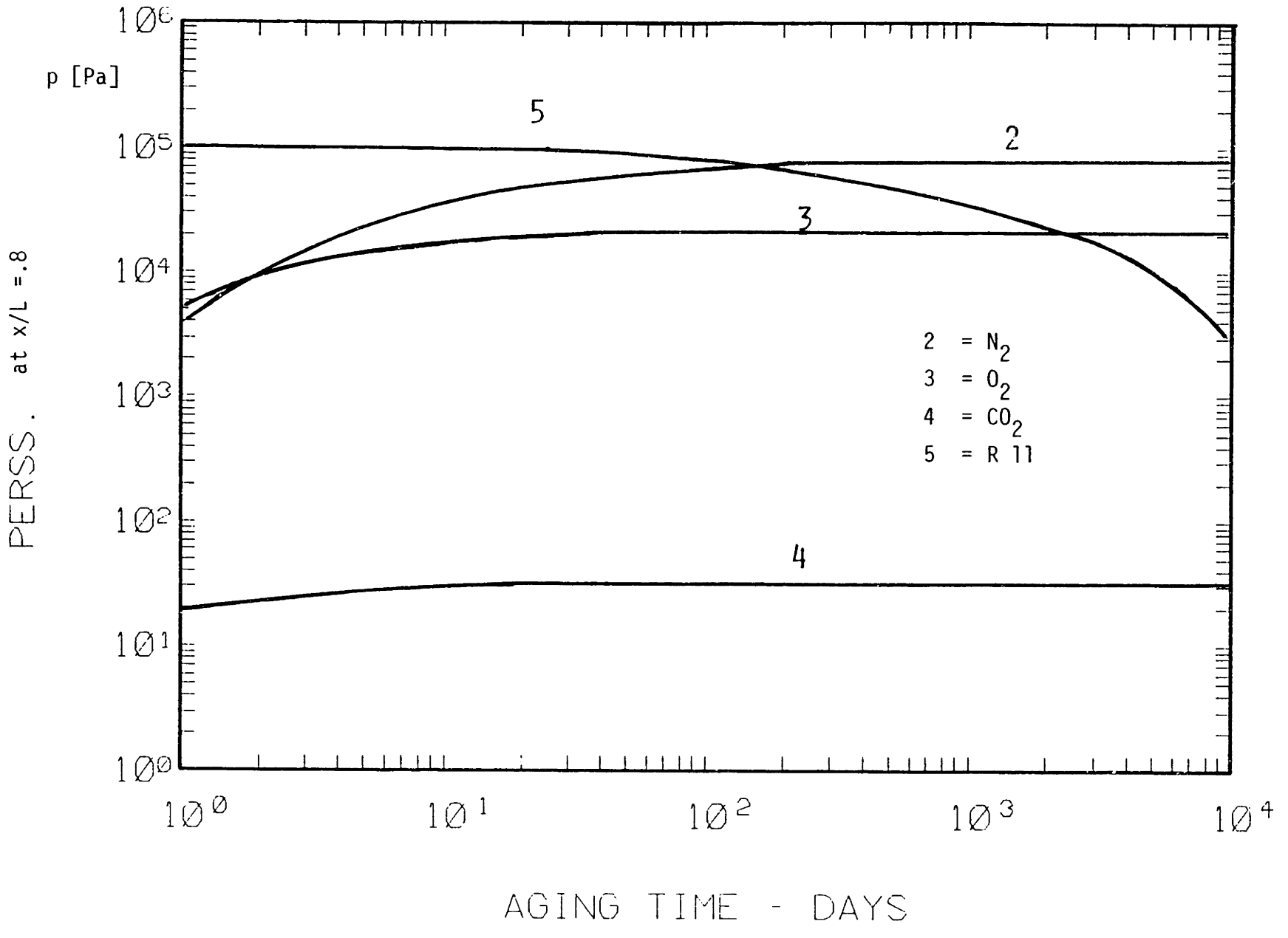

Fig. 9.6 PARTIAL PRESSURE OF N_2, O_2, CO_2 AND FLUOROCARBON 11 AS A FUNCTION OF THE AGING TIME ($T_1 = T_2 = 25\ ^{o}C$; Specimen thickness = 2.54 cm; Next to surface node)

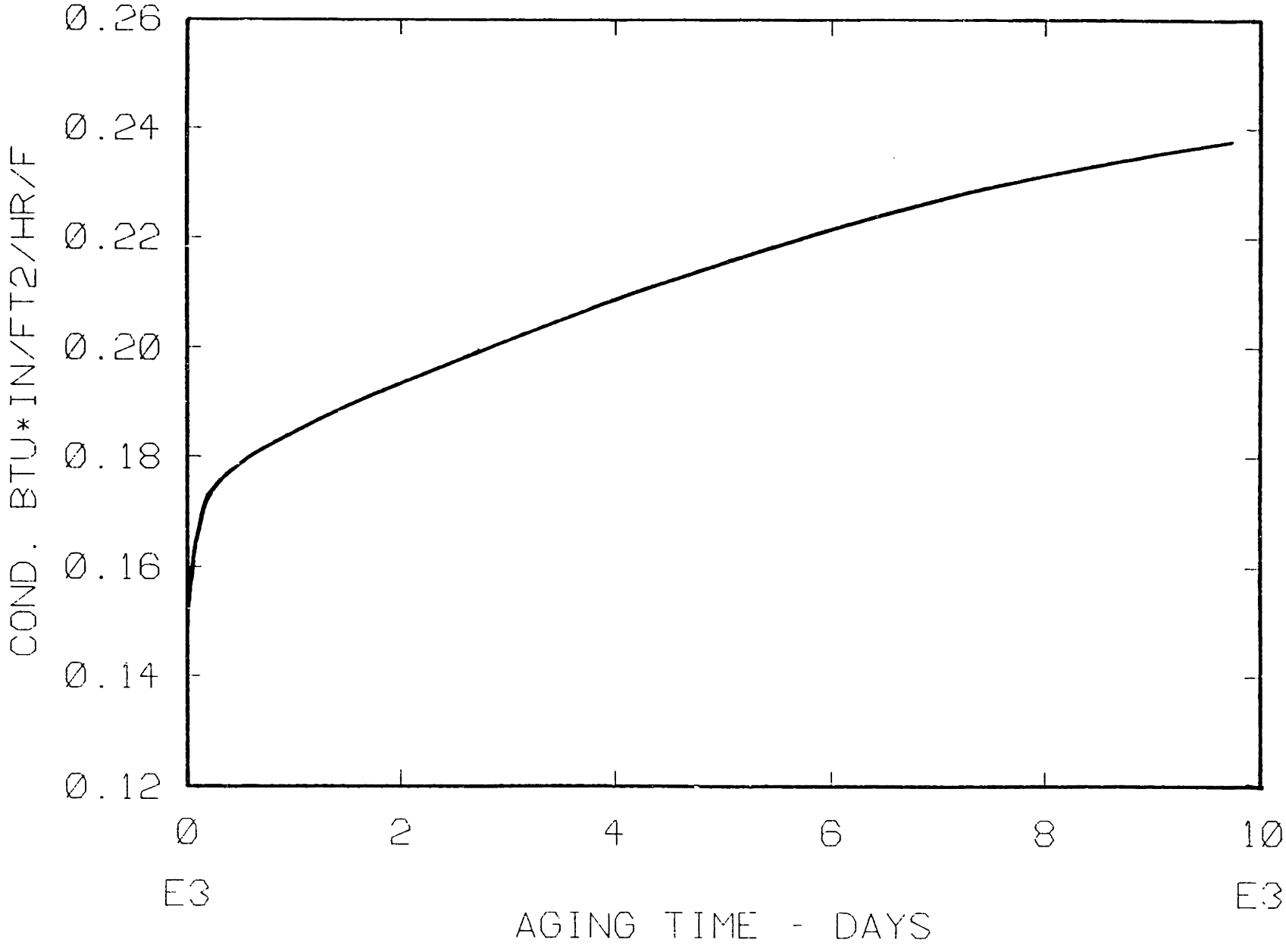

Fig. 9.7 EFFECTIVE CONDUCTIVITY OF A FOAM PANEL AS A FUNCTION OF THE AGING TIME
($T_1 = T_2 = 25\ ^{o}C$; Panel thickness = 2.54 cm)

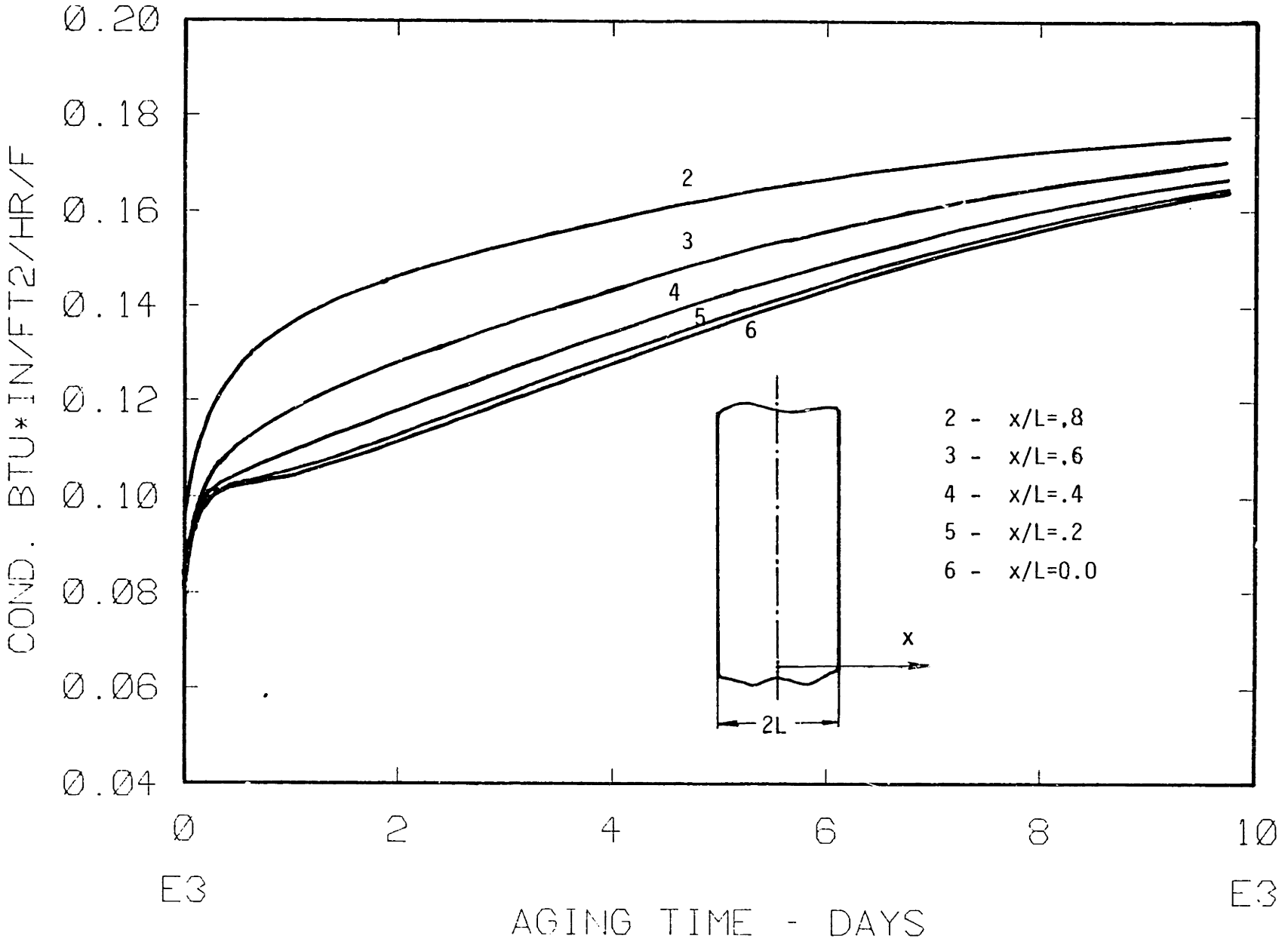

Fig 9.8 GAS MIXTURE CONDUCTIVITY INSIDE A FOAM PANEL AS A FUNCTION OF THE AGING TIME
($T_1 = T_2 = 25\ ^{o}C$; Panel thickness = 2.54 cm)

conductivity of the gas mixture inside the foam panel with the aging time up to 10^{+4} days, and at different axial positions.

9.6 Diffusion Barriers

The permeability tests of the foil materials have shown that aluminum foils present infinite diffusion resistance compared to the diffusion resistance of the foam. On contrary, the felt material is porous and offers no resistance to gas molecules.

Typical results of the leak test are shown on Fig. 8.2. These results indicate that open paths exist parallel to the foam/foil interface. The open paths have a diameter much greater than the mean free path of the air molecules. Their diameters are probably equal to the diameter of foam cells. Thus the surface of the foam underneath the facing are exposed to air through the open paths, in effect bypassing the facings.

Results obtained by the dye tests are shown on Fig 9.9 to 9.11. The ratio of the dyed to the undyed area of the foam/foil interface presents the porosity of the interface according to the equation (8.12). It can be readily shown that a faced foam having as many pores as the foam in Fig. 9.9 ages almost as fast as the unfaced foam.

The dye test also pointed out the existance of porous layers inside the foam. The layer appears as a plane parallel to the surface. several cell diameters away from the one of the interfaces of aluminum faced foams, Fig. 9.10. In all tested samples the foil interface adjacent to the porous foam layer is not porous, Fig. 9.10. The other

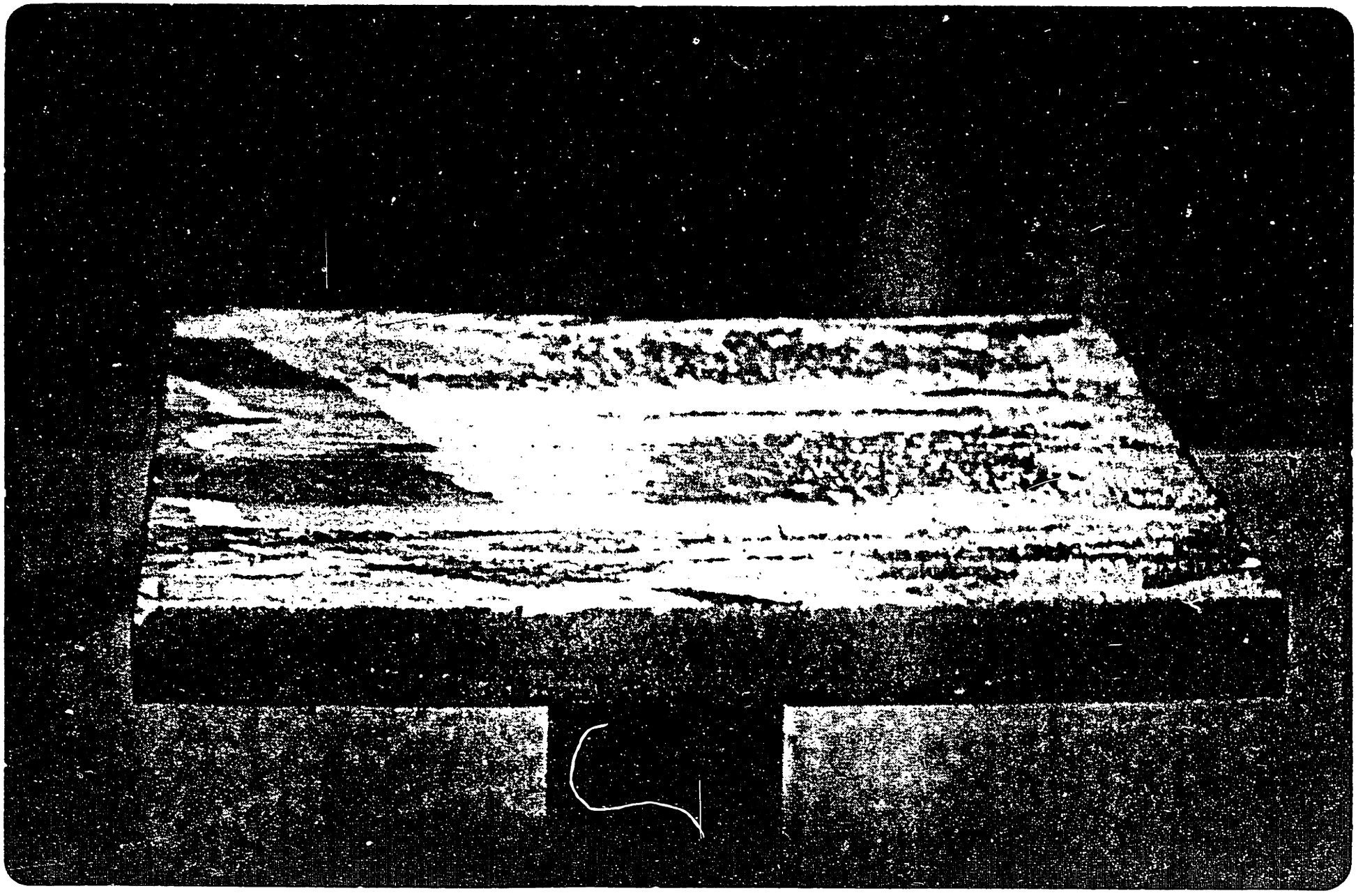

Fig. 9.9 [illegible] POROUS FOAM/[illegible] INTERFACE [illegible]

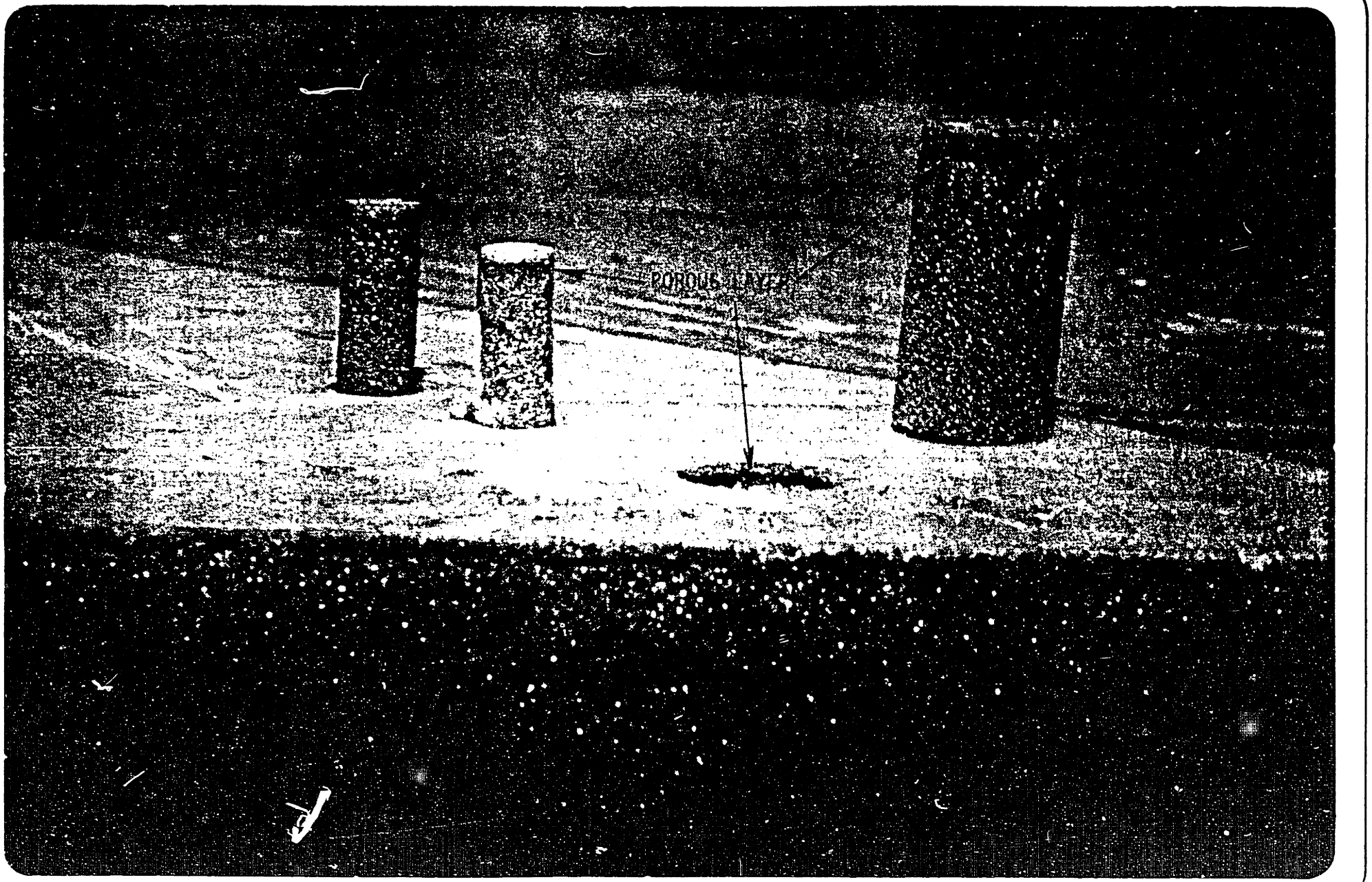

Fig. 9.10 PHOTOGRAPH OF A POROUS LAYER SEVERAL CELL DIAMETERS AWAY FROM THE INTERFACE OBTAINED BY [illegible] TECHNIQUE

interface was found to be very porous in all tested samples.

10. CONCLUSION

It was shown that gas diffusion in closed-cell foams is driven by partial pressure only and not by temperature gradient.

The value of the foam effective thermal conductivity can be predicted rapidlly and accurately by the developed ECVA code, when the diffusion coefficients of N_2, O_2, CO_2 and fluorocarbon 11 are known. The code can predict the aging rate in different thermal enviriioments. Therefore, for specific operating conditions the foam aging rate can be estimated more accurately by use of the code than by extrapolation of the data obtained in long-term or accelerated aging tests that are at present performed by industry.

The effective diffusion coefficient can be obtained with sufficiant accuracy from the analytical or electrical model, or can be measured directly by the rapid steady state technique. The analytical model will be imporved adequately by taking into account the effect of the open cells.

For reliable use of the analytical and electrical models in variety of closed cell foams, more data on the permeability of the cell walls having different chemical composition are needed.

The rapid steady state foam test enables accurate and reliable measurement of the foam effective diffusion coefficient. The rapid test is at least ten times faster than the long term steady state tests, with equal accuracy. Compared to the accelerated aging tests, the rapid steady state foam test is a factor of 5 to 25 faster,

depending on the thickness of the foam panels.

Most of the presently used diffusion barriers were found to be inefficient. The tests developed for the diffusion barriers enable fast tests of the facing efficiency and allow for fast feed-backed between production conditions and quality of the facing.

It was found that porrous layers exist at the foam/facing interface and inside of the poam panels. By eliminating these layers, the aging performance of the foam can be substantialy improved.

REFERENCES

1. Federal Register, Vol 44, #167, August 27, 1979.
2. Cuddihy, E.F., Moacanin, J., "Diffusion of Gases in Polymeric Foams", J.of Cellular Plastics 3, pp. 73-80 (1967).
3. Norton, F.J., "Diffusion of Chlorofluoro Carbon Gases in Polymer Films and Foams", J. of Cellular Plastics, pp. 300-318 (1982).
4. Reitz, D.W., Schuetz, M.A., Glicksman, L.R., "A Basic Study of Aging of Foam Insulation", J. of Cellular Plastics, 20, 2, pp. 104-113, (1984).
5. Hallinan, M.R., Himmler, W.A., Kaplan, M., "Advances in the Technology of Rigid Urethane Foams", Eighteenth Annual Technical Conference of the Society of Plastics Engineers, Sect. 20-4, 2 (1962).
6. Reitz, D.W.,"A Basic Study of Gas Diffusion in Foam Insulation", S.M. Thesis, Dept. of Mech. Eng., Massachusetts Institute of Technology (1983).
7. Lee W.M., Brown C.N., "Gas Permeability Determination in Urethane Foams", Journal of Thermal Insulation, Vol 6, Jan 1983.
8. Ball G.W., Hurd R., Walker M.G., "The Thermal Conductivity on Rigid Urethane Foams", Journal of Cellular Plastics, March/April 1970.
9. Norton, F.J., "Thermal Conductivity and Life of Polymer Foams", J. of Cellular Plastics 23, (1967).
10. Brandreth, D.A., Ingersole, H.G., "Accelerated Aging of Rigid Polyurethane Foam", unpublished report, E.I. du Pont de Nemours and Co., Wilmington, Delaware.

11. Bauman G., "R Value study of Rigid Polyurethane Foam, an S.P.I. Research Project", Proceedings of the S.P.I. Annual Conference, 1982.

12. Gibbs J.W., Scientific Papers, Dover, Reprint, Vol I and II, N.Y. 1961.

13. Levich V.G., Physicochemical Hydrodynamics, Prentice Hall Inc., 1962.

14. Onsager L., "Reciprocal Relations in Irreversible Processes I.", Physical Review, Vol 37,p. 405 - 426, February 15, 1931.

15. Onsager L., "Reciprocal Relations in Irreversible Processes II.", Physical Review, Vol 38,p. 405 - 426, December 15, 1931.

16. De Groot S.R., Thermodynamics of Ireversible Proceses, North-Holand Publishing Company, Amsterdam, 1951

17. Hatsopulos G.N., and Giftopulos E. P., Thermionic Energy Conversion, Vol. 2, Ch 8, M.I.T. Press Cambridge, 1980.

18. Geankoplis C.J., Mass Transfer Phenomena, Holt, Rinehard and Winston, Inc.

19. Van Krevelen D. W., Properties of Polymers, Elsevier, 1976.

20 Kreith F., Principles of Heat Transfer, International Textbook Company, Second Ed. 1967, p.92 to 96.

21. Encyclopedia of Polymer Science and Technology, Vol 9, John Wiley and Sons, Inc., 1968.

22. Carslaw H.S., Jaeger J.C., Conduction of Heat in Solids, Oxford University Press, Second Edition, 1959.

23. Shirtlliffe C. J., "Establishing Steady State Thermal Conditions in Flat Slab Speciments", ASTM Special Technical Publication, 544

24. Tsederberg N.V., Thermal Conductivity of Gases and Liquids, The

M.I.T. Press, 1965.

25. Arpaci V. S., Conduction Heat Transfer, Addison-Wesley Publishing Comp., 1966

26. Roth A., Vacuum Technology, North-Holland Publishing Company, 1976.

APPENDIX I
CONVERSION FACTORS FOR QUANTITIES IN GAS DIFFUSION USED IN THE PRESENT RESEARCH

1) Conversion into Centimeter, Gram, Second, (CGS) System of Units

NAME OF THE USED QUANTITY	(USED UNITS)	x (CONVERSION FACTOR)			= (CGS UNITS)
		N_2	O_2	CO_2	
mass	[cm^3_{STP}]	1.134E-3	1.292E-3	1.785E-3	[g]
concentration	[cm^3_{STP}/cm^3]	1.134E-3	1.292E-3	1.785E-3	[g/cm^3]
permeability	[sm^3_{STP}/cm-s-atm]	1.112E-3	1.267E-3	1.750E-3	[g/sm-s-bar]*
solubility	[cm^3_{STP}/cm^3-atm]	1.112E-3	1.267E-3	1.750E-3	[g/cm^3-bar]*
Diff. coeff.	[cm^2/s]	1	1	1	[cm^2/s]

* 1bar = 10^{+6} dyn/cm^2=10^{+5} Pa; 1dyn = 1 g-cm/s2 = 10^{-5} N

2) Conversion into Meter, Kilogram, Second, (MKS) System of Units

NAME OF THE USED QUANTITY	(USED UNITS)	x (CONVERSION FACTOR)			= (MKS UNITS)
		N_2	O_2	CO_2	
mass	[cm^3_{STP}]	1.134E-6	1.292E-6	1.785E-6	[kg]
concentration	[cm^3_{STP}/cm^3]	1.134	1.292	1.785	[kg/m^3]
permeability	[sm^3_{STP}/cm-s-atm]	1.112E-9	1.267E-9	1.750E-9	[kg/m-s-Pa]
solubility	[cm^3_{STP}/cm^3-atm]	1.112E-5	1.267E-5	1.750E-5	[kg/m^3-Pa]
Diff. coeff.	[cm^2/s]	1E-4	1E-4	1E-4	[m^2/s]

3) Some Other Units for Permeability

(USED UNITS)	x (CONVERSION FACTOR)	= (OTHER UNITS)
[cm^3_{STP}/cm-s-atm]	1/7.6	[cm^3_{STP}-mm/cm2-s-cmHg]
[cm^3_{STP}/cm-s-atm]	2.212E+10	[cc-mil/100in^2-day-atm]

```
C        APPENDIX II: LISTING OF THE COMPUTER CODE ECVA
C A. OSTROGORSKY, M.I.T., FEB. 1985.
C
C THIS IS THE AGE PROGRAM.
C AGE COMPUTES THE 1-D TIME CHANGE OF THE
C         * GAS COMPOSITION
C         * GAS CONDUCTIVITY
C ISINDE OF AN INFINITE CLOSED CELL FOAMS LAB,
C AND ADDS IT TO THE CONDUCTIVITY OF SOLID AND
C CONDUCTANCE DUE TO RADIATION.
C
C THE INPUT PARAMETERS ARE
C
C GEOMETRY (METERS):
C         THICKNESS L
C
C INITIAL CONDITIONS:
C         TEMPERATURE  T1(Z=0)
C         TEMPERATURE  T2(Z=1)
C         PARTIAL PRESSURE OF N2
C         PARTIAL PRESSURE OF O2
C         PARTIAL PRESSURE OF CO2
C         PARTIAL PRESSURE OF FREON
C
C
      REAL PRESS0(5,200),PRESS2(5,200),PRESS3(5,200),PRESS4(5,200),
     1 PRESS5(5,200),XSCL(4),ARRKON(6,200),ARRK(2,200)
      REAL KGM(51),K(5),KSOL,KRAD,MOL(5)
      REAL AP(100),BP(100),CP(100),T(200,51)
      REAL AT(51),BT(51),CT(51),ACON(51)
      COMMON/BLK1/ PN2(200,51),PO2(200,51),PCO2(200,50),PFR(200,51),
     1 PTOT(51)
      COMMON/BLK7/ S(5),SS(5,5)
      COMMON/BLK2/ DN2(51),DO2(51),DCO2(51),DFR(51)
      COMMON/BLK6/ RN2,RO2,RCO2,RFR
      COMMON/BLK5/ PEN2O,PEO2O,PECO2O,PEFRO,EN2,EO2,ECO2,EFR
      COMMON/BLK8/IPR,DZ,DT,ITEMP
C
C
      OPEN(UNIT=6,FILE='M.OUT',STATUS='NEW')
      R=8314.
      RN2=R/28.
      RO2=R/32.
      RCO2=R/44.
      RFR=R/137.4
      IT=1
      ITIME=1
      ILIN=0
      IPR=2
C
C MOL WEIGHTS:
      MOL(1)=28.
      MOL(2)=32.
      MOL(3)=44.
      MOL(4)=137.4
C CONST. FOR KG MIXTURE
      S(1)=1.5*(273.-195.8)
      S(2)=1.5*(273.-182.962)
      S(3)=1.5*(273.-78.476)
```

```
      S(4)=1.5*(273.+10.)
      DO 20 I=1,4
      DO 20 J=1,4
   20 SS(I,J)=(S(I)*S(J))**.5
C
C
      WRITE(6,110)
  110 FORMAT(3X,'THIS IS THE "AGE" PROGRAM.',/,
     1'   AGE WAS WRITEN AT M.I.T. BY A. G. OSTROGORSKY UNDER THE',/,
     1'   GUIDANCE OF L. R. GLICKSMAN.',//,
     1'   AGE COMPUTES 1-D CHANGE WITH TIME OF:',/,
     1'          * GASS PARTIAL PRESSURE IN THE FOAM CELLS',/,
     2'          * MIXTURE KONDUCTIVITY IN THE FOAM CELLS',/,
     3'          * TOTAL CHANGE OF THE FOAM CONDUCTANCE.',//)
C
C  R E A D  T H E  I N P U T  F I L E  MAIN.DAT
C
      OPEN(UNIT=4,FILE='M.DAT',STATUS='OLD')
      READ(4,*)THIC,NZ,TIME,DTI,IPR,ITEMP,
     1 PEN2O,EN2,PEO2O,EO2,PECO2O,ECO2,PEFRO,EFR,
     2 T(1,NZ),T(1,1),
     2 PN2(1,2),PO2(1,2),PCO2(1,2),PFR(1,2),
     3 KSOL,KRAD
C
C
      DT=DTI
      DZ=THIC/(NZ-1)
      NT=TIME/DTI
      DTI=DTI*3600.*24.
      WRITE(6,178)DT,TIME,NZ,DZ
  178 FORMAT(3X,'INITIAL TIME STEP(DAYS)=',F6.2,/,
     1 '   AGING TIME (DAYS)=',F8.2,/,
     2 '   # OF NODES      =',I8,/,
     3 '   NODE (CM)       =',F8.2,//)
C CONVERT TIMES TO SEC.
      DT=DTI
      TIME=3600.*24.*TIME
C
C COMPUTE THE CONSTANT MATRIX COEF.
      DO 6 IZ=1,NZ
      BP(IZ)=1.
    6 CP(IZ)=1.
C
C SET INITIAL FOAM TEMPERATURE = 25 C
      DO 66 IZ=2,NZ-1
   66 T(1,IZ)=298.
C
C PARTIAL PRESS. OUTSIDE THE FOAM (STANDARD PARTIAL
C PRESSURES COND.):
      PPP=1.0132E+5
      PN2(1,1)=.78084*PPP
      PN2(1,NZ)=.78084*PPP
      PO2(1,1)=.2095*PPP
      PO2(1,NZ)=.2095*PPP
      PCO2(1,1)=.000314*PPP
      PCO2(1,NZ)=.000314*PPP
      PFR(1,1)=0.0*PPP
      PFR(1,NZ)=0.0*PPP
```

```
      WRITE(6,103)
  103 FORMAT(3X,'INITIAL PRESSURE INSIDE THE FOAM @ 25 C',//,
     1 '                PN2            PO2            PCO2            PFR')
C
C COMPUTE THE INITIAL PARTIAL PRESSURES IN THE FOAM:
C
      DO 11 IZ=3,NZ-1
      PN2(1,IZ)=PN2(1,2)
      PO2(1,IZ)=PO2(1,2)
      PCO2(1,IZ)=PCO2(1,2)
      PFR(1,IZ)=PFR(1,2)
   11 CONTINUE
      DO 108 IZ=1,NZ
    9 WRITE(6,111)IZ,PN2(1,IZ),PO2(1,IZ),PCO2(1,IZ),PFR(1,IZ)
  111 FORMAT(3X,'# =',I2,'    ',E11.4,'    ',E11.4,
     1'    ',E11.4,'    ',E11.4)
  108 CONTINUE
C
C
C TEMP. PROFILE IS LINEAR
C
      T(2,1)=T(1,1)
      T(2,NZ)=T(1,NZ)
      DO 4 IZ=1,NZ-2
      T(2,IZ+1)=T(1,1)+IZ*(T(1,NZ)-T(1,1))/(NZ-1)
    4 CONTINUE
C
C *************** TIME DEPENDANT LOOP ******************************
C
      IT=0
 2000 CONTINUE
      IT=IT+1
      TIM=TIM+DT
      IF(TIM.GT.TIME)GOTO 1000
C
C SET THE B.C
C PRESSURE:
      PN2(IT+1,1)=PN2(1,1)
      PN2(IT+1,NZ)=PN2(1,1)
      PO2(IT+1,1)=PO2(1,1)
      PO2(IT+1,NZ)=PO2(1,1)
      PCO2(IT+1,1)=PCO2(1,1)
      PCO2(IT+1,NZ)=PCO2(1,1)
      PFR(IT+1,1)=PFR(1,1)
      PFR(IT+1,NZ)=PFR(1,1)
C TEMPERATURE:
      T(IT+2,1)=T(1,1)
      T(IT+2,NZ)=T(1,NZ)
C
      IF(IPR.LT.1)GOTO 113
      WRITE(6,114)
  114 FORMAT(//,3X,'IMPOSED TEMPERATURE IN THE FOAM:',/)
      DO 113 IZ=1,NZ
      WRITE(6,112)IZ,T(IT+1,IZ)
  112 FORMAT(3X,'NODE#=',I2,'      T=',F9.4)
  113 CONTINUE
C
C COMPUTE THE PRESSURE CHANGE DUE TO TEMPERATURE CHANGE
      DO 67 IZ=2,NZ-1
      PN2(IT,IZ)=PN2(IT,IZ)*T(IT+1,IZ)/T(IT,IZ)
```

```
      PO2(IT,IZ)=PO2(IT,IZ)*T(IT+1,IZ)/T(IT,IZ)
      PCO2(IT,IZ)=PCO2(IT,IZ)*T(IT+1,IZ)/T(IT,IZ)
   67 PFR(IT,IZ)=PFR(IT,IZ)*T(IT+1,IZ)/T(IT,IZ)
C
C COMPUTE THE CHANGE OF THE GASS PARTIAL PRESSURES
      CALL PPRESS(IT,NT,NZ,T,AP,BP,CP)
C
      DT1=DT/24./3600.
      TIM1=TIM/24./3600.
      IF(IPR.GE.1)WRITE(6,1800)IT+1,DT1,TIM1
 1800 FORMAT(//,3X,'LOOP #            =',I10,/,
     1 '   TIME  STEP (DAYS)=',F10.4,/,
     1 '   AGING TIME (DAYS)=',F10.4,/)
C
      IF(IPR.LT.2)GOTO 1801
      WRITE(6,1803)
 1803 FORMAT(3X,'NEW PRESSURE DUE TO TEMPERATURE CHANGE:',//,
     1 '   NODE#     PN2         PO2         PCO2         PFR         PTOT',/)
C
      DO 1801 IZ=1,NZ
      WRITE(6,802)IZ,PN2(IT,IZ),PO2(IT,IZ),
     1 PCO2(IT,IZ),PFR(IT,IZ),PTOT(IZ)
 1801 CONTINUE
C
C
      IF(IPR.LT.1)GOTO 801
      WRITE(6,800)IT+1
  800 FORMAT(//,3X,'TIME ST  #=',I5,
     1 '   NEW PRESSURE DUE TO DIFFUSION:',//,
     1 '   NODE#     PN2         PO2         PCO2         PFR         PTOT',/)
      DO 801 IZ=1,NZ
      WRITE(6,802)IZ,PN2(IT+1,IZ),PO2(IT+1,IZ),
     1 PCO2(IT+1,IZ),PFR(IT+1,IZ),PTOT(IZ)
  801 CONTINUE
  802 FORMAT(3X,I5,5E11.4)
C
C COMPUTE THE CONDUCTIVITY OF THE GASS MIHTURE
      CALL KMIX(IT,IZ,NZ,T,KGM,MOL)
C
      CON=0.0
      DO 711 IZ=1,NZ
      IF(IPR.GE.1)WRITE(6,710)IZ,KGM(IZ)
      CON=CON+KGM(IZ)
  711 CONTINUE
  710 FORMAT(3X,'K.GASS(',I2,') =',E12.5)
      CONAV=(CON-KGM(1)-KGM(NZ))/(NZ-2)
C
      IF(IPR.GE.1)WRITE(6,700)KSOL,KRAD
  700 FORMAT(//,3X,'K.SOLID     =',E12.5,/,
     2 '   K.RADIATION=',E12.5)
C
      AKTOT=KSOL+KRAD+CONAV
      IF(IPR.GE.1)WRITE(6,720)CONAV,AKTOT
  720 FORMAT(3X,'K.GAS AVE. =',E12.5,/,
     1 '   TOTAL COD. =',E12.5,/)
C
C PLOT THE RESULTS:
C
      NPT=IT
C
```

```
C KONDUCTIVITY
C
      ARRKON(1,IT)=TIM/24./3600.
      ARRKON(2,IT)=KGM(2)/.14413
      ARRKON(3,IT)=KGM(3)/.14413
      ARRKON(4,IT)=KGM(4)/.14413
      ARRKON(5,IT)=KGM(5)/.14413
      ARRKON(6,IT)=KGM(NZ/2+1)/.14413
C
      ARRK(1,IT)=TIM/24./3600.
      ARRK(2,IT)=AKTOT/.14413
C
C PRESSURES AT THE NODE 2
C
      PRESS2(1,IT)=TIM/24./3600.
      PRESS2(2,IT)=PN2(IT,2)
      PRESS2(3,IT)=PO2(IT,2)
      PRESS2(4,IT)=PCO2(IT,2)
      PRESS2(5,IT)=PFR(IT,2)
C
C PRESSURES AT NODE 3
C
      PRESS3(1,IT)=TIM/24./3600.
      PRESS3(2,IT)=PN2(IT,3)
      PRESS3(3,IT)=PO2(IT,3)
      PRESS3(4,IT)=PCO2(IT,3)
      PRESS3(5,IT)=PFR(IT,3)
C
C PRESSURES AT NODE 4
C
      PRESS4(1,IT)=TIM/24./3600.
      PRESS4(2,IT)=PN2(IT,4)
      PRESS4(3,IT)=PO2(IT,4)
      PRESS4(4,IT)=PCO2(IT,4)
      PRESS4(5,IT)=PFR(IT,4)
C
C 1) PRESSURES AT THE C.L.
C
      PRESS5(1,IT)=TIM/24./3600.
      PRESS5(2,IT)=PN2(IT,5)
      PRESS5(3,IT)=PO2(IT,5)
      PRESS5(4,IT)=PCO2(IT,5)
      PRESS5(5,IT)=PFR(IT,5)
C
C
C PRESSURES AT THE C.L.
C
      PRESSO(1,IT)=TIM/24./3600.
      PRESSO(2,IT)=PN2(IT,NZ/2+1)
      PRESSO(3,IT)=PO2(IT,NZ/2+1)
      PRESSO(4,IT)=PCO2(IT,NZ/2+1)
      PRESSO(5,IT)=PFR(IT,NZ/2+1)
C
C
      IF(DT.GT.8.6E+6)GOTO 1333
      DT=DTI+PN2(IT,NZ/2)/ABS(PN2(IT+1,NZ/2)-PN2(IT,NZ/2))*DTI
 1333 IF(DT.GT.8.64E+6)DT=8.64E+6
      IF(IT.GT.NT-1)GOTO 1000
C
C COMPUTE THE NEW TEMPERATURE
```

```
C
C COMPUTE THE FOAM RESISTANCE
      REZ=0.0
      DO 900 IZ=2,NZ-1
  900 REZ=REZ+DZ/KGM(IZ)
      REZT=1/(1/REZ+(KSOL+KRAD)/THIC)
C COMPUTE THE HEAT FLUX
      QFLUX=(T(IT+1,NZ)-T(IT+1,1))/REZT
      DO 905 IZ=2,NZ-1
      T(IT+2,IZ)=T(IT+2,IZ-1)+QFLUX*DZ/
     1 ((KGM(IZ-1)+KGM(IZ))/2.+KSOL/NZ+KRAD/NZ)
  905 CONTINUE
      IF(IPR.GE.1)WRITE(6,910)REZ,REZT,QFLUX
  910 FORMAT(3X,'R.GAS=',E12.5,'   R.TOT=',E12.5,
     1 '   HEAT FLUX=',E12.5,///)
C
      GO TO 2000
 1000 CONTINUE
C
C PLOT TE RESULRS:
      NROW=5
      NPTS=NPT-2
      XSCL(1)=1.
      XSCL(2)=10000.
      XSCL(3)=1.
      XSCL(4)=.12E+6
      CALL QPICTR(PRESS2,NROW,NPTS,QY(2,3,4,5),QX(1),
     1 QXLAB(' AGING TIME - DAYS'),QYLAB('PERSS. @ Z=.2'),QMOVE(0),
     2 QLABEL(4),QXSCL(XSCL),QISCL(28))
      CALL QPICTR(PRESS3,NROW,NPTS,QY(2,3,4,5),QX(1),
     1 QXLAB(' AGING TIME - DAYS'),QYLAB('PERSS. @ Z=.4'),QMOVE(0),
     2 QLABEL(4),QXSCL(XSCL),QISCL(28))
      CALL QPICTR(PRESS4,NROW,NPTS,QY(2,3,4,5),QX(1),
     1 QXLAB(' AGING TIME - DAYS'),QYLAB('PERSS. @ Z=.6'),QMOVE(0),
     2 QLABEL(4),QXSCL(XSCL),QISCL(28))
      CALL QPICTR(PRESS5,NROW,NPTS,QY(2,3,4,5),QX(1),
     1 QXLAB(' AGING TIME - DAYS'),QYLAB('PERSS. @ Z=.8'),QMOVE(0),
     2 QLABEL(4),QXSCL(XSCL),QISCL(28))
      CALL QPICTR(PRESS0,NROW,NPTS,QY(2,3,4,5),QX(1),
     1 QXLAB(' AGING TIME - DAYS'),QYLAB('PERSS. @ Z=1.'),QMOVE(0),
     2 QLABEL(4),QXSCL(XSCL),QISCL(28))

      NROW=6
      XSCL(1)=0.0
      XSCL(2)=10000.
      XSCL(3)=.050
      XSCL(4)=.190
C
C      CALL QPICTR(ARRKON,NROW,NPTS,QY(2,3,4,5,6),QX(1),
C     1 QXLAB(' AGING TIME - DAYS'),QYLAB('COND. BTU*IN/FT2/HR/F'),
C     2 QMOVE(0),QLABEL(4),QXSCL(XSCL),QISCL(-2))
C
      NROW=2
      XSCL(1)=0.0
      XSCL(2)=10000.
      XSCL(3)=.120
      XSCL(4)=.260
C
C      CALL QPICTR(ARRK,NROW,NPTS,QY(2),QX(1),
C     1 QXLAB(' AGING TIME - DAYS'),QYLAB('COND. BTU*IN/FT2/HR/F'),
```

```
C      2 QMOVE(0),QLABEL(4),QXSCL(XSCL),QISCL(-2))
C
       STOP
       END
C END OF THE MAIN PROGRAM
C
CCCCCCCCCCCCCCCCCCCCCCCCCCCCCCCCCCCCCCCCCCCCCCCCCCCCCCCCCCCCCCCCCCCCC
C
C
       SUBROUTINE PPRESS(IT,NT,NZ,T,AP,BP,CP)
C
       REAL AP(100),BP(100),CP(100),APRESS(51),QQQ(51),TTT(51)
       REAL T(200,51),L(100),D(100),U(100)
       COMMON/BLK1/ PN2(200,51),PO2(200,51),PCO2(200,50),PFR(200,51),
      1 PTOT(51)
       COMMON/BLK2/ DN2(51),DO2(51),DCO2(51),DFR(51)
       COMMON/BLK6/ RN2,RO2,RCO2,RFR
       COMMON/BLK5/ PEN2O,PEO2O,PECO2O,PEFRO,EN2,EO2,ECO2,EFR
       COMMON/BLK8/ IPR,DZ,DT,ITEMP
C
C THIS SUBROUTINE COMPUTES THE CHANGE OF GASS PARTIAL PRESSURE
C WITH TIME
C
C DIFUSION COEFICIENT AS FUNCTION OF TEMPERATURE
C
       IT1=IT+1
       IF(IPR.GT.3)WRITE(6,212)IT,NT,NZ
  212 FORMAT(//,3X,3I6,//)
C      NITROGEN DIFF. COEF.
       DO 10 IZ=2,NZ-1
       DN2(IZ)=PEN2O*EXP(-EN2/T(IT+1,IZ))*T(IT+1,IZ)/298.
       IF(IPR.GE.3)WRITE(6,213)IT,IZ,T(IT+1,IZ),EN2,PEN2O,RN2,DN2(IZ)
  213 FORMAT(3X,2I4,E12.5,3E12.3,'  DN2=',E11.4)
   10 CONTINUE
C
C      OXIGEN DIFF. COEF
       DO 12 IZ=2,NZ-1
   12  DO2(IZ)=PEO2O*EXP(-EO2/T(IT+1,IZ))*T(IT+1,IZ)/298.
C
C      CO2 DIF. COEF.
       DO 14 IZ=2,NZ-1
   14  DCO2(IZ)=PECO2O*EXP(-ECO2/T(IT+1,IZ))*T(IT+1,IZ)/298.
C
C      FREON DIFF. COEF.
       DO 16 IZ=2,NZ-1
   16  DFR(IZ)=PEFRO*EXP(-EFR/T(IT+1,IZ))*T(IT+1,IZ)/298.
CCC   16  DFR(IZ)=1.E-7/30.*3.5
C
       IF(IPR.GE.1)WRITE(6,18)
   18  FORMAT(//,'    C.V.#            DN2            DO2            DCO2',
      1 '             DFR')
       DO 17 IZ=2,NZ-1
       IF(IPR.GE.1)WRITE(6,19)IZ,DN2(IZ),DO2(IZ),DCO2(IZ),DFR(IZ)
   19 FORMAT(3X,I5,4E14.4)
   17 CONTINUE
C
C THE PRESSURE CHANGE FOR N2
C
       APRESS(2)=DZ*DZ/(DT*DN2(2)*.5)
       AP(2)=-(2.+APRESS(2))
```

```
      APRESS(NZ-1)=DZ*DZ/(DT*DN2(NZ-1)*.5)
      AP(NZ-1)=-(2.+APRESS(NZ-1))
      QQQ(2)=-(2.*PN2(IT,1)-PN2(IT,2)*
     1 (2.-APRESS(2))+PN2(IT,3))
      QQQ(NZ-1)=-(PN2(IT,NZ-2)-PN2(IT,NZ-1)*
     1 (2.-APRESS(NZ-1))+2.*PN2(IT,NZ))
C
      DO 600 IZ=3,NZ-2
      APRESS(IZ)=DZ*DZ/(DT*DN2(IZ)*.5)
      AP(IZ)=-(2.+APRESS(IZ))
      QQQ(IZ)=-(PN2(IT,IZ-1)-PN2(IT,IZ)*
     1 (2.-APRESS(IZ))+PN2(IT,IZ+1))
      IF(IPR.GE.3)WRITE(6,222)IT,IZ,AP(IZ),QQQ(IZ)
  222 FORMAT(5X,2I3,' AP=',E12.5,' QQQ=',E12.5)
  600 CONTINUE
      CALL LUDE(AP,BP,CP,L,D,U,NZ)
      CALL FBACK(L,D,U,QQQ,TTT,NZ)
C
      DO 610 IZ=2,NZ-1
      PN2(IT+1,IZ)=TTT(IZ)
  610 CONTINUE
C
      DO 623 IZ=1,NZ
      IF(IPR.GE.3)WRITE(6,622)IT1,IZ,PN2(IT+1,IZ)
  622 FORMAT(3X,' IT+1=',I3,'  IZ=',I3,'   P.N2=',E12.5)
  623 CONTINUE
C
C THE PRESSURE CHANGE FOR O2
C
      APRESS(2)=DZ*DZ/(DT*DO2(2)*.5)
      AP(2)=-(2.+APRESS(2))
      APRESS(NZ-1)=DZ*DZ/(DT*DO2(NZ-1)*.5)
      AP(NZ-1)=-(2.+APRESS(NZ-1))
      QQQ(2)=-(2.*PO2(IT,1)-PO2(IT,2)*
     1 (2.-APRESS(2))+PO2(IT,3))
      QQQ(NZ-1)=-(PO2(IT,NZ-2)-PO2(IT,NZ-1)*
     1 (2.-APRESS(NZ-1))+2.*PO2(IT,NZ))
C
      DO 609 IZ=3,NZ-2
      APRESS(IZ)=DZ*DZ/(DT*DO2(IZ)*.5)
      AP(IZ)=-(2.+APRESS(IZ))
      QQQ(IZ)=-(PO2(IT,IZ-1)-PO2(IT,IZ)*
     1 (2.-APRESS(IZ))+PO2(IT,IZ+1))
  609 CONTINUE
C
      CALL LUDE(AP,BP,CP,L,D,U,NZ)
      CALL FBACK(L,D,U,QQQ,TTT,NZ)
C
      DO 611 IZ=2,NZ-1
      PO2(IT+1,IZ)=TTT(IZ)
  611 CONTINUE
C
      DO 635 IZ=1,NZ
      IF(IPR.GE.3)WRITE(6,634)IT1,IZ,PO2(IT+1,IZ)
  634 FORMAT(3X,' IT+1=',I3,'  IZ=',I3,'   P.O2=',E12.5)
  635 CONTINUE
C
C THE PRESSURE CHANGE FOR CO2
C
      APRESS(2)=DZ*DZ/(DT*DCO2(2)*.5)
```

```
      AP(2)=-(2.+APRESS(2))
      APRESS(NZ-1)=DZ*DZ/(DT*DCO2(NZ-1)*.5)
      AP(NZ-1)=-(2.+APRESS(NZ-1))
      QQQ(2)=-(2.*PCO2(IT,1)-PCO2(IT,2)*
     1 (2.-APRESS(2))+PCO2(IT,3))
      QQQ(NZ-1)=-(PCO2(IT,NZ-2)-PCO2(IT,NZ-1)*
     1 (2.-APRESS(NZ-1))+2.*PCO2(IT,NZ))
CCCCCCCCCCCCCCCCCCCCCCCCCCCC
      DO 608 IZ=3,NZ-2
      APRESS(IZ)=DZ*DZ/(DT*DCO2(IZ)*.5)
      AP(IZ)=-(2.+APRESS(IZ))
      QQQ(IZ)=-(PCO2(IT,IZ-1)-PCO2(IT,IZ)*
     1 (2.-APRESS(IZ))+PCO2(IT,IZ+1))
 608  CONTINUE
C
      CALL LUDE(AP,BP,CP,L,D,U,NZ)
      CALL FBACK(L,D,U,QQQ,TTT,NZ)
C
      DO 612 IZ=2,NZ-1
      PCO2(IT+1,IZ)=TTT(IZ)
 612  CONTINUE
C
      DO 637 IZ=1,NZ
      IF(IPR.GE.3)WRITE(6,624)IT1,IZ,PCO2(IT+1,IZ)
  624 FORMAT(3X,' IT+1=',I3,'  IZ=',I3,'   P.CO2=',E12.5)
  637 CONTINUE
C
C THE PRESSURE CHANGE FOR FR
C
      APRESS(2)=DZ*DZ/(DT*DFR(2)*.5)
      AP(2)=-(2.+APRESS(2))
      APRESS(NZ-1)=DZ*DZ/(DT*DFR(NZ-1)*.5)
      AP(NZ-1)=-(2.+APRESS(NZ-1))
      QQQ(2)=-(2.*PFR(IT,1)-PFR(IT,2)*
     1 (2.-APRESS(2))+PFR(IT,3))
      QQQ(NZ-1)=-(PFR(IT,NZ-2)-PFR(IT,NZ-1)*
     1 (2.-APRESS(NZ-1))+2.*PFR(IT,NZ))
C
      DO 607 IZ=3,NZ-2
      APRESS(IZ)=DZ*DZ/(DT*DFR(IZ)*.5)
      AP(IZ)=-(2.+APRESS(IZ))
      QQQ(IZ)=-(PFR(IT,IZ-1)-PFR(IT,IZ)*
     1 (2.-APRESS(IZ))+PFR(IT,IZ+1))
 607  CONTINUE
C
      CALL LUDE(AP,BP,CP,L,D,U,NZ)
      CALL FBACK(L,D,U,QQQ,TTT,NZ)
C
      DO 613 IZ=2,NZ-1
      PFR(IT+1,IZ)=TTT(IZ)
 613  CONTINUE
C
      DO 638 IZ=1,NZ
      IF(IPR.GE.3)WRITE(6,625)IT1,IZ,PFR(IT+1,IZ)
  625 FORMAT(3X,' IT+1=',I3,'IZ=',I3,'   P.FREON=',E12.5)
  638 CONTINUE
C
      DO 630 IZ=1,NZ
      PTOT(IZ)=PN2(IT+1,IZ)+PO2(IT+1,IZ)+PCO2(IT+1,IZ)+
     1 +PFR(IT+1,IZ)
```

```
  630 CONTINUE
      RETURN
      END
C
CCCCCCCCCCCCCCCCCCCCCCCCCCCCCCCCCCCCCCCCCCCCCCCCCCCCCCCCCCCCCCCCCCCC
C
      SUBROUTINE KMIX(IT,IZ,NZ,T,KGM,MOL)
C
C THE SUBROUTINE COMPUTES THE CONDUCTIVITY OF THE GAS MIXTURE
C INSIDE THE CLOSED FOAM CELLS AS A FUNCTION OF COMPOSITION
C IN AXIAL DIRECTION Z
C

      REAL KGM(51),KN2,KO2,KCO2,KFR
      REAL T(200,51),YA(5),RT(51),TMEM(51)
      REAL ETA(5),XN2(51),XO2(51),XCO2(51),XFR(51),AA(5,5),MOL(5)
C
      COMMON/BLK1/ PN2(200,51),PO2(200,51),PCO2(200,50),PFR(200,51),
     1 PTOT(51)
      COMMON/BLK7/ S(5),SS(5,5)
      COMMON/BLK6/ RN2,RO2,RCO2,RFR
      COMMON/BLK8/ IPR,DZ,DT,ITEMP
C
      RRR=8314./29.7
      IF(ITEMP.NE.25)GOTO 436
C
      DO 436 IZ=1,NZ
      TMEM(IZ)=T(IT,IZ)
      T(IT,IZ)=298.
  436 CONTINUE
C
C  THE MIHTURE TRANSPORT PROPERTIES:
C
C
C COMPUTE THE  THERMAL PROPERTIES:
C
C MOL FRACTIONS:
C
      IF(IPR.GT.1)WRITE(6,437)
  437 FORMAT(//,'   MOL FRACTIONS:',/,
     1 '    NODE#      XN2          XO2         XCO2         XFR         XTOT',/)
      DO 210 IZ=1,NZ
      XN2(IZ)=PN2(IT+1,IZ)/PTOT(IZ)
      XO2(IZ)=PO2(IT+1,IZ)/PTOT(IZ)
      XCO2(IZ)=PCO2(IT+1,IZ)/PTOT(IZ)
      XFR(IZ)=PFR(IT+1,IZ)/PTOT(IZ)
      XTOT=XN2(IZ)+XO2(IZ)+XCO2(IZ)+XFR(IZ)
      IF(IPR.GT.1)WRITE(6,432)IZ,XN2(IZ),XO2(IZ),XCO2(IZ),
     1 XFR(IZ),XTOT
  432 FORMAT(3X,I5,5E11.4)
  210 CONTINUE
      WRITE(6,438)
  438 FORMAT(//)
C
C MIXTURE CONDUCTIVITY KGM(IZ):
C
      DO 230 IZ=1,NZ
C
C VISCOSITIES:
      ETA(1)=(17.84+(T(IT,IZ)-300.)/100.*4.14)*1.E-6
```

```
      ETA(2)=(20.63+(T(IT,IZ)-300.)/50.*2.53)*1.E-6
      ETA(3)=(14.958+(T(IT,IZ)-300.)/50.*2.247)*1.E-6
      ETA(4)=20.000E-6
C
      DO 229 IR=1,4
      IF(IPR.GE.3)WRITE(6,228)IR,S(IR),SS(2,IR),ETA(IR)
  228 FORMAT(9X,I3,3E12.5)
  229 CONTINUE
      DO 225 I=1,4
      DO 220 J=1,4
      IF(I.EQ.J)AA(I,J)=0.0
      IF(I.EQ.J)GOTO 220
      AA(I,J)=.25*(1.+SQRT(ETA(I)/ETA(J)*(MOL(J)/MOL(I))**.75*
     1 (T(IT,IZ)+S(I))/(T(IT,IZ)+S(J))))**2.*(T(IT,IZ)+SS(I,J))
     2 /(T(IT,IZ)+S(I))
  220 CONTINUE
C
      YA(I)=XN2(IZ)*AA(I,1)+XO2(IZ)*AA(I,2)
     1 +XCO2(IZ)*AA(I,3)+XFR(IZ)*AA(I,4)
      IF(IPR.GE.3)WRITE(6,334)I,J,YA(I)
  225 CONTINUE
  334 FORMAT(3X,2I3,'  YA=',E11.4)
C
C KODUCTIVITIES:
      KN2=.02620+(T(IT,IZ)-300.)/100.*.00715
      KO2=.02676+(T(IT,IZ)-300.)/50.*.00394
      KCO2=.016572+(T(IT,IZ)-300.)/50.*.003898
      KFR=8.3022E-3+(9.426E-3-8.3022E-3)/27.8
     1 *(T(IT,IZ)-310.93)
C
      KGM(IZ)=KN2*XN2(IZ)/(XN2(IZ)+YA(1))
     1 +KO2*XO2(IZ)/(XO2(IZ)+YA(2))
     1 +KCO2*XCO2(IZ)/(XCO2(IZ)+YA(3))
     1 +KFR*XFR(IZ)/(XFR(IZ)+YA(4))
  230 CONTINUE
C
      DO 233 IZ=1,NZ
      T(IT,IZ)=TMEM(IZ)
  233 CONTINUE
C
      RETURN
      END
C
CCCCCCCCCCCCCCCCCCCCCCCCCCCCCCCCCCCCCCCCCCCCCCCCCCCCCCCCCCCCCCCCCCCCCCCCC
      SUBROUTINE FBACK(L,D,U,QQQ,TTT,N)
      REAL L(100),D(100),U(100),QQQ(100),Y(100),TTT(100)
      COMMON/BLK8/ IPR,DX,DT
C
C     [A]*[TTT]=[QQQ]
C     [L]*[U]*[TTT]=[QQQ]
C     [[U]*[T]=[Y]
C     [L]*[Y]=[QQQ]
C     N - MATRIX ORDER
C     TTT SOLUTION VECTOR
C
      Y(2)=QQQ(2)
C
      DO 20 I=3,N-1
   20 Y(I)=QQQ(I)-L(I)*Y(I-1)
```

```
      TTT(N-1)=Y(N-1)/D(N-1)
C
      DO 21 I=2,N-2
      J=N-I
      TTT(J)=(Y(J)-U(J)*TTT(J+1))/D(J)
   21 IF(IPR.GE.3)WRITE(6,121)J,TTT(J),QQQ(J)
  121 FORMAT(3X,' J=',I3,2E12.4)
      RETURN
      END
C
CCCCCCCCCCCCCCCCCCCCCCCCCCCCCCCCCCCCCCCCCCCCCCCCCCCCCCCCCCCCCCCCCCCC
      SUBROUTINE LUDE(A,B,C,L,D,U,N)
      REAL A(100),B(100),C(100),L(100),D(100),U(100)
C
C     THIS SUBR. DECOMPOSES A TRIDIAGONAL MATRIX BY L-U METHOD
C
C     B(I) LOWER OFF DIAG. EL. OF TRIDIAGONAL MATRIX
C     A(I) DIAG. EL.OF TRIDIAGONAL MATRIX
C     C(I) UPPER OF DIAG. EL. OF TRIDIAGONAL MATRIX
C
C     L(I) LOWER OF DIEG. EL. OF THE LOWER DIAG. MATRIX
C     D(I) DIAG. EL OF UPPER DIAG. MATRIX
C     U(I) UPPER OFF DIAG. EL OF THE UPPRE DIAG. MATRIX
C
C     N - MATRIX ORDER
C
      D(2)=A(2)
      U(2)=C(2)
C
      DO 10 I=3,N-1
      L(I)=B(I)/D(I-1)
      D(I)=A(I)-L(I)*U(I-1)
      U(I)=C(I)
   10 CONTINUE
      RETURN
      END
C
CCCCCCCCCCCCCCCCCCCCCCCCCCCCCCCCCCCCCCCCCCCCCCCCCCCCCCCCCCCCCCCCCCCC
C
C SPEC HEAT (V=CONST):
C       CVN2=1.0408-R+(T(IT,IZ)-300.)/100.*.0051
C       CVO2=.9203-R+(T(IT,IZ)-300.)/50.*.0088
C       CVCO2=.871-R+(T(IT,IZ)-300.)/50.*.0029
C       CVFR=1.8
C       CVM(IZ)=CVN2*XN2(IZ)+CVO2*XO2(IZ)+CVCO2*XCO2(IZ)+
C      1 CVFR*XFR(IZ)
C RHOM:
C       RHOM(IZ)=(PN2(IT,IZ)+PO2(IT,IZ)+PCO2(IT,IZ)
C      1 +PFR(IT,IZ))/T(IT,IZ)/RRR
C       WRITE(6,321)IZ,CVM(IZ),RHOM(IZ)
```

Input Data File M.DAT

The input data include:

THICK - Thickness of the foam panel [cm]
NZ - Number of nodes, up to 51 (see Fig 7.1)
TIME - Aging time [days]
DTI - Initial time step [days]
IPR - Integer specifying the code output: IPR=2 prints a detailed output, IPR=1 prints only partial pressures and mixture conductivities.
ITEMP - Integer equal to 25 if conductivity of gas mixture has to be computed at 25°C
PN20,PE020,PEC020,PEFR0
- Reference values of N_2, O_2, CO_2 and R 11 permeability coefficients, [$sm^3_{STP}/cm\text{-}s\text{-}atm$], (see equation 5.1)
EN2,E02,EC02,EFR
- activation energy divided by ideal gas constant (see equation 5.1)
T(1,NZ) - Temperature imposed on the foam surface, [°K], (node NZ)
T(1,1) - Temperature imposed on the foam surface, [°K], (node 1)
PN2(1,2) - Initial partial pressure of N_2 inside the foam panel, [atm], (constant in all nodes)
P02(1,2) - Initial partial pressure of O_2 inside the foam panel, [atm], (constant in all nodes)
PC02(1,2)- Initial partial pressure of CO_2 inside the foam panel, [atm], (constant in all nodes)
FR(1,2) - Initial partial pressure of R 11 inside the foam panel, [atm], (constant in all nodes)
KSOL - Effective conductivity of the solid polymer cell structure, [W/m-°K]
KRAD - Apparent conductivity of the solid polymer due to radiation, [W/m-°K].